Gradient-based shape optimization of 2D wave barriers using the Boundary Element Method and the Finite Element Method

Jacob David Rodríguez Bordón

Instituto Universitario SIANI - Universidad de Las Palmas de Gran Canaria

supervised by

Prof. Dr. Geert Lombaert

Structural Mechanics Section (Department of Civil Engineering) - KU Leuven

February 2016

Acknowledgements

This report is a result from the work done during a three-month (September to November 2015) research stay at Structural Mechanics Section (Department of Civil Engineering) of KU Leuven under the supervision of Professor Geert Lombaert. I would like to deeply thank Professor Lombaert for allowing me to work alongside him and such an enthusiastic research team, and for his guidance, advice and patience.

I would like to thank immensely my advisors, Professors Juan José Aznárez and Orlando Maeso, and also Luis Alberto Padrón, for encouraging me to live this experience, and for their constant support and help whenever it is required. I would like to express my gratitute to Pedro Galvín for facilitating this stay at the initial stages.

I would like to thank Professor Mattias Schevenels and Cedric Van hoorickx for their support and advice during the stay.

I would also like to thank all the Department, especially my friends and colleages Manthos, Dimitrios, Bram, Matthias, Jie, Hernán, Arne, Ramses, Kristof, Weili, Pengchao, Avisek and Kirsty.

Thank you all for the warmth that everyone has shown.

Thank you María.

Abstract

This report is concerned with the gradient-based shape optimization of two dimensional wave barriers using the Boundary Element Method (BEM) and the Finite Element Method (FEM) in the time harmonic domain. The advantages and disadvantages of both numerical methods are widely known, and the problem at hand is one of those problems where they complement very well. The main focus is on the development of the formulation required for the calculation of shape sensitivities, which is usually the costlier stage of a gradient-based shape optimization. Shape sensitivities are calculated using a Direct Differentiation Method (DDM) rather than an Adjoint Variable Method (AVM) because a small number of design variables is considered. For the sake of completeness and usefulness, the formulation is described in such a level of detail that its implementation is relatively straightforward. From the FEM point of view, the formulation is developed for wave propagation through isotropic elastic solids. From the BEM point of view, the formulation is developed for wave propagation through inviscid fluids, and anti-plane and in-plane wave propagation through isotropic elastic solids. An entire chapter is devoted to the optimization of wave barriers, where the developments of the present work are applied to the optimization of a simple wave barrier. The studied problem exploit partially the BEM–FEM coupling as it can also be solved by using a BEM–BEM model. However, it serves as an application of the methodology, which will remain valid for future developments based on this work.

Contents

Organization of the report

Chapter 1 gives an overview of the subject by describing several concepts related to wave barriers and optimization.

Chapter 2 gives an overview of shape sensitivity analysis using the Finite Element Method, and describes in detail the formulation for 2D solid finite elements.

Chapter 3 gives an overview of shape sensitivity analysis using the Boundary Element Method, and develops the Singular Boundary Integral Equations for 2D shape sensitivity analysis of Laplace (heat conduction, electrostatics, potential flow), Helmholtz (wave propagation in inviscid fluids, anti-plane elastodynamics), in-plane elastostatics, and in-plane elastodynamics problems.

Chapter 4 describes BEM-BEM and BEM-FEM coupling for sensitivity analysis.

Chapter 5 contains the application of the described methodologies to the shape optimization of a simple wave barrier. This chapter also gives the main conclusions and ideas for further research.

Chapter 1

Introduction

1.1   Wave barriers

Machinery and vehicles are a source of vibrations that can travel through the soil to nearby constructions, where they can annoy people or cause equipment malfunctioning or even damage. In order to reduce the vibrations, one or more wave barriers can be installed along the transmission path as a passive isolation system. The design of each system depends on the source of vibrations, the properties of the transmission path, and the isolation requirements. Open trenches are very efficient as wave barriers because its stress-free boundaries act as perfect reflectors of elastic waves. The efficiency of open trenches greatly depends on the ratio between the Rayleigh wavelength and the trench depth. However, a pure open trench can not be excavated to any desired depth for soil stability reasons. Thus, other systems such as in-filled trenches, or the installation of sheet piles or rows of piles, are often used. Another option is reinforcing the open trench by installing retaining sheet piles or concrete walls on both sides of the trench.

The literature about the design and analysis of wave barriers is vast. Before the numerical computing era, only experimental studies were performed in order to assess these problems. Barkan [10] conducted experiments to study the efficiency of open trenches in dry and water saturated soils, and sheet piles barriers in a dry soil. Woods [60] performed a more systematic set of field tests to study the effect of the geometry of open trenches over their efficiency. They confirmed experimentally the well known fact that the efficiency of open trenches mostly depends on the depth to Rayleigh wavelength ratio. Woods found that the width of the trench has little influence on efficiency. Nowadays, analytical, semi-analytical and numerical methods are being used, although experimental methods are still being used to confirm or parametrize mathematical models. Three kinds of wave barriers have been extensively studied: open and in-filled trenches, and rows of piles; mainly using the Boundary Element Method (BEM). The open and in-filled trenches have been studied through two-dimensional BEM models by Emad et al. [30], Beskos et al. [16, 40], and even formulas for a simplified design have been given by Ahmad et al. [2]. They were studied in three-dimensional problems using BEM models by Banerjee et al. [9] and Dasgupta et al. [27]. The vibration isolation produced by rows of piles have been studied by Avilés et al. [7] analytically, and by Kattis et al. [39] using a three-dimensional BEM model.

Most of the effort has been directed towards the analysis of wave barriers in general

situations in order to obtain useful design rules, where the influences of the source, wave barrier, soil, and receiver are evaluated by doing parametric studies. A step forward is being taken for obtaining better designs by applying optimization algorithms to this problem [35]. The optimization of wave barriers leads to better designs for both general and particular situations, but specially for the latter as it allows obtaining the best solution taking into account specific economic and engineering constraints.

1.2 Optimization

Nowadays, design optimization is a crucial field in engineering. When facing a design problem, the very first step is to come out with a solution or a concept that simply works, i.e. the design does what is required. In our competitive environment this is not enough, and the design must fulfill several constraints and perform well under different conditions. Furthermore, the main objectives are usually accompanied by other secondary objectives, which can be even conflicting objectives. An appropriate methodology to do such an optimization is using optimization algorithms and numerical simulation of the problem.

The mathematical formulation of an optimization problem can be written as [48]:

$$\min_{a \in \mathbb{R}^n} f_i(a), \, i \in \mathcal{F} \text{ subject to } \begin{cases} g_i(a) \leq 0, \, i \in \mathcal{I} \\ h_i(a) = 0, \, i \in \mathcal{E} \end{cases} \tag{1.1}$$

where f_i, g_i and h_i are scalar valued functions of the variables a, and $\mathcal{F}$, $\mathcal{I}$ and $\mathcal{E}$ are sets of indices. The variable a is the vector of design variables. The functions f_i are the objective functions, g_i the inequality constraints, and h_i the equality constraints. Optimization is a very active field of research because of its complexity and usefulness. There are a plethora of optimization algorithms, each of one designed to target a range of problems. They can be mainly divided into deterministic and heuristic approaches. The deterministic approach take analytical properties of the problem to generate points that converge to optimal solutions. The heuristic approach is more flexible than the deterministic one, but the quality of the obtained solution cannot be guaranteed and the number of evaluations of the objective function is usually greater. A good reference on deterministic algorithms is [48], and on heuristic algorithms [34, 28].

The structural optimization problem can be explained using the paradigm of three interacting models [5]: the design model, the analysis model and the optimization model. Here, we give a slightly broader definition of this paradigm in order to include other aspects than geometry.

The design model is a subset of all possible designs. Thus, it is a decisive step that needs some knowledge about the problem at hand. The description of a design model comprises information about its geometry, materials and conditions. The most important piece of information is the geometrical one. All others are somehow supported on it. The geometric description consists of information related to the topology, i.e. number of sub-domains and their connectivity, and information related to the shape of each sub-domain. The material information offers data about the type of material and its properties at each point of the domain. Each sub-domain is usually made of the same type of material with homogeneous properties, but in general the properties could vary over it. The description about conditions consists of support, interface and load information. All this information

must be expressed in a mathematical form as a set of equations, inequalities and variables (continuous or discrete). Eventually, some of the variables become constants, parameters or design variables, being these latter those that actually change during the optimization process.

The analysis model allows evaluation of objective and constraint functions, and their gradient or even Hessian if needed by the optimization model. This model must be equivalent to the design model, but ready to be used by an analysis procedure. The analysis procedure can be a closed-form analytical solution, but more often is a semi-analytical or numerical procedure.

The optimization model selects the best design according to the objective and constraint functions from the possibilities offered by the design model. For a multi-objective optimization, it gives a range of designs which defines the Pareto front. The model requires the definition of the design variables and their domains, the objective and constraint functions, and the optimization algorithm. The optimization model acts as the job manager in the optimization process, i.e. it decides at each step what designs have to be analysed and then takes further decisions using the analysis results.

1.3 Sensitivity analysis

Most of the analyses consist in obtaining the response of a given design, these are the usual zero-order static, time harmonic, transient, modal, etc. analyses. In order to study the influence of some design parameters, it is possible to run several zero-order analyses with different values of these design parameters, i.e. a parametric study. It is appropriate when the engineer would like to have a global idea of the performance of the design for a range of variation of a small number of parameters. For other purposes like optimization, identification or reliability studies, zero-order analyses are usually not enough. Sensitivity analyses consist in obtaining first- and second-order static, time harmonic, transient, modal, etc. analyses of a design with respect to the variation of continuous design parameters [25].

Let $\mathbf{a}$ be a vector of continuous design parameters, and $f = f(\mathbf{a})$ a field variable (displacement, velocity, stress, etc.) or combination of field variables (performance, constraints, etc.). If f is smooth enough ($f \in C^2$), it is possible to build a Taylor's approximation of f near a given set of values of the design parameters $\mathbf{a}^0$:

$$f(\mathbf{a}) = f^0 + f_{,j}^0 \left(a_j - a_j^0\right) + f_{,jk}^0 \left(a_j - a_j^0\right)\left(a_k - a_k^0\right) + O\left[(\Delta a)^3\right] \qquad (1.2)$$

where f^0 is obtained from a zero-order analysis, $f_{,j}^0$ from a first-order sensitivity analysis (gradient), and $f_{,jk}^0$ from a second-order sensitivity analysis (Hessian), all at $\mathbf{a} = \mathbf{a}^0$. Note that indicial notation, comma notation for derivatives with respect to the design parameters, and Einstein summation convention are used in Equation (1.2). Most of the literature about sensitivity analysis is focused on first-order analysis. Second-order analysis, although useful for checking optimality conditions, is seldom performed because of its computational cost and its comparatively narrow range of applications [25]. Therefore, in the following, the term "sensitivity" is used as a synonym of "first-order sensitivity".

There are four major methodologies for obtaining sensitivities [59]: overall or global finite differences, continuum derivatives, discrete derivatives and computational or automatic differentiation. The last three methodologies can be formulated as direct and adjoint

9

methods. In the direct approach, the derivatives of the entire structural response are obtained, and then the performance functions can be obtained by using the chain rule of differentiation. In the adjoint approach, an adjoint problem is formulated for each performance function, and hence not all derivatives of the structural response are obtained. Roughly speaking, the direct approach focuses on structural response, while the adjoint approach focuses on structural performance. The former is appropriate for a small number of design variables and a big number of performance functions, and the latter is appropriate for the opposite. In both approaches, the obtained matrix of the linear system of equations (stiffness or influence matrix) is exactly equal to that of the zero-order analysis, and thus its factorization could be used for the sensitivity analysis. The effort is employed in building the vector of the linear system of equations (load vector). Van Keulen et al. [59] give a very complete review of methods of structural sensitivity analysis. Next, a brief overview is given.

The Global Finite Differences (GFD) methodology is based on estimating the performance sensitivity $f_{,j}^0$ by using a finite difference formula which requires only zero-order analyses:

$$f_{,j}^0 \simeq \text{FD}\left[f^0, \Delta a_j^0\right] \tag{1.3}$$

where the FD operator can represent a forward, central, 4-point central, etc. finite difference formula with a perturbation Δa_j^0 on the j-th design variable. It is the easiest method to implement. However, it is computationally inefficient and unreliable as an appropriate value of the perturbation is needed. Furthermore, not always is possible to find a finite difference formula and a value of the perturbation that lead to a sensitivity with the required precision. Therefore, GFD should be the last resort for computing sensitivities.

In the Continuum Derivatives (CD) approach, the sensitivities are obtained by differentiating the continuum governing equations (partial differential or integro-differential equations). It leads to a set of continuum sensitivity equations which are then usually solved numerically. For shape sensitivities, because the domain itself becomes a design variable, a material differentiation approach or a control volume approach must be used [6].

In the Discrete Derivatives (DD) approach, the sensitivities are obtained by differentiating the discretized set of equations. Thus, in the DD approach the differentiation and discretization processes are reversed with respect to the CD approach. For some cases, if the same numerical method and discretization is used, it has been proven that both approaches lead to the same solution [5]. The element-wise matrices obtained after differentiation involves derivatives of the stiffness and load matrices. Although these derivatives can be evaluated analytically, they are particularly involved and lengthy for shape sensitivities. Therefore, they are usually approximated by finite differences, which not only is much more easy to implement, but also is cheaper computationally. In this case, the approach is called semi-analytical.

Automatic Differentiation (AD) approach consists in the differentiation of the computer code itself. Although finite element codes are composed of many more or less complex subroutines and functions, they are basically a collection of elementary functions. AD approach defines the partial derivatives of these elementary functions, and then the derivatives of complicated subroutines and functions are computed using propagation and the chain rule of differentiation. Although it may appear to be simple and straightforward,

it is not. It requires enough skills to apply the tools to the source code, and a judicious choice of where to apply it in order to get an efficient code. Furthermore, it could require the modification of the original code before applying the tools.

1.4   Parametrization

Parametrization (or parameterization) is the process by which some entity is described in terms of parameters. In our context, this is done over the description of the design model. The parametrization of a design is not unique nor trivial, it has a huge impact on the result of an optimization process. In fact, it materializes the design model by setting a set of parameters and mathematical expressions that defines the geometry, material and conditions of a design model. The parameters that are used in an optimization process are the design variables.

In structural design, there are mainly five kinds of parameters [25]: material parameters (Young's modulus, fiber orientation, etc.), size parameters (thickness, cross-section, etc.), shape parameters (length, radius, etc.), configuration parameters (orientation and location of structural elements), and topological parameters (number and connectivity of structural elements). Note that some of them are closely related, and, for example, the last four could be grouped as geometrical parameters. These parameters can be also classified as discrete (boolean or integer) or continuous (real) parameters.

The literature about geometric parametrization is vast and specialized, particularly in shape parametrization, which is probably the most involved. Before going further, it is necessary to define some concepts related to shape parametrization and sensitivity analysis. For first-order analyses, each shape parameter is studied independently from others, i.e. the sensitivities are obtained without considering other shape parameters. Although several parameters could be linked through some constraints in order to obtain a feasible design, this is something managed by the optimization algorithm and does not influence the first-order sensitivity analysis. For this reason, it is possible to build a Taylor's expansion of the geometrical design with respect to the parameter a around a given state $a = a^0$:

$$\tilde{\mathbf{x}} = \mathbf{x} + \mathbf{v}\left(a - a^0\right) + O\left[\left(a - a^0\right)^2\right] \tag{1.4}$$

where $\mathbf{x}$ is a point of the domain $\Omega(a^0)$, $\mathbf{v} = \mathbf{v}(\mathbf{x}, a^0) = (\partial \mathbf{x}/\partial a)_{a^0}$ is the design velocity field, and $\tilde{\mathbf{x}} = \tilde{\mathbf{x}}(\mathbf{x}, a)$ is the new location of the point $\mathbf{x}$ for a parameter value a. This is a linear mapping of points of the domain $\Omega(a^0)$ to $\tilde{\Omega}$, that approximates the domain for a small variation of a, see Fig. 1.1. It must obviously be continuous, i.e. $\mathbf{v} \in C^0$, otherwise the mapping breaks the domain.

For first-order shape sensitivity analysis, the design velocity field $\mathbf{v}$ of each design variable has to be defined for all points of the domain. There are a large number of strategies to build and update this mapping during optimization processes [58, 54, 25, 26, 5]. Although it is difficult to classify all these strategies, there are three main philosophies:

Based on geometry. In order to build the geometry, it is necessary to use a CAD (Computer Aided Design) tool which can use a Boundary REPresentation (BREP), Function REPresentation (FREP), Constructive Solid Geometry (CSG) or other representation. Since the representation is based on a set of equations and parameters,
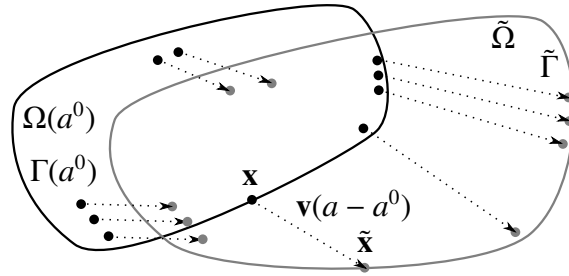
Figure 1.1: Taylor's expansion of the shape parametrization

these parameters are available as design variables. Once the mesh is obtained from the CAD model by a mesher, the design velocity field of each design variable can be inherited to the nodes of the mesh by differentiation of the representation with respect to the design variable at the position of the nodes.

Based on mesh. Instead of working with the representation given by the CAD model, it is possible to use the representation provided by the mesh. The nodal coordinates are used as design variables, which lead to a big set of design variables. It is also called parameter-free or FE-based parametrization.

Based on a free-form deformation. An auxiliary design mesh consisting of isoparametric elements, B-splines or NURBS is defined in order to deform the CAD model or the mesh. The points of the CAD model or the nodes of the mesh are connected to the design mesh by position, i.e. there is a one-to-one correspondence (a mapping) between the design model and the CAD model or mesh. The design mesh acts as a canvas where the CAD model or the mesh is stuck, and any deformation applied to the canvas is accordingly done over them. The design variables can be the nodal coordinates or control points of the design mesh.

None of the strategies are of general applicability. The strategies based on geometry are useful for clearly defined shape optimizations, for example when the design variables are radii, lengths or positions of straight or arc-like lines. If the CAD model allows patches of variable order, then it would be possible to obtain more complicated shapes. A major drawback is that CAD tools do not usually come with all the necessary features to apply these strategies easily. The strategies based on mesh movement offer more freedom to the shape optimization. However, this freedom comes with some additional costs. Regularization and remeshing processes are needed after each optimization step in order to obtain a feasible design and a valid mesh. Furthermore, because of the number of design variables and the post-processing stages after each iteration, they can be relatively expensive computationally. The strategies based on a free-form deformation have characteristics of the latter two. They offer a selective in-between flexibility with respect to shape variations, from very simple and constrained shapes to very complex shapes. Moreover, they have much less problems associated with the distortion of the mesh, and thus regularization and remeshing are hardly needed.

Chapter 2

Shape sensitivities using the Finite Element Method

2.1 Introduction

As pointed out in Section 1.3, the calculation of shape sensitivities can be done in several ways. Apart from the unreliable Global Finite Difference (GFD) approach, the other three approaches are somehow equivalent, but very different with respect to where and how much effort is required. From the point of view of the Finite Element Method (FEM), the Discrete Derivatives approach is probably the most appropriate. Its starting point is the system of equations obtained from the discretization.

Consider the global system of equations resulting from the discretization of an elastic domain by using the FEM:

$$\mathbf{K}\mathbf{u} = \mathbf{f} \tag{2.1}$$

where $\mathbf{K}$ is the stiffness matrix, $\mathbf{u}$ is the degrees of freedom vector of dimension N_{dof}, and $\mathbf{f}$ is the load vector. Consider also N_{f} objective or constraint functions ψ_i, and the vector of design variables $\mathbf{a}$ of dimension N_{dv}:

$$\psi_i = \psi_i\left(\mathbf{a}, \mathbf{u}\left(\mathbf{a}\right)\right), \quad i = 1, \dots, N_{\text{f}} \tag{2.2}$$

By differentiating Equation (2.1) with respect to the design variables:

$$\mathbf{K}\frac{\partial \mathbf{u}}{\partial a_i} = \frac{\partial \mathbf{f}}{\partial a_i} - \frac{\partial \mathbf{K}}{\partial a_i}\mathbf{u}, \quad i = 1, \dots, N_{\text{dv}} \tag{2.3}$$

where $\partial \mathbf{u}/\partial a_i$ is the vector of sensitivities of $\mathbf{u}$ with respect to a_i, and $\partial \mathbf{f}/\partial a_i$ and $\partial \mathbf{K}/\partial a_i$ are derivatives with respect to a_i, which can be calculated by using the design parametrization. In the so-called semi-analytical approach, these derivatives are calculated by finite differences, which is relatively simple but accurate. Because compatibility and equilibrium conditions also hold for the displacement and traction sensitivities, these derivatives can be calculated element-wise and then assembled into the global system of equations as usual. By differentiating Equation (2.2) with respect to the design variables:

$$\frac{\mathrm{d}\psi_i}{\mathrm{d}a_j} = \frac{\partial \psi_i}{\partial a_j} + \frac{\partial \psi_i}{\partial u_k}\frac{\partial u_k}{\partial a_j}, \quad i = 1, \dots, N_{\text{f}}, \ j = 1, \dots, N_{\text{dv}}, \ k = 1, \dots, N_{\text{dof}} \tag{2.4}$$

where indicial notation and Einstein summation convention are used. This approach can be formulated as a Direct Differentiation Method (DDM) or as an Adjoint Variable Method (AVM). DDM consists in performing the following steps:

1. Solve Equation (2.1), i.e. zero-order analysis.

2. Solve Equation (2.3), i.e. first-order sensitivity analysis.

3. Substitute results in Equation (2.4) in order to obtain the gradient of each objective or constraint function.

AVM requires a reformulation of Equation (2.4) by substituting $\partial u_k / \partial a_j$ obtained from Equation (2.3):

$$\frac{\mathrm{d}\psi_i}{\mathrm{d}a_j} = \frac{\partial \psi_i}{\partial a_j} + \frac{\partial \psi_i}{\partial u_k} K_{lk}^{-1} \left(\frac{\partial f_l}{\partial a_j} - \frac{\partial K_{lk}}{\partial a_j} u_k \right) = \frac{\partial \psi_i}{\partial a_j} + \lambda_l \left(\frac{\partial f_l}{\partial a_j} - \frac{\partial K_{lk}}{\partial a_j} u_k \right) \tag{2.5}$$

$$\frac{\partial \psi_i}{\partial u_k} = \lambda_l K_{lk} \tag{2.6}$$

where $l = 1, \ldots, N_{\mathrm{dof}}$, and Equation (2.6) represents the adjoint problem with λ_l as the adjoint variables and $\partial \psi_i / \partial u_k$ as the adjoint loads. Note that this problem has the same stiffness matrix as the original problem, although transposed. Adjoint loads are explicit and known once the objective or constraint functions are defined. Therefore, AVM consists in performing the following steps:

1. Solve Equation (2.1), i.e. zero-order analysis of the original problem.

2. Obtain the loads from Equation (2.3), i.e. the loads required for solving first-order sensitivity analysis.

3. Solve Equation (2.5), i.e. zero-order analysis of the adjoint problem.

4. Substitute results in Equation (2.5) in order to obtain the gradient of each objective or constraint function.

Both methods require solving the zero-order analysis of the original problem, and also the calculation of the stiffness matrix and load vector derivatives with respect to the design variables. The main difference is the additional linear system of equations that must be solved. DDM requires solving as many systems as the number of design variables, while AVM requires solving as many systems as the number of objective or constraint functions that require the calculation of their gradients. A very concise comparison between both methods can be found in [25]. In the present work, DDM is used because a small number of design variables are considered.

The rest of the chapter is organized as follows. In Section 2.2, the 2D solid isoparametric finite element is described, including the matrices derivatives, their approximation by finite differences, and their analytical evaluation. In Section 2.3, an example is solved analytically and numerically in order to validate the formulation and its implementation.

2.2 2D solid isoparametric finite element

Although widely known, the 2D solid isoparametric finite element formulation is going to be briefly described for the sake of completeness. It also allows describing the basic semi-analytical approach as well as an exact method [49] for the evaluation of the matrices derivatives.

2.2.1 Basic formulation

A 2D solid isoparametric finite element with N_n nodes is built using the same interpolation for the geometry and the displacement field:

$$\mathbf{x} = \sum_{i=1}^{i=N_\mathrm{n}} N^{(i)} \mathbf{x}^{(i)} = \left[\; N^{(1)}\mathbf{I} \;\; \ldots \;\; N^{(i)}\mathbf{I} \;\; \ldots \;\; N^{(N_\mathrm{n})}\mathbf{I} \;\right] \left\{ \begin{array}{c} \mathbf{x}^{(1)} \\ \ldots \\ \mathbf{x}^{(i)} \\ \ldots \\ \mathbf{x}^{(N_\mathrm{n})} \end{array} \right\} = \mathbf{N}^{(\mathrm{e})}\mathbf{x}^{(\mathrm{e})} \tag{2.7}$$

$$\mathbf{u} = \mathbf{N}^{(\mathrm{e})}\mathbf{u}^{(\mathrm{e})} \tag{2.8}$$

where $\mathbf{x}^{(i)}$ is the position vector of the i-th node in global coordinates, $N^{(i)} = N^{(i)}(\xi_1, \xi_2)$ is the shape function associated the the i-th node, ξ_1 and ξ_2 are the local curvilinear coordinates, and $\mathbf{I}$ is the 2×2 identity matrix. The transformation between local curvilinear coordinates and global cartesian coordinates is governed by the Jacobian matrix:

$$\frac{\partial f}{\partial \xi_i} = \frac{\partial f}{\partial x_j}\frac{\partial x_j}{\partial \xi_i} = J_{ij}\frac{\partial f}{\partial x_j} \quad \mathbf{G} = \mathbf{J}^{-1} \xrightarrow{} \quad \frac{\partial f}{\partial x_i} = G_{ij}\frac{\partial f}{\partial \xi_j} \tag{2.9}$$

where:

$$\mathbf{J} = \left[\begin{array}{cc} \dfrac{\partial x_1}{\partial \xi_1} & \dfrac{\partial x_2}{\partial \xi_1} \\[2ex] \dfrac{\partial x_1}{\partial \xi_2} & \dfrac{\partial x_2}{\partial \xi_2} \end{array} \right] = \sum_{i=1}^{i=N_\mathrm{n}} \left[\begin{array}{cc} \dfrac{\partial N^{(i)}}{\partial \xi_1}x_1^{(i)} & \dfrac{\partial N^{(i)}}{\partial \xi_1}x_2^{(i)} \\[2ex] \dfrac{\partial N^{(i)}}{\partial \xi_2}x_1^{(i)} & \dfrac{\partial N^{(i)}}{\partial \xi_2}x_2^{(i)} \end{array} \right] = \left[\begin{array}{cc} J_{11} & J_{12} \\[2ex] J_{21} & J_{22} \end{array} \right] \tag{2.10}$$

and its determinant relates infinitesimal domains in both spaces:

$$\mathrm{d}\Omega = |\mathbf{J}|\;\mathrm{d}\xi_1\mathrm{d}\xi_2 \tag{2.11}$$

The relevant strain tensor components can be arranged in a column-vector $\boldsymbol{\epsilon}$, whose relationship with the displacement field is:

$$\boldsymbol{\epsilon} = \left\{ \begin{array}{c} \epsilon_{11} \\ \epsilon_{22} \\ \gamma_{12} \end{array} \right\} = \left[\begin{array}{cc} \dfrac{\partial}{\partial x_1} & 0 \\[2ex] 0 & \dfrac{\partial}{\partial x_2} \\[2ex] \dfrac{\partial}{\partial x_2} & \dfrac{\partial}{\partial x_1} \end{array} \right] \left\{ \begin{array}{c} u_1 \\ u_2 \end{array} \right\} = \mathbf{S}\mathbf{u} = \left[\; \mathbf{B}^{(1)} \;\; \ldots \;\; \mathbf{B}^{(i)} \;\; \ldots \;\; \mathbf{B}^{(N_\mathrm{n})} \;\right]\mathbf{u}^{(\mathrm{e})} = \mathbf{B}^{(\mathrm{e})}\mathbf{u}^{(\mathrm{e})}$$

$$\tag{2.12}$$

where $\mathbf{B}^{(i)} = \mathbf{S}N^{(i)}$ is built using Equation (2.9):

$$\frac{\partial N^{(i)}}{\partial x_j} = G_{jk}\frac{\partial N^{(i)}}{\partial \xi_k} \tag{2.13}$$

The relevant stress tensor components can also be arranged in a column-vector σ, and its relationship with the strain vector is done through the general constitutive matrix $\mathbf{D}$:

$$\sigma = \left\{ \begin{array}{c} \sigma_{11} \\ \sigma_{22} \\ \tau_{12} \end{array} \right\} = \left[\begin{array}{ccc} d_{11} & d_{12} & 0 \\ d_{11} & d_{12} & 0 \\ 0 & 0 & d_{33} \end{array} \right] \left\{ \begin{array}{c} \epsilon_{11} \\ \epsilon_{22} \\ \gamma_{12} \end{array} \right\} = \mathbf{D}\epsilon \tag{2.14}$$

where for plane strain ($\epsilon_{33} = \gamma_{13} = \epsilon_{23} = 0$):

$$d_{11} = d_{22} = \frac{E(1-\nu)}{(1+\nu)(1-2\nu)}$$

$$d_{12} = d_{21} = \frac{E\nu}{(1+\nu)(1-2\nu)} \tag{2.15}$$

$$d_{33} = \frac{E}{2(1+\nu)} = \mu$$

By changing d_{ij} is possible to consider plane stress or orthotropy [50].

Consider a two-dimensional domain Ω with boundary $\Gamma = \partial\Omega$ and thickness t. The Principle of Virtual Work for 2D elasticity problems can be written in matrix form as:

$$\int_\Omega \delta\epsilon^T \sigma t \, d\Omega = \int_\Omega \delta\mathbf{u}^T \mathbf{b}t \, d\Omega + \int_\Gamma \delta\mathbf{u}^T \mathbf{t}t \, d\Gamma + \sum_{i=1}^{N_{pl}} \delta\mathbf{u}_i^T \mathbf{p}_i \tag{2.16}$$

where $t = 1$ for plain strain, and t is the real thickness for plain stress. The virtual field is indicated as usual with the prefix δ, $\mathbf{b}$ is the vector of body loads, $\mathbf{t}$ is the vector of boundary loads, and $\mathbf{p}_i$ is the i-th point load. Once discretized into elements, by using the same interpolation for virtual and real displacements it leads to the classical local equilibrium equation for a given element $\Omega^{(e)}$:

$$\mathbf{K}^{(e)}\mathbf{u}^{(e)} - \mathbf{f}^{(e)} = \mathbf{q}^{(e)} \tag{2.17}$$

where the element-wise stiffness matrix $\mathbf{K}^{(e)}$ is:

$$\mathbf{K}^{(e)} = \int_{\Omega^{(e)}} \left(\mathbf{B}^{(e)}\right)^T \mathbf{D}^{(e)}\mathbf{B}^{(e)}t \, d\Omega \tag{2.18}$$

the element-wise load vector $\mathbf{f}^{(e)}$ consist of equivalent nodal forces due to body loads $\mathbf{f}_b^{(e)}$ and boundary loads $\mathbf{f}_t^{(e)}$:

$$\mathbf{f}^{(e)} = \mathbf{f}_b^{(e)} + \mathbf{f}_t^{(e)} \tag{2.19}$$

and $\mathbf{q}^{(e)}$ is the element-wise vector of equilibrating nodal forces. A body load $\mathbf{b}$ with the same interpolation as the displacement field lead to the following equivalent nodal forces:

$$\mathbf{f}_b^{(e)} = \int_{\Omega^{(e)}} \left(\mathbf{N}^{(e)}\right)^T \mathbf{b}t \, d\Omega = \left[\int_{\Omega^{(e)}} \left(\mathbf{N}^{(e)}\right)^T \mathbf{N}^{(e)}t \, d\Omega\right]\mathbf{b}^{(e)} = \mathbf{Q}_b^{(e)}\mathbf{b}^{(e)} \tag{2.20}$$

16

When a boundary load $\mathbf{t}$ is applied along $\Gamma^{(\text{be})}$, the produced equivalent nodal forces are obtained from:

$$\mathbf{f}_{\text{t}}^{(\text{e})} = \int_{\Gamma^{(\text{be})}} \left(\mathbf{N}^{(\text{e})} \right)^T \mathbf{t} t \, \text{d}\Gamma = \left[\int_{\Gamma^{(\text{be})}} \left(\mathbf{N}^{(\text{e})} \right)^T \mathbf{N}^{(\text{be})} t \, \text{d}\Gamma \right] \mathbf{t}^{(\text{be})} = \mathbf{Q}_{\mathbf{t}}^{(\text{be})} \mathbf{t}^{(\text{be})} \tag{2.21}$$

where $\mathbf{t}$ is interpolated using a boundary element with N_{n}^{be} nodes:

$$\mathbf{t} = \left[\begin{array}{ccccc} N^{(\text{be})(1)}\mathbf{I} & \cdots & N^{(\text{be})(i)}\mathbf{I} & \cdots & N^{(\text{be})(N_{\text{n}}^{\text{be}})}\mathbf{I} \end{array} \right] \left\{ \begin{array}{c} \mathbf{t}^{(1)} \\ \cdots \\ \mathbf{t}^{(i)} \\ \cdots \\ \mathbf{t}^{(N_{\text{n}}^{\text{be}})} \end{array} \right\} = \mathbf{N}^{(\text{be})}\mathbf{t}^{(\text{be})} \tag{2.22}$$

and $N^{(\text{be})(i)} = N^{(\text{be})(i)}(\eta)$, being η the local curvilinear coordinate of the load element. The load element is connected to the element by defining the coordinate $\xi^{(j)}$ of the j-th node of the load element, thus:

$$\xi_i = \sum_{j=1}^{j=N_{\text{n}}^{\text{be}}} N^{(\text{be})(j)} \xi_i^{(j)} \tag{2.23}$$

and:

$$\frac{\text{d}\xi_i}{\text{d}\eta} = \sum_{j=1}^{j=N_{\text{n}}^{\text{be}}} \frac{\text{d}N^{(\text{be})(j)}}{\text{d}\eta} \xi_i^{(j)} = J_i^\eta \tag{2.24}$$

$$\frac{\text{d}x_i}{\text{d}\eta} = \frac{\partial x_i}{\partial \xi_j} \frac{\text{d}\xi_j}{\text{d}\eta} = J_{ji} J_j^\eta = J_i^{(\text{be})} \tag{2.25}$$

$$\text{d}\Gamma = \sqrt{J_j^{(\text{be})} J_j^{(\text{be})}} \, \text{d}\eta = \left| \mathbf{J}^{(\text{be})} \right| \, \text{d}\eta \tag{2.26}$$

The global equilibrium equation is obtained by establishing that the sum of all equilibrating nodal forces balances the point loads:

$$\mathbf{K}\mathbf{u} = \mathbf{f} \tag{2.27}$$

where $\mathbf{f}$ includes body, boundary and point loads.

For time harmonic analysis, displacements, stresses, loads, etc. can be expressed as $v(\mathbf{x},t) = v(\mathbf{x},\omega)\,\text{e}^{i\omega t}$. All the equations written above hold, although now the variables are complex amplitudes $v(\mathbf{x},\omega)$ which depend on the real circular frequency ω. Inertial forces due to the movement of the continuous distribution of mass can be included as a body load $\mathbf{b} = -\rho\ddot{\mathbf{u}}$:

$$\mathbf{f}_{\text{m}}^{(\text{e})} = -\int_{\Omega^{(\text{e})}} \left(\mathbf{N}^{(\text{e})} \right)^T \rho \ddot{\mathbf{u}} t \, \text{d}\Omega = \omega^2 \rho \mathbf{Q}_{\mathbf{b}}^{(\text{e})} \mathbf{u}^{(\text{e})} \text{e}^{i\omega t} = \omega^2 \mathbf{M}^{(\text{e})} \mathbf{u}^{(\text{e})} \text{e}^{i\omega t} \tag{2.28}$$

where $\mathbf{M}^{(\text{e})}$ is the mass matrix. Taking into account that the exponential terms cancel out, the local equilibrium equation for time harmonic analysis can be written as:

$$\left(\mathbf{K}^{(\text{e})} - \omega^2 \mathbf{M}^{(\text{e})} \right) \mathbf{u}^{(\text{e})} - \mathbf{f}^{(\text{e})} = \mathbf{q}^{(\text{e})} \quad \Rightarrow \quad \tilde{\mathbf{K}}^{(\text{e})} \mathbf{u}^{(\text{e})} - \mathbf{f}^{(\text{e})} = \mathbf{q}^{(\text{e})} \tag{2.29}$$

which is completely analogous to Equation (2.17).

2.2.2 Element matrices differentiation

The basic semi-analytical approach consist in the numerical differentiation of the element matrices by using finite difference formulas. This simple black-box procedure is appropriate and leads to accurate results most of the times. It fails when dealing with structural finite elements in shape sensitivity analysis [49, 17], especially with Euler-Bernoulli/Kirchoff kinematics. There exist several ways to overcome this, but the procedures proposed by Olhoff et al. [49] are particularly general (solid and structural elements), accurate and robust.

Consider a shape design variable a which produces a design velocity field $\mathbf{v}$, the partial derivative of any field variable f with respect to a can be expressed as a function of $\mathbf{v}$ by using the chain rule of differentiation:

$$\frac{\partial f}{\partial a} = \frac{\partial f}{\partial x_j}\frac{\partial x_j}{\partial a} = \frac{\partial f}{\partial x_j}v_j \tag{2.30}$$

where the Einstein summation convention is implied. The finite difference formula can be applied to estimate $\partial/\partial a$ or $\partial/\partial x_j$:

$$\frac{\partial f}{\partial a} \simeq \mathrm{FD}\left[f, \Delta a\right] \tag{2.31}$$

$$\frac{\partial f}{\partial x_j} \simeq \mathrm{FD}\left[f, \Delta x_j\right] \Rightarrow \frac{\partial f}{\partial a} \simeq \frac{\partial f}{\partial x_j}v_j \tag{2.32}$$

where in the latter case Equation (2.30) is applied in order to build the required $\partial/\partial a$. Although both methods are equivalent, there are differences in terms of robustness and computational effort. The former is simpler and computationally cheaper, however is unreliable because choosing an appropriate Δa is not straightforward. The latter is computationally more expensive, but also more robust since a clear criteria based on the size of the element can be used to estimate an appropriate value of Δx_j. With this in mind, the partial derivative of the element-wise stiffness matrix $\mathbf{K}^{(e)}$ with respect to a can be written as:

$$\frac{\partial \mathbf{K}^{(e)}}{\partial a} = \frac{\partial \mathbf{K}^{(e)}}{\partial x_j^{(k)}}\frac{\partial x_j^{(k)}}{\partial a} = \frac{\partial \mathbf{K}^{(e)}}{\partial x_j^{(k)}}v_j^{(k)} \tag{2.33}$$

where $\mathbf{v}^{(k)}$ is the design velocity field at the k-th node, and the summation convention is implied for indices j and k. The same holds true for other element-wise matrices ($\mathbf{Q}_\mathbf{b}^{(e)}$, $\mathbf{Q}_\mathbf{t}^{(be)}$, $\mathbf{M}^{(e)}$, etc.).

Since the stiffness matrix is explicit for the linear triangle, see e.g. [50], its derivatives with respect to the nodal coordinates can be easily calculated analytically by any computer algebra system. These derivatives are rational polynomial functions of nodal coordinates, where both are 4-th degree polynomials. Therefore, even for such a simple element, the finite difference can provide only an approximation. The perturbation $\Delta x_j^{(k)}$ is chosen as $\Delta x_j^{(k)} = D \cdot \Delta h$, where D is the diameter of the bounding ball of the element and Δh is a dimensionless perturbation. Using the linear triangle, a convergence study has been performed for several finite difference formulas. Table 2.1 shows the RMS error between analytical and numerical estimation of $\partial \mathbf{K}^{(e)}/\partial x_k^{(j)}$ for an equilateral triangle with $E = 1$

and $\nu = 1/3$. The dimensionless perturbation Δh behaves with the expected convergence rate up to a point where round-off and truncation error start becoming relevant. Framed cells show the minimum error and indicate the best value of Δh for each finite difference formula. This criteria can be used not only for the stiffness matrix, but also for the load matrices.

$\Delta h = \Delta x_k^{(j)}/D$	Forward FD	Central FD	4P Central FD	6P Central FD
10^{-1}	$4 \cdot 10^{-1}$	$4 \cdot 10^{-2}$	$2 \cdot 10^{-3}$	$4 \cdot 10^{-4}$
10^{-2}	$4 \cdot 10^{-2}$	$4 \cdot 10^{-4}$	$2 \cdot 10^{-7}$	$3 \cdot 10^{-10}$
10^{-3}	$4 \cdot 10^{-3}$	$4 \cdot 10^{-6}$	$2 \cdot 10^{-11}$	$\boxed{5 \cdot 10^{-13}}$
10^{-4}	$4 \cdot 10^{-4}$	$4 \cdot 10^{-8}$	$\boxed{6 \cdot 10^{-12}}$	$6 \cdot 10^{-12}$
10^{-5}	$4 \cdot 10^{-5}$	$4 \cdot 10^{-10}$	$5 \cdot 10^{-11}$	$7 \cdot 10^{-11}$
10^{-6}	$4 \cdot 10^{-6}$	$\boxed{5 \cdot 10^{-11}}$	$7 \cdot 10^{-10}$	$7 \cdot 10^{-10}$
10^{-7}	$4 \cdot 10^{-7}$	$4 \cdot 10^{-10}$	$7 \cdot 10^{-9}$	$8 \cdot 10^{-9}$
10^{-8}	$\boxed{7 \cdot 10^{-8}}$	$4 \cdot 10^{-9}$	$7 \cdot 10^{-8}$	$7 \cdot 10^{-8}$
10^{-9}	$5 \cdot 10^{-7}$	$2 \cdot 10^{-8}$	$4 \cdot 10^{-7}$	$6 \cdot 10^{-7}$

Table 2.1: $\partial \mathbf{K}^{(e)}/\partial x_k^{(j)}$ RMS error using several FD formulas (linear equilateral triangle)

Other linear triangles with aspect ratios up to $1/5$ have been studied, and their behaviour with respect to Δh is a little bit worse. Despite high-order finite difference formulas can lead to almost exact results, it is achieved at the expense of evaluating the matrix many times. Note that the computational effort is proportional to the the total number of matrix evaluations, which is equal to the product of the number of nodes, the number of dimensions, and the number of points of the finite difference formula.

Analytical differentiation

The explained basic finite difference approach is simple, easy to implement and applicable to all kind of elements and design variables. However, its lack of accuracy when applied to structural elements in shape sensitivity analysis and its high computational cost have motivated researchers to find for better solutions. Olhoff et al. developed a semi-analytical but exact procedure using inexpensive forward finite differences, being [49] probably their most complete paper. In general, the strategy consists in performing the analytical differentiation over the integrand and then decomposing it in order to find polynomial terms that can be numerically differentiated exactly. In the case of solid isoparametric elements, this procedure can be easily used to obtain an analytical solution (except for the numerical integration). Next, this analytical solution is going to be described for 2D elements, although the extension to 3D elements is straightforward.

For the stiffness matrix, the starting point is the derivative of Equation (2.18) once the integration domain is transformed into the local space through the determinant of the Jacobian matrix $|\mathbf{J}|$. Then, taking into account that $\mathbf{D}^{(e)}$ is symmetric, the derivative can

be written as:

$$\frac{\partial \mathbf{K}^{(e)}}{\partial x_j^{(k)}} = \frac{1}{2} \left\{ \left[\int_{\Omega^{(e)}} \left(\mathbf{B}^{(e)}\right)^T \mathbf{D}^{(e)} \hat{\mathbf{B}}^{(e)} t \, |\mathbf{J}| \, \mathrm{d}\xi_1 \mathrm{d}\xi_2 \right] + \left[\int_{\Omega^{(e)}} \left(\mathbf{B}^{(e)}\right)^T \mathbf{D}^{(e)} \hat{\mathbf{B}}^{(e)} t \, |\mathbf{J}| \, \mathrm{d}\xi_1 \mathrm{d}\xi_2 \right]^T \right\}$$

(2.34)

where:

$$\hat{\mathbf{B}}^{(e)} = 2\frac{\partial \mathbf{B}^{(e)}}{\partial x_j^{(k)}} + \frac{1}{|\mathbf{J}|} \frac{\partial |\mathbf{J}|}{\partial x_j^{(k)}} \mathbf{B}^{(e)}$$

(2.35)

The difference between Equation (2.34) and Equation (2.18) is only $\hat{\mathbf{B}}^{(e)}$, which even contains several already calculated terms. Thus, relatively small additional effort is needed with respect to the calculation of the stiffness matrix, only the calculation of $\partial \mathbf{B}^{(e)}/\partial x_j^{(k)}$ and $\partial |\mathbf{J}|/\partial x_j^{(k)}$. By examining Equation (2.10), it is easy to write the derivative of $\mathbf{J}$ with respect to $x_j^{(k)}$ as:

$$\frac{\partial \mathbf{J}}{\partial x_j^{(k)}} = \begin{bmatrix} \dfrac{\partial J_{11}}{\partial x_j^{(k)}} & \dfrac{\partial J_{12}}{\partial x_j^{(k)}} \\[2mm] \dfrac{\partial J_{21}}{\partial x_j^{(k)}} & \dfrac{\partial J_{22}}{\partial x_j^{(k)}} \end{bmatrix} = \begin{bmatrix} \dfrac{\partial N^{(k)}}{\partial \xi_1}\delta_{j1} & \dfrac{\partial N^{(k)}}{\partial \xi_1}\delta_{j2} \\[2mm] \dfrac{\partial N^{(k)}}{\partial \xi_2}\delta_{j1} & \dfrac{\partial N^{(k)}}{\partial \xi_2}\delta_{j2} \end{bmatrix} \Rightarrow \frac{\partial J_{mn}}{\partial x_j^{(k)}} = \frac{\partial N^{(k)}}{\partial \xi_m}\delta_{jn}$$

(2.36)

By applying the chain rule, the derivative of the determinant can be written as:

$$\frac{\partial |\mathbf{J}|}{\partial x_j^{(k)}} = \frac{\partial |\mathbf{J}|}{\partial J_{mn}} \frac{\partial J_{mn}}{\partial x_j^{(k)}}$$

(2.37)

where the Einstein summation convention is implied for both indices. From the definition of the determinant in terms of its cofactors, it is clear that its derivative with respect to each element of the matrix is:

$$\frac{\partial |\mathbf{J}|}{\partial J_{mn}} = \text{cofactor}\,(J_{mn}), \quad \text{cofactor}\,(J_{mn}) = (-1)^{m+n}\text{minor}\,(\mathbf{J}, m, n)$$

(2.38)

where the minor is the determinant of the submatrix obtained when removing the m-th row and the n-th column of the matrix $\mathbf{J}$. The inverse of a matrix can be expressed as a function of its adjugate and its determinant:

$$\mathbf{G} = \mathbf{J}^{-1} = \frac{1}{|\mathbf{J}|}\text{adjugate}\,(\mathbf{J}) = \frac{1}{|\mathbf{J}|}\left[\text{cofactor}\,(J_{mn})\right]^T = \frac{1}{|\mathbf{J}|}\left[\text{cofactor}\,(J_{nm})\right]$$

(2.39)

$$G_{mn} = \frac{1}{|\mathbf{J}|}\text{cofactor}\,(J_{nm}) \Rightarrow \frac{\partial |\mathbf{J}|}{\partial J_{mn}} = |\mathbf{J}|\,G_{nm}$$

(2.40)

Therefore, Equation (2.37) can now be written as:

$$\frac{\partial |\mathbf{J}|}{\partial x_j^{(k)}} = \frac{\partial |\mathbf{J}|}{\partial J_{mn}} \frac{\partial N^{(k)}}{\partial \xi_m}\delta_{jn} = \frac{\partial |\mathbf{J}|}{\partial J_{mj}} \frac{\partial N^{(k)}}{\partial \xi_m} = |\mathbf{J}|\,G_{jm}\frac{\partial N^{(k)}}{\partial \xi_m} = |\mathbf{J}|\,\frac{\partial N^{(k)}}{\partial x_j}$$

(2.41)

20

which is composed by terms already calculated. The derivative of $\mathbf{B}^{(e)}$ with respect to $x_j^{(k)}$ can be written as:

$$\frac{\partial \mathbf{B}^{(e)}}{\partial x_j^{(k)}} = \left[\begin{array}{ccccc} \dfrac{\partial \mathbf{B}^{(1)}}{\partial x_j^{(k)}} & \cdots & \dfrac{\partial \mathbf{B}^{(i)}}{\partial x_j^{(k)}} & \cdots & \dfrac{\partial \mathbf{B}^{(N_n)}}{\partial x_j^{(k)}} \end{array} \right] \tag{2.42}$$

where with the help of Equation (2.13):

$$\frac{\partial \mathbf{B}^{(i)}}{\partial x_j^{(k)}} = \frac{\partial}{\partial x_j^{(k)}} \begin{bmatrix} \dfrac{\partial N^{(i)}}{\partial x_1} & 0 \\[2ex] 0 & \dfrac{\partial N^{(i)}}{\partial x_2} \\[2ex] \dfrac{\partial N^{(i)}}{\partial x_2} & \dfrac{\partial N^{(i)}}{\partial x_1} \end{bmatrix} \tag{2.43}$$

$$\frac{\partial}{\partial x_j^{(k)}} \left(\frac{\partial N^{(i)}}{\partial x_m} \right) = \frac{\partial G_{mn}}{\partial x_j^{(k)}} \frac{\partial N^{(i)}}{\partial \xi_n} \tag{2.44}$$

The derivative of G_{mn} with respect to $x_j^{(k)}$ is difficult to compute directly. Instead, from the identity $\mathbf{J}\mathbf{J}^{-1} = \mathbf{J}\mathbf{G} = \mathbf{I}$, it can be written as:

$$\frac{\partial \mathbf{J}}{\partial x_j^{(k)}} \mathbf{G} + \mathbf{J} \frac{\partial \mathbf{G}}{\partial x_j^{(k)}} = \mathbf{0} \Rightarrow \frac{\partial \mathbf{G}}{\partial x_j^{(k)}} = -\mathbf{G} \frac{\partial \mathbf{J}}{\partial x_j^{(k)}} \mathbf{G} \Rightarrow \frac{\partial G_{mn}}{\partial x_j^{(k)}} = -G_{mr} \frac{\partial J_{rs}}{\partial x_j^{(k)}} G_{sn} \tag{2.45}$$

where substituting Equation (2.36) and considering Equation (2.13):

$$\frac{\partial G_{mn}}{\partial x_j^{(k)}} = -G_{mr} \frac{\partial N^{(k)}}{\partial \xi_r} \delta_{js} G_{sn} = -G_{mr} \frac{\partial N^{(k)}}{\partial \xi_r} G_{jn} = -\frac{\partial N^{(k)}}{\partial x_m} G_{jn} \tag{2.46}$$

Substituting this last result into Equation (2.44) and considering again Equation (2.13):

$$\frac{\partial}{\partial x_j^{(k)}} \left(\frac{\partial N^{(i)}}{\partial x_m} \right) = -\frac{\partial N^{(k)}}{\partial x_m} G_{jn} \frac{\partial N^{(i)}}{\partial \xi_n} = -\frac{\partial N^{(k)}}{\partial x_m} \frac{\partial N^{(i)}}{\partial x_j} \tag{2.47}$$

which is a simple product of terms already calculated. The substitution of this result into Equation (2.43) allows building the matrix $\partial \mathbf{B}^{(e)} / \partial x_j^{(k)}$ defined by Equation (2.42).

For the body load matrix (and mass matrix), one has to consider the derivative of $\mathbf{Q}_b^{(e)}$ (Equation (2.20)) once the integration domain is transformed into the local space:

$$\frac{\partial \mathbf{Q}_b^{(e)}}{\partial x_j^{(k)}} = \int_{\Omega^{(e)}} \left(\mathbf{N}^{(e)} \right)^T \mathbf{N}^{(e)} t \frac{\partial |\mathbf{J}|}{\partial x_j^{(k)}} \, d\xi_1 d\xi_2 = \int_{\Omega^{(e)}} \left(\mathbf{N}^{(e)} \right)^T \mathbf{N}^{(e)} t \frac{\partial N^{(k)}}{\partial x_j} |\mathbf{J}| \, d\xi_1 d\xi_2 \tag{2.48}$$

where Equation (2.41) has been used. For the boundary load matrix, the same procedure is followed, the derivative of $\mathbf{Q}_t^{(be)}$ (Equation (2.21)) can be written as:

$$\frac{\partial \mathbf{Q}_t^{(be)}}{\partial x_j^{(k)}} = \int_{\Gamma^{(be)}} \left(\mathbf{N}^{(e)} \right)^T \mathbf{N}^{(be)} t \frac{\partial |\mathbf{J}^{(be)}|}{\partial x_j^{(k)}} \, d\eta \tag{2.49}$$

where $\partial\left|\mathbf{J}^{(\text{be})}\right|/\partial x_j^{(k)}$ can be calculated considering equations (2.25), (2.26) and (2.36):

$$\frac{\partial\left|\mathbf{J}^{(\text{be})}\right|}{\partial x_j^{(k)}} = \frac{J_j^{(\text{be})}}{\left|\mathbf{J}^{(\text{be})}\right|}\frac{\partial N^{(k)}}{\partial \xi_m}J_m^\eta \tag{2.50}$$

These analytical solutions has been checked against the basic semi-analytical approach with finite differences, except for the linear triangle which has a explicit analytical solution. When comparing the solution by finite differences against these analytical solutions, the same rates of convergence and optimum values of Δh as those shown in Table 2.1 are observed as expected. As an example, Table 2.2 shows RMS errors for the calculation of the stiffness matrix derivative of a quadratic triangular element (equilateral, $E = 1$, $v = 1/3$).

$\Delta h = \Delta x_k^{(j)}/D$	**Forward FD**	**Central FD**	**4P Central FD**	**6P Central FD**
10^{-1}	$3 \cdot 10^{-1}$	$7 \cdot 10^{-2}$	$9 \cdot 10^{-2}$	$4 \cdot 10^{-1}$
10^{-2}	$2 \cdot 10^{-2}$	$7 \cdot 10^{-4}$	$3 \cdot 10^{-6}$	$4 \cdot 10^{-8}$
10^{-3}	$2 \cdot 10^{-3}$	$7 \cdot 10^{-6}$	$3 \cdot 10^{-10}$	$\boxed{1 \cdot 10^{-13}}$
10^{-4}	$2 \cdot 10^{-4}$	$7 \cdot 10^{-8}$	$\boxed{8 \cdot 10^{-13}}$	$9 \cdot 10^{-13}$
10^{-5}	$2 \cdot 10^{-5}$	$7 \cdot 10^{-10}$	$9 \cdot 10^{-12}$	$9 \cdot 10^{-12}$
10^{-6}	$2 \cdot 10^{-6}$	$\boxed{6 \cdot 10^{-11}}$	$8 \cdot 10^{-11}$	$9 \cdot 10^{-11}$
10^{-7}	$2 \cdot 10^{-7}$	$6 \cdot 10^{-10}$	$9 \cdot 10^{-10}$	$9 \cdot 10^{-10}$
10^{-8}	$\boxed{3 \cdot 10^{-8}}$	$7 \cdot 10^{-9}$	$9 \cdot 10^{-9}$	$9 \cdot 10^{-9}$
10^{-9}	$1 \cdot 10^{-7}$	$6 \cdot 10^{-8}$	$8 \cdot 10^{-8}$	$9 \cdot 10^{-8}$

Table 2.2: $\partial\mathbf{K}^{(\text{e})}/\partial x_k^{(j)}$ RMS error using several FD formulas (quadratic equil. triangle)

In summary, two approaches have been shown with their own advantages and disadvantages. The classical semi-analytical approach using finite differences is easy to implement and accurate for any element, except for Euler-Bernoulli/Kirchoff structural elements. However, it is computationally expensive, and an appropriate selection of the perturbation is needed, which depends on the finite difference formula and the required accuracy. The analytical approach gives exact results with minimum computational cost at the expense of the effort required to obtain and implement the formulation. At least for solid isoparametric elements, the resulting formulation is simple and its implementation is straightforward.

2.3 Validation example

Analytical solution

Consider an elastic two-dimensional rectangular domain Ω with the geometry and boundary conditions that Figure 2.1 shows. The domain Ω has a density ρ, shear modulus μ and Poisson's ratio v. Despite being a two-dimensional domain, boundary conditions lead to a
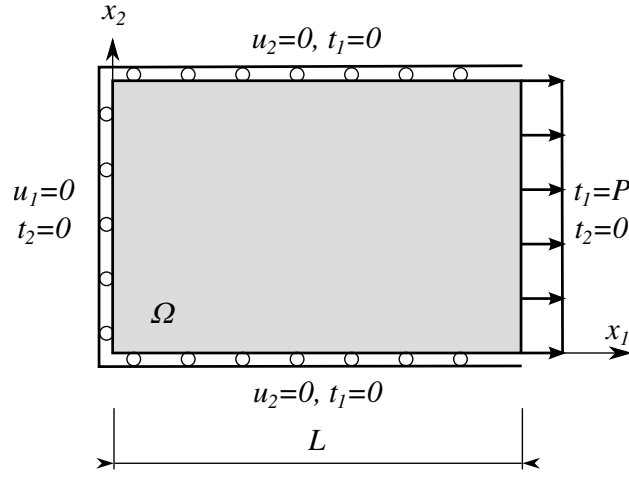
Design velocity field: $v_1(x) = x/L$, $v_2(x) = 0$

Figure 2.1: Problem layout

one-dimensional behaviour. The solution of the time harmonic elastodynamic governing equations consists of two waves travelling in opposite directions along x_1:

$$u_1(x_1) = A e^{-ikx_1} + B e^{ikx_1} \tag{2.51}$$

where A and B are the amplitudes of the waves, $k = \omega/c_P$ is the wavenumber, ω is the circular frequency, and $c_P = \sqrt{(\lambda + 2\mu)/\rho}$ is the P-wave propagation speed. Once boundary conditions are considered, the displacement u_1 and stress σ_{11} can be written as:

$$u_1(x_1) = \frac{P}{\rho c_P^2 \cos kL} \frac{\sin kx_1}{k} \tag{2.52}$$

$$\sigma_{11}(x_1) = \frac{P}{\cos kL} \cos kx_1 \tag{2.53}$$

If L is taken as the shape design variable with a design velocity field $\mathbf{v} = (x/L, 0)$, then the sensitivities are:

$$\delta u_1(x_1) = \frac{P}{\rho c_P^2} \left(\frac{\sin kL}{\cos^2 kL} \sin kx_1 + \frac{1}{\cos kL} \frac{x_1}{L} \cos kx_1 \right) \tag{2.54}$$

$$\delta \sigma_{11}(x_1) = Pk \left(\frac{\sin kL}{\cos^2 kL} \cos kx_1 - \frac{1}{\cos kL} \frac{x_1}{L} \sin kx_1 \right) \tag{2.55}$$

where $\delta = \mathrm{d}/\mathrm{d}L = \partial/\partial L + (\partial/\partial x_j)v_j$ is the simplified notation for the field variable sensitivity (or material derivative).

FEM solution

This problem is solved numerically by using the FEM-DDM where the derivatives are calculated with the analytical procedure explained in the previous section. The domain is considered to be a square with side length L, and is meshed using different element sizes ($L/4$, $L/10$), different topologies (structured, unstructured), different element shapes
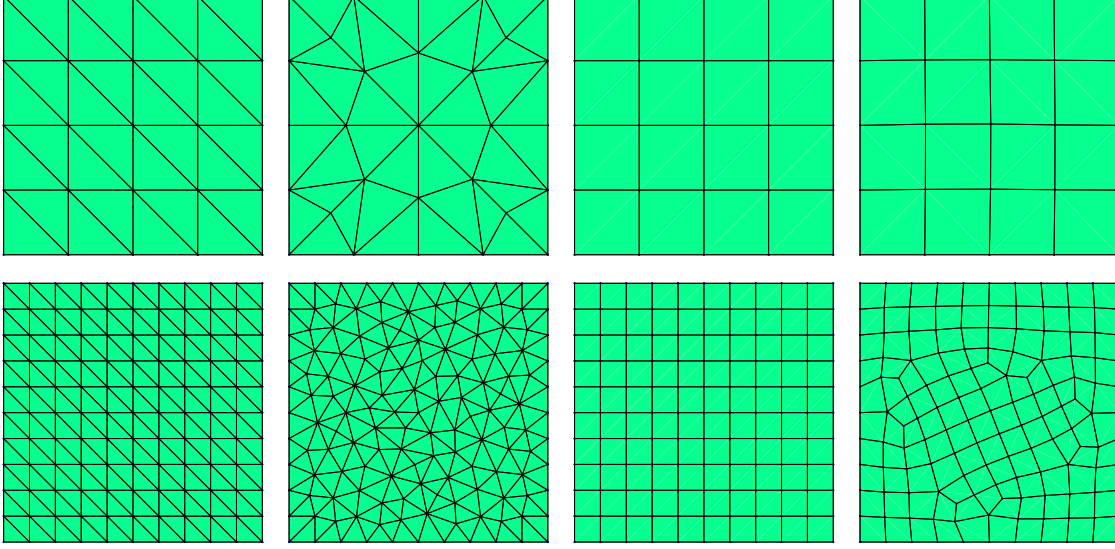
Figure 2.2: Meshes with $L/4$ and $L/10$ element sizes, structured/unstructured topology and triangular/quadrilateral elements.

(triangular, quadrilateral) and different element order (linear, quadratic), see Figure 2.2. By doing so, h and p convergence can be checked for triangular and quadrilateral meshes with structured or unstructured topologies. Poisson's ratio is assumed to be $\nu = 1/4$. Dimensionless frequency $a_0 = \omega L/c_P$ is used, which varies between 0 and 3 for linear elements, and between 0 and 6 for quadratic elements.

The design velocity field $\mathbf{v}$ is assigned to each physical node by defining a design mesh (auxiliary mesh) connected to the physical mesh by position, i.e. the so-called free-form deformation approach (see Section 1.4). The geometry and the design velocity field are interpolated similarly (isoparametric):

$$\mathbf{x} = \mathbf{N}^{(de)}\mathbf{x}^{(de)} \tag{2.56}$$

$$\mathbf{v} = \mathbf{N}^{(de)}\mathbf{v}^{(de)} \tag{2.57}$$

Given a physical node i with position $\mathbf{x}^{(i)}$ and design velocity $\mathbf{v}^{(i)}$, located within a design element, its design velocity field is calculated as:

$$\mathbf{x}^{(i)} = \mathbf{N}^{(de)}\left(\boldsymbol{\xi}^{(i)}\right)\mathbf{x}^{(de)} \tag{2.58}$$

$$\mathbf{v}^{(i)} = \mathbf{N}^{(de)}\left(\boldsymbol{\xi}^{(i)}\right)\mathbf{v}^{(de)} \tag{2.59}$$

where $\boldsymbol{\xi}^{(i)}$ is the local coordinate of the physical node i within the design element. The connectivity between all physical nodes and the design mesh and the calculation of $\mathbf{v}^{(i)}$ are done just one time as an initialization stage in the solver.

The complete design velocity field is defined by a design mesh containing only one 4-node quadrilateral element covering the domain Ω, and appropriate values of $\mathbf{v}$ are assigned to the four nodes in order to define $\mathbf{v} = \partial\mathbf{x}/\partial L = (x_1/L, 0)$, see Figure 2.3 (Left). In order to reduce computational cost, instead of using the complete domain deformation, only boundary nodes that produce a change in the shape can be used in the deformation field. The change of the shape of the domain remains exactly the same, however the
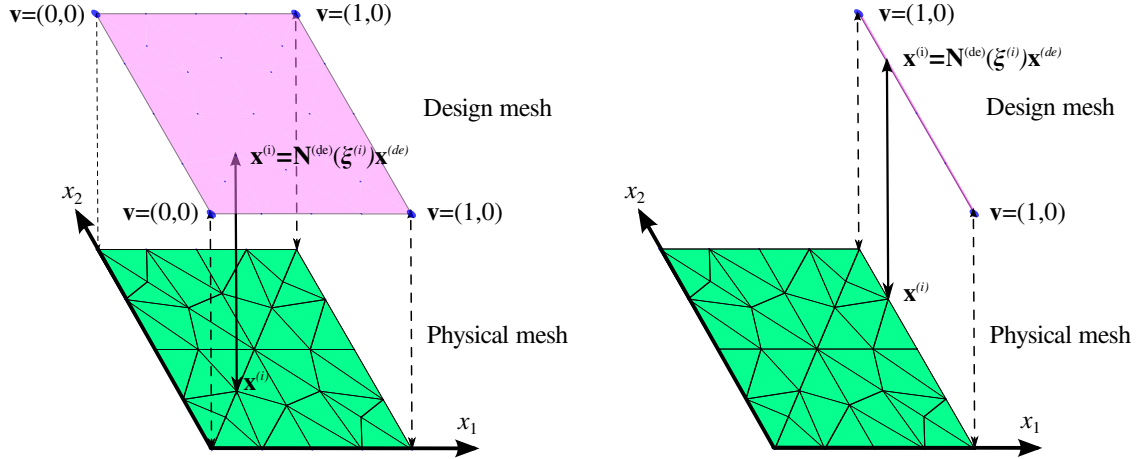
Figure 2.3: Physical mesh and design mesh. Left: complete design velocity field. Right: boundary layer technique.

design velocity field becomes less smooth as the design velocity is assumed null in other nodes. This approach is called boundary layer technique. In our example, this can be done by defining a design mesh with just one 2-node line element covering the right boundary ($x_1 = L$, $x_2 = [0, L]$), see Figure 2.3 (Right). Note that both design velocity fields lead to the same sensitivities only on the right boundary ($x_1 = L$), but not at other points.

Figures 2.4 to 2.7 show normalized displacements and displacement sensitivities, and their relative errors, at the point $\mathbf{x} = (L, L/2)$ for all the meshes using the complete design velocity field. Figure 2.8 shows the displacement sensitivity errors at $\mathbf{x} = (L, L/2)$ for all meshes using the boundary layer technique.

Given that the same mesh is used for the whole frequency range, the error increases with the frequency because the number of elements per wavelength decreases. As expected, the error levels are similar between displacements and displacement sensitivities for the same element size and order. This is not the case for unstructured meshes when using the boundary layer technique, although the error levels are acceptable. Some unacceptable error peaks start to appear in all cases when the number of elements per wavelength is less than 8-10 for linear elements, and less than 4-5 for quadratic elements. These peaks in the numerical solution can be mitigated by using a small damping in the system.

Convergence and robustness are clearly observed by comparing these graphs. Therefore, it can be said that the formulation and the implementation have been correctly developed.

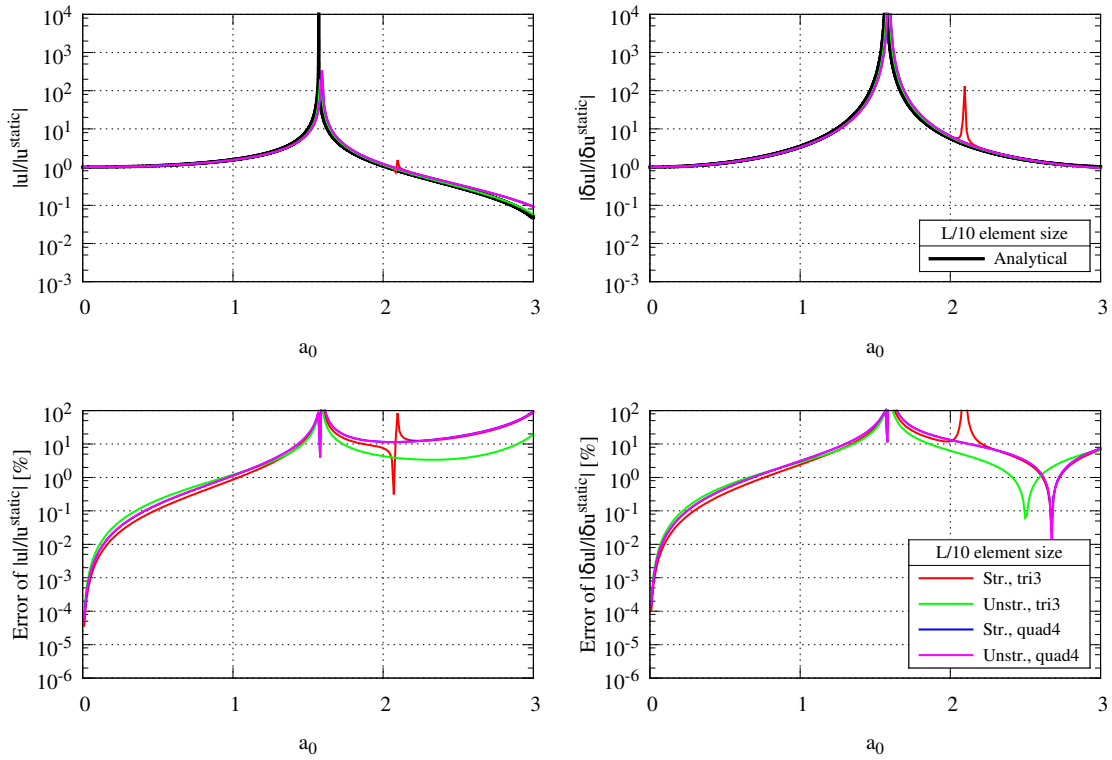Figure 2.4: Linear elements with $L/4$ size using complete design velocity field
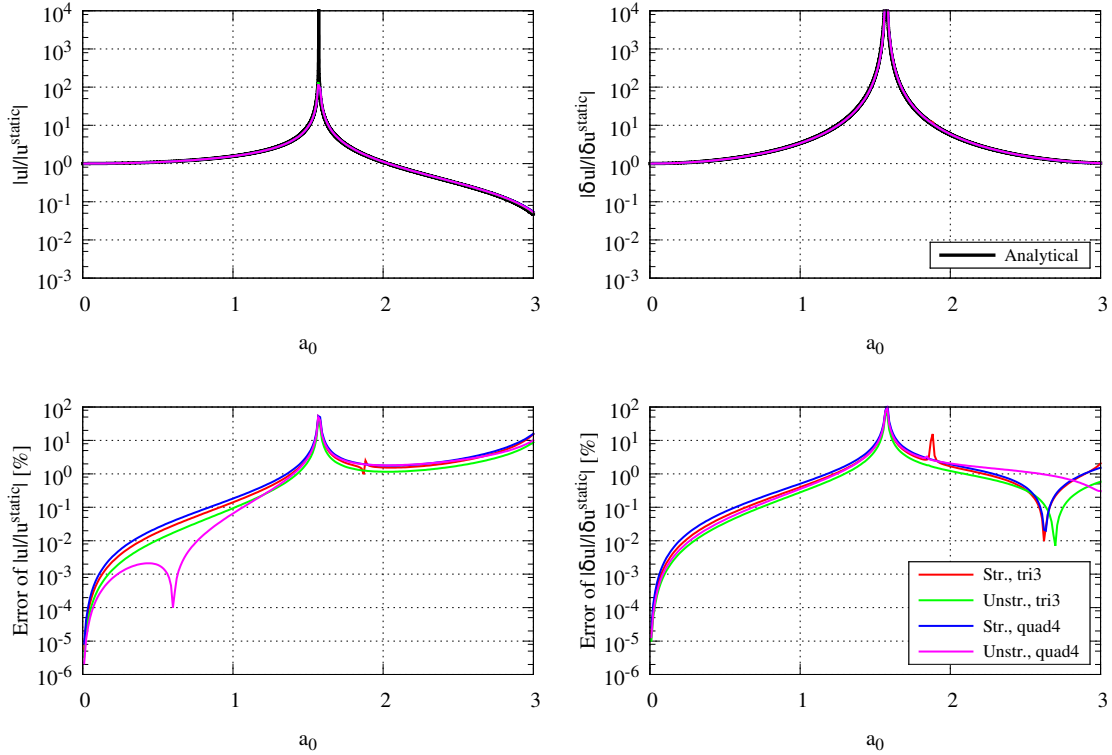

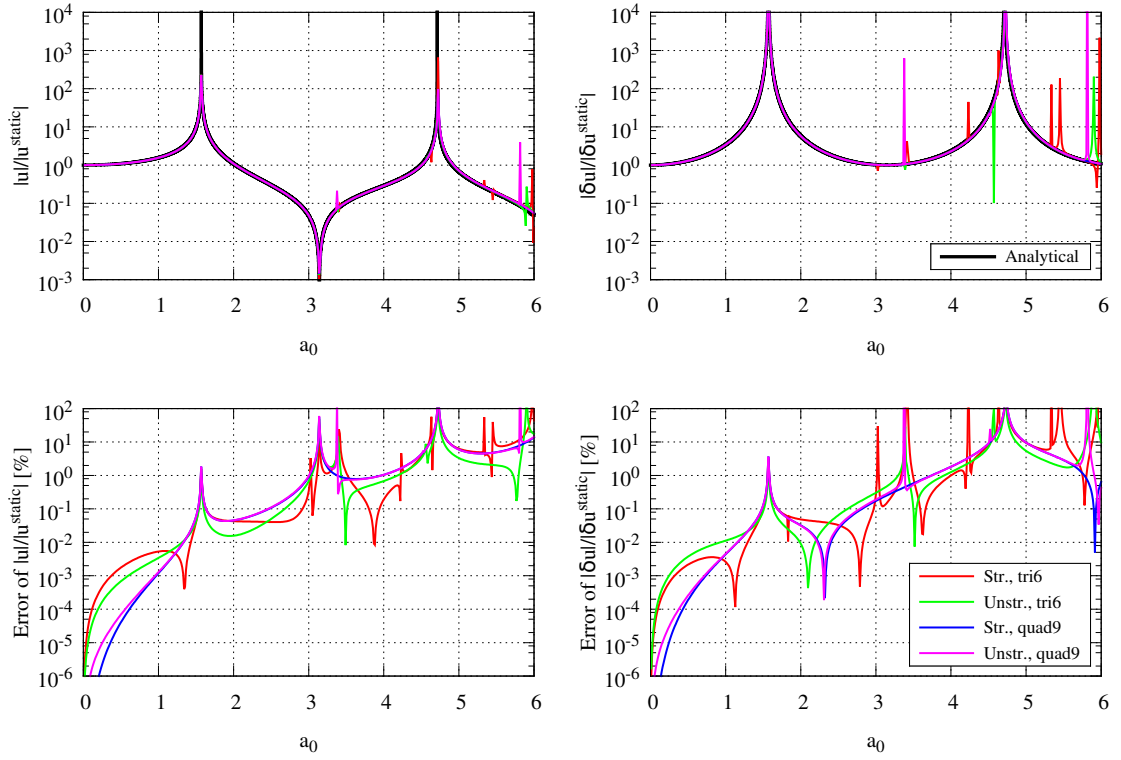Figure 2.5: Linear elements with $L/10$ size using complete design velocity field

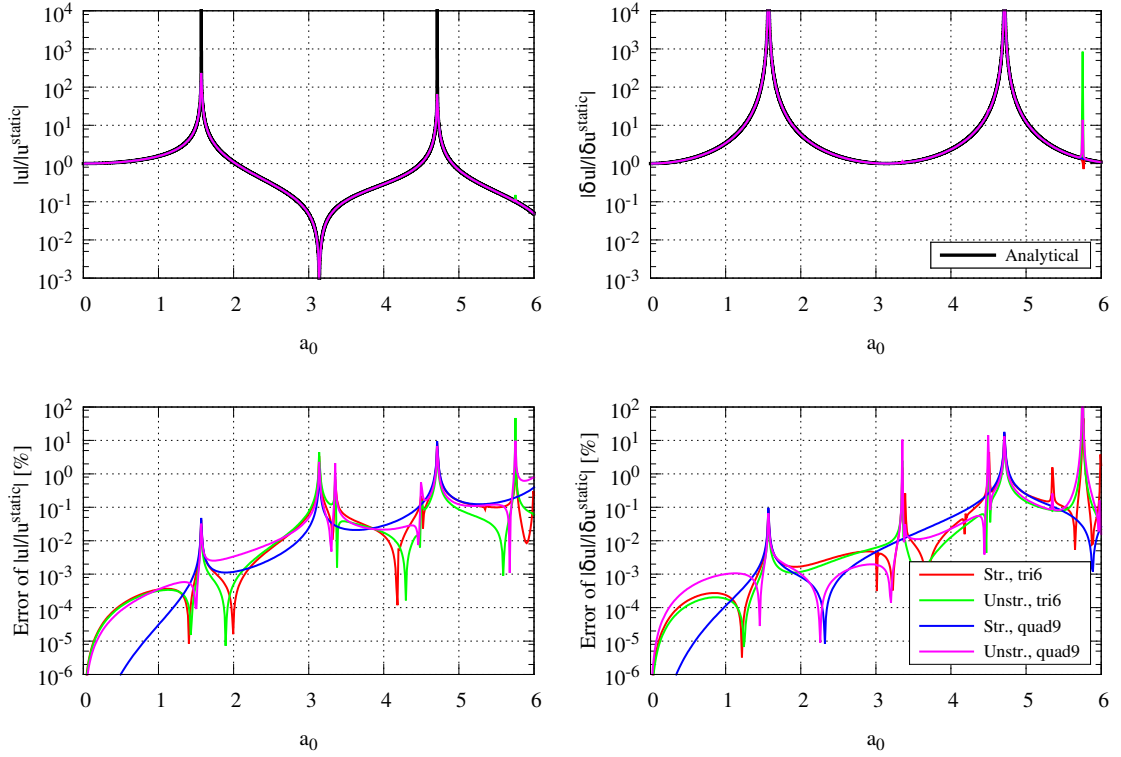Figure 2.6: Quadratic elements with $L/4$ size using complete design velocity field

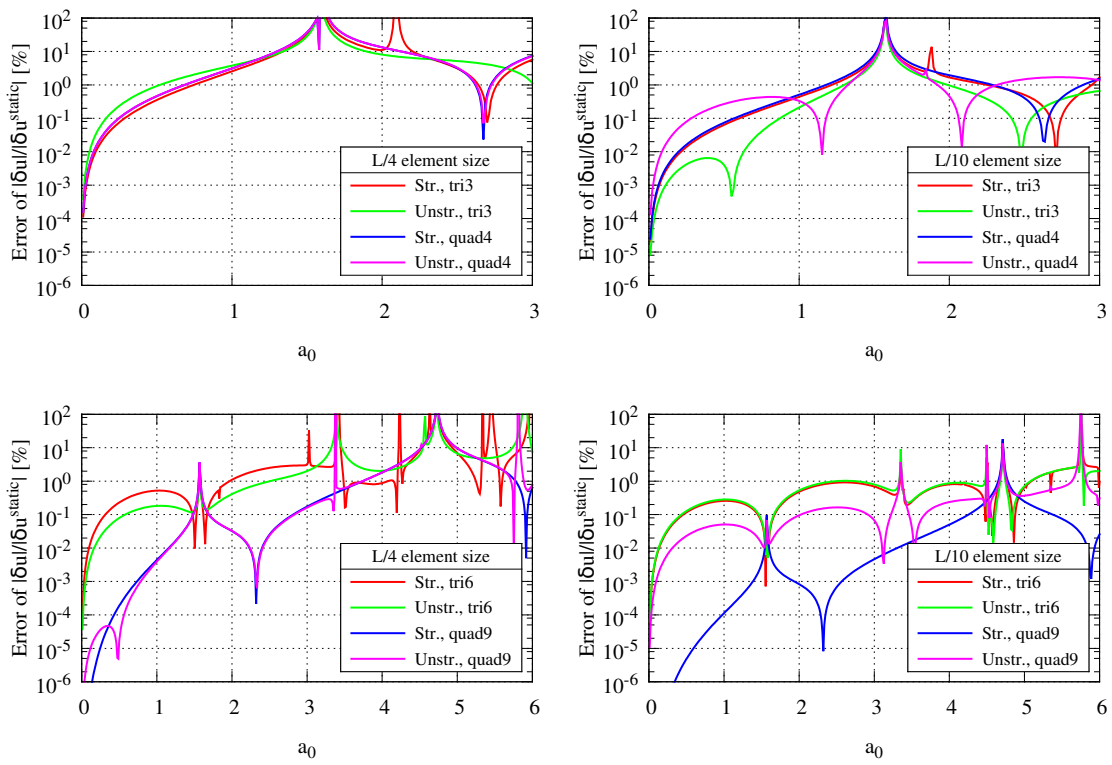Figure 2.7: Quadratic elements with $L/10$ size using the complete design velocity field

Figure 2.8: Sensitivity errors when using the boundary layer technique

28

Chapter 3

Shape sensitivities using the Boundary Element Method

3.1   Introduction

As seen in the previous chapter, sensitivity analysis can be done more or less straightfor-
wardly with the Finite Element Method (FEM) by differentiation of the discretized equa-
tions, and then calculating the derivatives in an approximate manner by finite differences
(semi-analytical approach) or exactly by analytical differentiation where possible. As it
is well known, the FEM is not naturally adapted to the analysis of unbounded regions. In
this case, the Boundary Element Method (BEM) is a more appropriate numerical method.
Furthermore, the BEM only requires the discretization of the boundary of the domain,
i.e. the shape of the body, thus it perfectly fits with shape sensitivity analysis and opti-
mization. On the other hand, the BEM is considerably more involved mathematically and
numerically than the FEM.

   Although less common than the FEM, the application of the BEM to sensitivity anal-
ysis is an active research field that started in the early 1980s. Barone et al. [11] applied
a special form of the BEM to the optimal arrangement of holes in a two-dimensional do-
main. Meric used the BEM with the Adjoint Variable Method (AVM) in order to study
heat transfer and mechanical behaviour of solids [44, 45, 46]. Mota Soares et al. [55]
applied the BEM to optimal shape design for minimum compliance. Kane et al. [38]
used implicit differentiation of the discretized equations for plane elasticity. Barone et al.
[12, 13] used the material derivative over the Boundary Integral Equations (BIE), includ-
ing the Hypersingular (stress) BIE (HBIE), for three-dimensional elasticity. Aithal and
Saigal [3, 4] applied the AVM and the material derivative to obtain the shape sensitivities
for thermal and elasticity problems.

   Besides being useful by itself or for shape optimization, shape sensitivity analysis us-
ing the BEM fits particularly well with inverse problems. Mellings and Aliabadi [42, 43]
used the BEM and the Dual BEM for identification of cavities and cracks on potential
and elastic problems. Also, Nishimura and Kobayashi [47] developed a BEM formula-
tion for identification of cracks with complex shapes. Bonnet [18, 19, 22, 23] covered
almost all aspects of shape sensitivity analysis using the BEM and a rigurous mathemati-
cal treatment. In particular, Bonnet [20] proved that material differentiation formulas for
regular integrals still hold true for strongly singular and hypersingular integrals, which

demonstrated that material differentiation can be applied to non-regularized as well as regularized BIEs. Gallego, Rus and Suarez [33, 32, 51, 52, 53] used the BEM for cavities and crack identification on potential and elastic problems using a free-form approach for the flaw parametrization, and a sensitivity BIE derived from the Taylor's expansion of the shape perturbation. In the present work, the latter approach is used to obtain the sensitivity or variation BIE (δBIE) which is the fundamental ingredient to build the BEM for sensitivity analysis. It is esentially similar to applying the material differentiation formulas to the BIE.

The chapter is organized as follows. In Section 3.2, several geometrical aspects, the discretization scheme and the notation that will be needed in the rest of the chapter are described. From Section 3.3 to 3.6, the Singular BIEs for sensitivity analysis are developed for Laplace, Helmholtz, elastostatics and elastodynamics problems, respectively. Last, Section 3.7 shows the validation of the presented formulation and its implementation.

3.2 Generalities

The superscript i over a symbol $\square$ representing a position vector, unit normal, field variable, etc., i.e. $\square^i$, is used to indicate if the object is associated with the collocation point, rather than with the observation point. It is not an index, thus no summation is implied for it.

Let Ω be a region in $\mathbb{R}^2$ with boundary $\Gamma = \partial\Omega$ whose orientation is defined by the outward unit normal vector $\mathbf{n} = (n_1, n_2)$. Following the usual convention, the orientation of Γ can be equally defined by the unit tangent vector $\mathbf{t} = (t_1, t_2) = (-n_2, n_1)$. Consider a boundary element $\Phi \subset \Gamma$ with N_n^Φ nodes, then any point $\mathbf{x}$ of the boundary element is described by:

$$x_j = \phi_p x_{jp}^\Phi \tag{3.1}$$

where $j = 1, 2$ is the coordinate index, $p = 1, \ldots, N_n^\Phi$ is the node index of the boundary element, x_{jp}^Φ is the j-th component of the position vector of the p-th node, $\phi_p = \phi_p(\xi)$ is the shape function of the p-th node, and ξ is the local curvilinear coordinate. The transformation between the local curvilinear coordinate and the global cartesian coordinates is governed by the Jacobian vector $\mathbf{J}$:

$$J_j = \frac{\partial x_j}{\partial \xi} = \frac{\mathrm{d}\phi_p}{\mathrm{d}\xi} x_{jp}^\Phi \tag{3.2}$$

$$\mathrm{d}\Gamma = \sqrt{J_j J_j}\, \mathrm{d}\xi = |\mathbf{J}|\, \mathrm{d}\xi \tag{3.3}$$

where summation convention is implied for j. Thus, the unit tangent can be calculated as $\mathbf{t} = \mathbf{J}/|\mathbf{J}|$ and the unit normal $\mathbf{n} = (t_2, -t_1)$.

For first-order shape sensitivity analysis, the region $\Omega = \Omega(a^0)$ is perturbed with respect to a given design velocity field $\mathbf{v} = \mathbf{v}(\mathbf{x}, a^0)$ that is produced by a design variable a when $a = a^0$, see Figure 3.1. The following linear mapping builds the perturbed domain $\tilde{\Omega}$ from the reference domain $\Omega = \Omega(a^0)$ for a small variation of a around a^0:

$$\tilde{\mathbf{x}} = \mathbf{x} + \mathbf{v}\left(a - a^0\right) \tag{3.4}$$
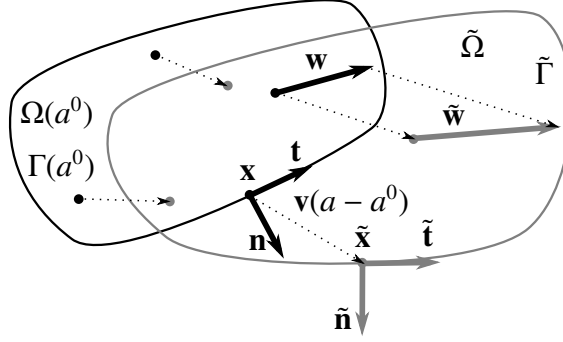
Figure 3.1: Taylor's expansion of the shape parametrization

The design velocity field acts basically as a displacement field, thus a constant design velocity field throughout the domain does not produce any shape variation. It can be easily seen that a material vector $\mathbf{w}$, i.e. a vector whose origin and orientation are sticked to a point, follows this linear mapping [21]:

$$\tilde{w}_i = w_i + v_{i,j} w_j \left(a - a^0 \right) \tag{3.5}$$

where the comma notation for derivatives with respect to x is implied. The following notation is going to be used for the vector sensitivity (or vector material derivative):

$$\delta w_i = v_{i,j} w_j \tag{3.6}$$

Thus, the linear mapping of the vector length is:

$$\tilde{w} = \tilde{w}_i \tilde{w}_i = w_i w_i + w_i v_{i,j} w_j \left(a - a^0 \right) = w + \delta w \left(a - a^0 \right) \tag{3.7}$$

where only linear terms are retained, and summation convention is implied for i and j. With this in mind, the linear mapping of an infinitesimal part of the boundary $d\Gamma$ is easily obtained by using the length variation of the unit tangent considered as a material vector:

$$d\tilde{\Gamma} = d\Gamma + t_i v_{i,j} t_j \, d\Gamma \left(a - a^0 \right) = d\Gamma + \delta J \, d\Gamma \left(a - a^0 \right) = \left(1 + \delta J \left(a - a^0 \right) \right) \, d\Gamma \tag{3.8}$$

The unit tangent and normal vectors are not material vectors. The unit tangent is only material with respect to orientation, and the unit normal is completely dependant on the tangent plane. Hence, the linear mapping of the unit tangent is similar to that of a material vector but substracting the length increase:

$$\tilde{t}_i = t_i + \left(v_{i,j} t_j - t_k v_{k,j} t_j t_i \right) \left(a - a^0 \right) = t_i + \left(v_{i,j} t_j - \delta J t_i \right) \left(a - a^0 \right) = t_i + \delta t_i \left(a - a^0 \right) \tag{3.9}$$

The variation of the unit tangent $\delta \mathbf{t}$ can only be perpendicular to the unit tangent $\mathbf{t}$. Hence, it can further be simplified to:

$$\delta t_i = v_{i,j} t_j - \delta J t_i \implies \delta t_i n_i = n_i v_{i,j} t_j \implies \delta t_k n_k n_i = \delta t_i = n_i n_k v_{k,j} t_j \tag{3.10}$$

The linear mapping of the unit normal is obtained by rotation of that of the unit tangent:

$$\epsilon_{ij} \tilde{t}_j = \epsilon_{ij} t_j + \epsilon_{ij} \delta t_j \left(a - a^0 \right) = \tilde{n}_i = n_i + \delta n_i \left(a - a^0 \right) \tag{3.11}$$

31

where ϵ_{ij} is the two-dimensional Levi-Civita symbol, and then $\delta n_i = -t_i n_k v_{k,j} t_j$.

The design velocity field $\mathbf{v} = \mathbf{v}(\mathbf{x}, a^0)$ throughout the domain is defined by using a design mesh (auxiliary mesh) connected to the physical mesh by position, i.e. the so-called free-form deformation approach (see Section 1.4). The geometry and the design velocity field of a design element $\Psi \subset \Omega$ with N_n^Ψ nodes are interpolated similarly (isoparametric):

$$x_j = \psi_q x_{jq}^\Psi \tag{3.12}$$

$$v_j = \psi_q v_{jq}^\Psi \tag{3.13}$$

where $q = 1, \ldots, N_n^\Psi$ is the node index of the design element, and x_{jq}^Ψ and v_{jq}^Ψ are the j-th components of the position vector and design velocity field of the q-th node, respectively. The element can be a one-dimensional or a two-dimensional element, i.e. shape functions can be $\psi_q = \psi_q(\eta)$ or $\psi_q = \psi_q(\eta_1, \eta_2)$, respectively. In general, they can be written as $\psi_q = \psi_q(\boldsymbol{\eta})$. As it will be seen later, shape functions $\psi_q(\boldsymbol{\eta})$ only appear in the calculation of the integrals. Thus, for an integration point i with position vector $\mathbf{x}^{(i)}$ located within a design element Ψ, the calculation of the local curvilinear coordinate $\boldsymbol{\eta}^{(i)}$ is required:

$$\boldsymbol{\eta}^{(i)} \text{ such that } x_j^{(i)} = \psi_q\left(\boldsymbol{\eta}^{(i)}\right) x_{jq}^\Psi \tag{3.14}$$

which can be done by a simple iterative minimization algorithm (convergent if $\mathbf{x}^{(i)} \in \Psi$). The connectivity between the physical mesh and the design mesh is built in the initialization stage of the solver, allowing a good initial guess for the minimization algorithm.

Strictly speaking, the design velocity field must be at least continuous throughout the domain, i.e. C^0, otherwise it breaks the domain. Hence, the design mesh should fill the whole domain, should be conforming, and only elements with the same dimension as the ambient space should be used. However, for shape sensitivity calculation using finite elements, the design velocities are required only at the nodes of the finite elements. Thus, neither the design mesh must fill the domain (by default a null design velocity field can be assigned to physical nodes not connected to the design mesh) nor the elements must have the same dimension as the ambient space. This fact justifies using the boundary layer technique as a way to reduce the computational cost (elements with null design velocity fields have null matrices derivatives with respect to the design variables) at the expense of a moderate but acceptable error increase in unstructured meshes (see Figure 2.8). As it will be shown later in this chapter, for shape sensitivity calculation using boundary elements, the design velocity field at the collocation point must be at least differentiable, i.e. C^1. The same strategy as with finite elements can be followed, although, in that case, a computationally expensive non-nodal collocation is required. In order to use nodal collocation, an element with the same dimension as the ambient space must be present at the collocation point. More details about these issues will be given later in this chapter.

As shown above, the calculation of the gradient of the design velocity field is needed. For a point located at a design element Ψ, it means that the derivatives of shape functions with respect to the global coordinates are required:

$$v_{i,j} = \psi_{q,j} v_{iq}^\Psi \tag{3.15}$$

If the design element is a one-dimensional element, then the shape functions are $\psi_q = \psi_q(\xi)$, and their derivatives with respect to the global coordinates are:

$$\psi_{q,j} = \frac{\partial \psi_q}{\partial x_j} = \frac{J_j}{|\mathbf{J}|^2} \frac{\partial \psi_q}{\partial \xi} \tag{3.16}$$

where the Jacobian vector is:

$$J_j = \frac{\partial x_j}{\partial \xi} = \frac{\partial \psi_q}{\partial \xi} x_{jq}^{\Psi} \tag{3.17}$$

If the design element is a two-dimensional element, then the shape functions are $\psi_q = \psi_q(\xi_1, \xi_2)$, and their derivatives with respect to the global coordinates are:

$$\psi_{q,j} = \frac{\partial \psi_q}{\partial x_j} = G_{jk} \frac{\partial \psi_q}{\partial \xi_k} \tag{3.18}$$

where $\mathbf{G} = \mathbf{J}^{-1}$ and the elements of the Jacobian matrix $\mathbf{J}$ are:

$$J_{jk} = \frac{\partial x_k}{\partial \xi_j} = \frac{\partial \psi_q}{\partial \xi_j} x_{kq}^{\Psi} \tag{3.19}$$

The linear mapping corresponding to a field variable u is:

$$\tilde{u} = u + \delta u \left(a - a^0 \right) = u + \left(\frac{\partial u}{\partial a} + \frac{\partial u}{\partial x_j} v_j \right)_{a=a^0} \left(a - a^0 \right) \tag{3.20}$$

where the sensitivity δu can be evaluated using the expression shown above only when u is explicit, as in Section 2.3. When used in the FEM or BEM sensitivity analysis, δu is a degree of freedom. Field variables and their sensitivities are interpolated using the same shape functions as the geometry, hence an isoparametric boundary element representation is considered. For a vector variable $\mathbf{u}$:

$$u_j = \phi_p u_{jp}^{\Phi} \tag{3.21}$$

$$\delta u_j = \phi_p \delta u_{jp}^{\Phi} \tag{3.22}$$

where $p = 1, \ldots, N_n^{\Phi}$ is the node index of the boundary element, and u_{jp}^{Φ} and δu_{jp}^{Φ} are the j-th components of the vector variable and its sensitivity of the p-th node, respectively.

3.3   Laplace problem

A problem governed by the Laplace equation is considered. The potential (primary variable) is denoted by p, while the flux is the potential derivative in the $\mathbf{n}$ direction (secondary variable) and is denoted by $q = \nabla p \cdot \mathbf{n}$.

3.3.1 δSBIE for non-boundary collocation points

The Singular BIE (SBIE) for an interior or exterior collocation point with respect to the reference domain Ω can be written as [29, 51]:

$$\delta_{\Omega}^i p^i + \int_{\Gamma} q^* p \, \mathrm{d}\Gamma = \int_{\Gamma} p^* q \, \mathrm{d}\Gamma, \quad \delta_{\Omega}^i = \begin{cases} 1, \ \mathbf{x}^i \in \Omega \\ 0, \ \mathbf{x}^i \notin \Omega \cup \Gamma \end{cases} \tag{3.23}$$

where:

$$p^* = -\frac{1}{2\pi} \ln r \tag{3.24}$$

$$p^*_{,j} = -\frac{1}{2\pi} \frac{1}{r} r_{,j} \tag{3.25}$$

$$q^* = p^*_{,j} n_j = -\frac{1}{2\pi} \frac{1}{r} \frac{\partial r}{\partial n} \tag{3.26}$$

$$r = |\mathbf{x} - \mathbf{x}^i| \tag{3.27}$$

and $\mathbf{x}$ and $\mathbf{x}^i$ are the observation and collocation points, respectively. Likewise, for the perturbed domain $\tilde{\Omega}$:

$$\delta^i_{\tilde{\Omega}} \tilde{p}^i + \int_{\tilde{\Gamma}} \tilde{q}^* \tilde{p} \, d\tilde{\Gamma} = \int_{\tilde{\Gamma}} \tilde{p}^* \tilde{q} \, d\tilde{\Gamma}, \quad \delta^i_{\tilde{\Omega}} = \begin{cases} 1, \ \mathbf{x}^i \in \tilde{\Omega} \\ 0, \ \mathbf{x}^i \notin \tilde{\Omega} \cup \tilde{\Gamma} \end{cases} \tag{3.28}$$

As seen in the previous section, the relationships of geometrical objects and variables between the reference domain Ω and the perturbed domain $\tilde{\Omega}$ are given by linear mappings:

$$\tilde{p}^i = p^i + \delta p^i \left(a - a^0\right) \tag{3.29}$$

$$\tilde{p} = p + \delta p \left(a - a^0\right) \tag{3.30}$$

$$\tilde{p}_j = p_j + \delta p_j \left(a - a^0\right) \tag{3.31}$$

$$\tilde{n}_j = n_j + \delta n_j \left(a - a^0\right) \tag{3.32}$$

$$\tilde{q} = \tilde{p}_j \tilde{n}_j = q + \left(p_j \delta n + \delta p_j n_j\right)\left(a - a^0\right) = q + \delta q \left(a - a^0\right) \tag{3.33}$$

$$d\tilde{\Gamma} = \left[1 + \delta J \left(a - a^0\right)\right] d\Gamma \tag{3.34}$$

where $(a - a^0)^2$ terms have been disregarded. Since the shape parametrization does not change the topology of the domain, i.e. an interior (or exterior) point remains interior (or exterior), then $\delta^i_{\tilde{\Omega}} = \delta^i_{\Omega}$. The fundamental solution p^* depends on the observation and collocation points $p^* = p^*(\mathbf{x}, \mathbf{x}^i)$, hence its linear mapping must be built from the Taylor's expansion with respect to both points:

$$\tilde{p}^* = p^* + \frac{\partial p^*}{\partial x_j} v_j \left(a - a^0\right) + \frac{\partial p^*}{\partial x^i_j} v^i_j \left(a - a^0\right) = p^* + p^*_{,j} \left(v_j - v^i_j\right)\left(a - a^0\right) \tag{3.35}$$

where $\square_{,j} = \partial\square/\partial x_j = -\partial\square/\partial x^i_j$ holds for any fundamental solution and its derivatives since $\mathbf{x}$ and $\mathbf{x}^i$ only appear inside of terms depending on the distance vector $\mathbf{r} = \mathbf{x} - \mathbf{x}^i$. Furthermore, from the linear mapping of observation and collocation points, it is possible to write:

$$\begin{aligned}
\tilde{\mathbf{x}} &= \mathbf{x} + \mathbf{v}\left(a - a^0\right) \\
\tilde{\mathbf{x}}^i &= \mathbf{x}^i + \mathbf{v}^i\left(a - a^0\right) \\
\tilde{\mathbf{x}} - \tilde{\mathbf{x}}^i &= \mathbf{x} - \mathbf{x}^i + \left(\mathbf{v} - \mathbf{v}^i\right)\left(a - a^0\right) \\
\tilde{\mathbf{r}} &= \mathbf{r} + \delta\mathbf{r}\left(a - a^0\right)
\end{aligned} \tag{3.36}$$

where it is obvious that $\delta\mathbf{r} \to \mathbf{0}$ as $\mathbf{x} \to \mathbf{x}^i$, i.e. $\delta\mathbf{r} = O(r)$. This important fact is used later to study the integration of the SBIE for collocation points located at the boundary. Therefore, $\tilde{p}^*$ can be written as:

$$\tilde{p}^* = p^* + p^*_{,j}\delta r_j \left(a - a^0\right) = p^* + \delta p^* \left(a - a^0\right) \tag{3.37}$$

The linear mapping of $\tilde{q}^*$ is built by using the linear mapping of its components:

$$\begin{aligned} \tilde{q}^* = \tilde{p}^*_{,j}\tilde{n}_j &= \left[p^*_{,j} + p^*_{,jm}\delta r_m \left(a - a^0\right)\right]\left[n_j + \delta n_j \left(a - a^0\right)\right] \\ &= q^* + \left(p^*_{,j}\delta n_j + p^*_{,jm}\delta r_m n_j\right)\left(a - a^0\right) = q^* + \delta q^* \left(a - a^0\right) \end{aligned} \tag{3.38}$$

where only linear terms are kept. Note that $p^*_{,jm}$ is obtained differentiating Equation (3.25):

$$p^*_{,jm} = -\frac{1}{2\pi}\frac{1}{r^2}\left(\delta_{jm} - 2r_{,j}r_{,m}\right) \tag{3.39}$$

where δ_{ij} is the Kronecker delta. Last, substituting all these linear mappings into Equation (3.28), keeping only linear terms $(a - a^0)$, substracting Equation (3.23) from it, and dropping out $(a - a^0)$ terms, give the sensitivity SBIE (or δSBIE):

$$\delta^i_\Omega \delta p^i + \int_\Gamma q^*\delta p \ \mathrm{d}\Gamma + \int_\Gamma (\delta q^* + q^*\delta J)\, p \ \mathrm{d}\Gamma = \int_\Gamma p^*\delta q \ \mathrm{d}\Gamma + \int_\Gamma (\delta p^* + p^*\delta J)\, q \ \mathrm{d}\Gamma \tag{3.40}$$

The first and third integrals are analogous to the integrals of the SBIE, except that instead of p and q, their sensitivities δp and δq appear. The second and fourth integrals are new integrals that depend on p and q, hence only once the zero-order solution is known they can be evaluated. Since the integration domain Γ does not contain the collocation point, all integrals are regular but nearly singular if the collocation point is close to Γ.

3.3.2 δSBIE for boundary collocation points

The δSBIE presented in Equation (3.40) is valid only for interior or exterior collocation points. In order to obtain the δSBIE for boundary collocation points ($\mathbf{x}^i \in \Gamma$), it is possible to perform the integration of Equation (3.40) but along a modified path avoiding the collocation point:

$$\Gamma = \lim_{\epsilon \to 0^+}\left[\left(\Gamma - e^i\right) + \Gamma^i\right] \tag{3.41}$$

where ϵ is the radius of a circular arc Γ^i that substitutes a neighbourhood e^i of the collocation point on Γ. As seen in Figure 3.2, this limiting process can be done from the interior ($\delta^i_\Omega = 1$) or from the exterior ($\delta^i_\Omega = 0$), both leading to the same final result. In the following, the former is used:

$$\delta p^i + \lim_{\epsilon \to 0^+}\int_{\Gamma - e^i} q^*\delta p \ \mathrm{d}\Gamma + \lim_{\epsilon \to 0^+}\int_{\Gamma^i} q^*\delta p \ \mathrm{d}\Gamma + \lim_{\epsilon \to 0^+}\int_{\Gamma - e^i}(\delta q^* + q^*\delta J)\, p \ \mathrm{d}\Gamma$$

$$+ \lim_{\epsilon \to 0^+}\int_{\Gamma^i}(\delta q^* + q^*\delta J)\, p \ \mathrm{d}\Gamma = \lim_{\epsilon \to 0^+}\int_{\Gamma - e^i} p^*\delta q \ \mathrm{d}\Gamma + \lim_{\epsilon \to 0^+}\int_{\Gamma^i} p^*\delta q \ \mathrm{d}\Gamma$$

$$+ \lim_{\epsilon \to 0^+}\int_{\Gamma - e^i}(\delta p^* + p^*\delta J)\, q \ \mathrm{d}\Gamma + \lim_{\epsilon \to 0^+}\int_{\Gamma^i}(\delta p^* + p^*\delta J)\, q \ \mathrm{d}\Gamma \tag{3.42}$$
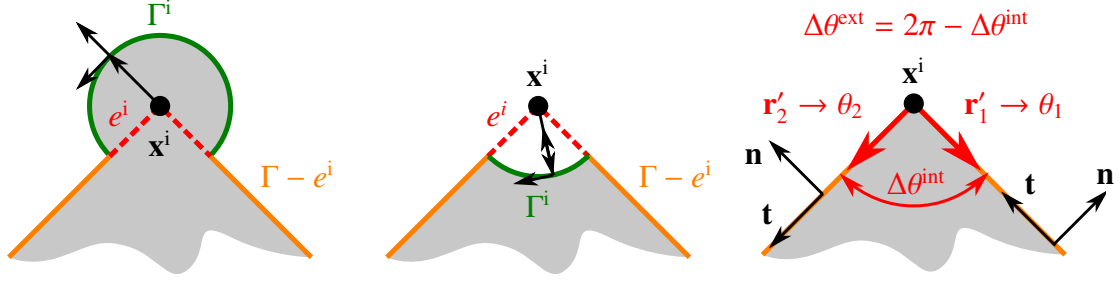
Figure 3.2: Integration path near boundary collocation points. Left: from the interior. Center: from the exterior. Right: criteria for angles θ_1 and θ_2

Integration over Γ^i   In order to evaluate the integrals along Γ^i, a polar system of coordinates (ϵ, θ) centered at the collocation point and oriented counterclockwise is considered. The polar angle θ is in the domain $\theta_1 \leq \theta \leq \theta_2$, where θ_1 and θ_2 are shown in Figure 3.2. The main geometrical terms along Γ^i are:

$$\mathbf{x}^i = \mathbf{0} \tag{3.43}$$

$$\mathbf{x} = (\epsilon \cos \theta, \epsilon \sin \theta) \tag{3.44}$$

$$\mathbf{r} = \mathbf{x}, \ r = \epsilon \tag{3.45}$$

$$r_{,j} = r_j/r \tag{3.46}$$

$$n_j = r_{,j}, \ \mathbf{n} = (\cos \theta, \sin \theta) \tag{3.47}$$

$$t_i = \epsilon_{ij} n_j, \ \mathbf{t} = (-\sin \theta, \cos \theta) \tag{3.48}$$

$$\partial r/\partial n = r_{,j} n_j = 1 \tag{3.49}$$

$$r_{,j} t_j = 0 \tag{3.50}$$

$$\mathrm{d}\Gamma = \epsilon \, \mathrm{d}\theta \tag{3.51}$$

where ϵ_{ij} is the two-dimensional Levi-Civita symbol. The evaluation of the first integral over Γ^i of Equation (3.42) gives:

$$\lim_{\epsilon \to 0^+} \int_{\Gamma^i} q^* \delta p \, \mathrm{d}\Gamma = -\frac{1}{2\pi} \lim_{\epsilon \to 0^+} \int_{\theta_1}^{\theta_2} \frac{1}{\epsilon} 1 \left(\delta p^i + O(\epsilon)\right) \epsilon \, \mathrm{d}\theta = -\frac{\theta_2 - \theta_1}{2\pi} \delta p^i = -\frac{\Delta\theta^{\mathrm{ext}}}{2\pi} \delta p^i \tag{3.52}$$

where a simple zero-order expansion $\delta p = \delta p^i + O(\epsilon)$ is required. The second integral over Γ^i is:

$$\lim_{\epsilon \to 0^+} \int_{\Gamma^i} (\delta q^* + q^* \delta J) p \, \mathrm{d}\Gamma = \lim_{\epsilon \to 0^+} \int_{\Gamma^i} \left(p^*_{,j} \delta n_j + p^*_{,jm} \delta r_m n_j + q^* \delta J\right) p \, \mathrm{d}\Gamma$$

$$= -\frac{1}{2\pi} \lim_{\epsilon \to 0^+} \int_{\theta_1}^{\theta_2} \left[\frac{1}{\epsilon} n_j \delta n_j + \frac{1}{\epsilon^2} \left(\delta_{jm} - 2 n_j n_m\right) \delta r_m n_j + \frac{1}{\epsilon} 1 \delta J\right] \left(p^i + O(\epsilon)\right) \epsilon \, \mathrm{d}\theta \tag{3.53}$$

where a zero-order expansion $p = p^i + O(\epsilon)$ is used. In order to evaluate the integral, expansions of several terms of the kernel around the collocation point are needed. For the

sensitivity of the unit normal δn_j, a zero-order expansion is required:

$$\delta n_j = -t_j n_m v^{\mathrm{i}}_{m,k} t_k + O(\epsilon) \tag{3.54}$$

Likewise, for the sensitivity of the boundary length δJ

$$\delta J = t_m v^{\mathrm{i}}_{m,j} t_j + O(\epsilon) \tag{3.55}$$

For the design velocity field, however, a first-order expansion is required:

$$v_m = v^{\mathrm{i}}_m + v^{\mathrm{i}}_{m,j}(x_j - x^{\mathrm{i}}_j) + O(r^2) = v^{\mathrm{i}}_m + v^{\mathrm{i}}_{m,j} r_j \epsilon + O(\epsilon^2) \tag{3.56}$$

and hence:

$$\delta r_m = v_m - v^{\mathrm{i}}_m = v^{\mathrm{i}}_{m,j} r_j \epsilon + O(\epsilon^2) \tag{3.57}$$

Therefore, since the gradient of the design velocity field at the collocation point $v^{\mathrm{i}}_{m,j}$ is required, the design velocity field must be differentiable, i.e. $\mathbf{v}(\mathbf{x}^{\mathrm{i}}) \in C^1$. Substituting these expansions into Equation (3.53) leads to:

$$\lim_{\epsilon \to 0^+} \int_{\Gamma^{\mathrm{i}}} (\delta q^* + q^* \delta J)\, p\; \mathrm{d}\Gamma = \frac{1}{2\pi}\left(\int_{\theta_1}^{\theta_2} n_m n_j\, \mathrm{d}\theta - \int_{\theta_1}^{\theta_2} t_m t_j\, \mathrm{d}\theta \right) v^{\mathrm{i}}_{m,j} p^{\mathrm{i}} = b^{\mathrm{i}}_{mj} v^{\mathrm{i}}_{m,j} p^{\mathrm{i}} \tag{3.58}$$

where b^{i}_{mj} is:

$$\left(b^{\mathrm{i}}_{mj}\right) = \frac{1}{4\pi}\begin{pmatrix} \sin 2\theta_2 - \sin 2\theta_1 & -(\cos 2\theta_2 - \cos 2\theta_1) \\ -(\cos 2\theta_2 - \cos 2\theta_1) & -(\sin 2\theta_2 - \sin 2\theta_1) \end{pmatrix} \tag{3.59}$$

which is null if the collocation point is located at a smooth point of the boundary, i.e $\Gamma(\mathbf{x}^{\mathrm{i}}) \in C^1 \Rightarrow b^{\mathrm{i}}_{mj} = 0$. The third integral over Γ^{i} is null:

$$\lim_{\epsilon \to 0^+} \int_{\Gamma^{\mathrm{i}}} p^* \delta q\; \mathrm{d}\Gamma = -\frac{1}{2\pi}\delta q\left(\lim_{\epsilon \to 0^+} \epsilon \ln \epsilon \right)\left(\int_{\theta_1}^{\theta_2} \mathrm{d}\theta \right) = 0 \tag{3.60}$$

where δq must be bounded. The fourth integral over Γ^{i} is also null:

$$\lim_{\epsilon \to 0^+} \int_{\Gamma^{\mathrm{i}}} (\delta p^* + p^* \delta J)\, q\; \mathrm{d}\Gamma = -\frac{1}{2\pi} \lim_{\epsilon \to 0^+} \int_{\theta_1}^{\theta_2} \left(\frac{1}{\epsilon} n_m v^{\mathrm{i}}_{m,j} \epsilon n_j + (\ln \epsilon)\, \delta J \right) q\epsilon\; \mathrm{d}\theta = 0 \tag{3.61}$$

where q must be bounded. Substituting all these results into Equation (3.42) gives:

$$c^{\mathrm{i}} \delta p^{\mathrm{i}} + b^{\mathrm{i}}_{mj} v^{\mathrm{i}}_{m,j} p^{\mathrm{i}} + \lim_{\epsilon \to 0^+} \int_{\Gamma - e^{\mathrm{i}}} q^* \delta p\; \mathrm{d}\Gamma + \lim_{\epsilon \to 0^+} \int_{\Gamma - e^{\mathrm{i}}} (\delta q^* + q^* \delta J)\, p\; \mathrm{d}\Gamma$$

$$= \lim_{\epsilon \to 0^+} \int_{\Gamma - e^{\mathrm{i}}} p^* \delta q\; \mathrm{d}\Gamma + \lim_{\epsilon \to 0^+} \int_{\Gamma - e^{\mathrm{i}}} (\delta p^* + p^* \delta J)\, q\; \mathrm{d}\Gamma \tag{3.62}$$

where $c^{\mathrm{i}} = \Delta \theta^{\mathrm{int}}/2\pi$ is the free-term similar to that of the SBIE, and b^{i}_{mj} is a new free-term appearing in the δSBIE. The integrals over $\Gamma - e^{\mathrm{i}}$ are at most strongly singular, and their evaluation requires additional work.

$$\frac{\partial r}{\partial \Gamma} = \frac{\mathbf{r}}{r} \cdot \mathbf{t} < 0, \left(\frac{\partial r}{\partial \Gamma}\right)^{\mathrm{i}} = -1 \qquad\qquad \frac{\partial r}{\partial \Gamma} = \frac{\mathbf{r}}{r} \cdot \mathbf{t} > 0, \left(\frac{\partial r}{\partial \Gamma}\right)^{\mathrm{i}} = 1$$

$$\frac{\partial r}{\partial n} = \frac{\mathbf{r}}{r} \cdot \mathbf{n} \to 0 \text{ when } r \to 0 \Rightarrow \frac{\partial r}{\partial n} = O(r)$$
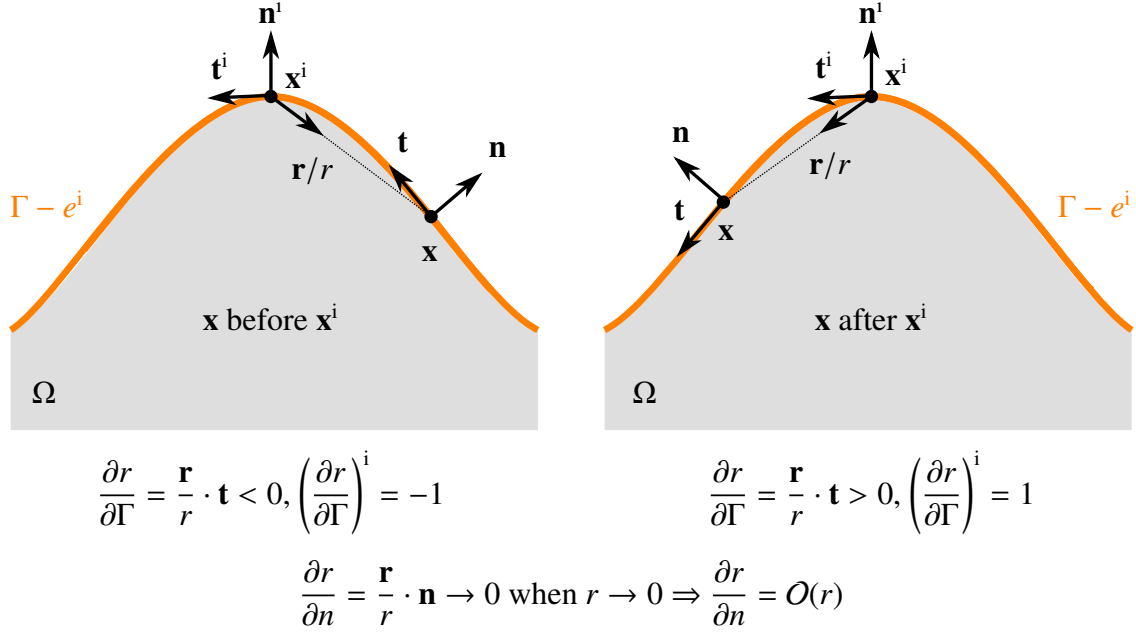
Figure 3.3: Limiting behaviour of geometrical vectors around the collocation point

Integration over $\Gamma - e^{\mathrm{i}}$ The evaluation of the integrals in Equation (3.62) can be performed in different ways, from a pure analytical approach (doable for straight elements) to a pure numerical approach using special quadrature formulae (Kutt's quadrature). In this work, an analytical regularization leading to at most weakly singular integrals is applied before any numerical integration is done. By doing so, only regular and weakly singular integrals are numerically managed, which are easily tractable and controllable.

   The integrands are composed mainly of geometrical terms and field variables, thus their behaviour near the collocation point must be studied. The behaviour of the relevant geometrical terms is illustrated in Figure 3.3. The field variables are at least bounded, and hence $p, q, \delta p, \delta q$ are $O(r^0)$. The first integral of Equation (3.62) is regular:

$$H = \lim_{\epsilon \to 0^+} \int_{\Gamma - e^{\mathrm{i}}} q^* \delta p \, \mathrm{d}\Gamma \text{ is regular } \because q^* = -\frac{1}{2\pi} \underbrace{\frac{1}{r}}_{O(r^{-1})} \underbrace{\frac{\partial r}{\partial n}}_{O(r^1)} = O\left(r^0\right) \tag{3.63}$$

The third integral is weakly singular:

$$G = \lim_{\epsilon \to 0^+} \int_{\Gamma - e^{\mathrm{i}}} p^* \delta q \, \mathrm{d}\Gamma \text{ is weakly singular } \because p^* = -\frac{1}{2\pi} \ln r = O\left(\ln r\right) \tag{3.64}$$

The fourth integral can be split into two parts:

$$\delta G = \lim_{\epsilon \to 0^+} \int_{\Gamma - e^{\mathrm{i}}} \left(\delta p^* + p^* \delta J\right) q \, \mathrm{d}\Gamma = \delta G^{\mathrm{R}} + \delta G^{\mathrm{J}} \tag{3.65}$$

where:

$$\delta G^{\mathrm{R}} = \lim_{\epsilon \to 0^+} \int_{\Gamma - e^{\mathrm{i}}} \delta p^* q \, \mathrm{d}\Gamma \text{ is regular } \because \delta p^* = \underbrace{p^*_{,j}}_{O(r^{-1})} \underbrace{\delta r_j}_{O(r^1)} = O\left(r^0\right) \tag{3.66}$$

$$\delta G^{\text{J}} = \lim_{\epsilon \to 0^+} \int_{\Gamma - e^{\text{i}}} p^* \delta J q \; \mathrm{d}\Gamma \text{ is weakly singular } \because \underbrace{p^*}_{O(\ln r)} \underbrace{\delta J}_{O(r^0)} = O(\ln r) \tag{3.67}$$

The second integral can be split into three parts:

$$\delta H = \lim_{\epsilon \to 0^+} \int_{\Gamma - e^{\text{i}}} \left(p^*_{,j} \delta n_j + p^*_{,jm} \delta r_m n_j + q^* \delta J \right) p \; \mathrm{d}\Gamma = \delta H^{\text{N}} + \delta H^{\text{R}} + \delta H^{\text{J}} \tag{3.68}$$

where:

$$\delta H^{\text{N}} = \lim_{\epsilon \to 0^+} \int_{\Gamma - e^{\text{i}}} p^*_{,j} \delta n_j p \; \mathrm{d}\Gamma \text{ is strongly singular } \because \underbrace{p^*_{,j}}_{O(r^{-1})} \underbrace{\delta n_j}_{O(r^0)} = O\left(r^{-1}\right) \tag{3.69}$$

$$\delta H^{\text{R}} = \lim_{\epsilon \to 0^+} \int_{\Gamma - e^{\text{i}}} p^*_{,jm} \delta r_m n_j p \; \mathrm{d}\Gamma \text{ is strongly sing. } \because \underbrace{p^*_{,jm}}_{O(r^{-2})} \underbrace{\delta r_m}_{O(r^1)} \underbrace{n_j}_{O(r^0)} = O\left(r^{-1}\right) \tag{3.70}$$

$$\delta H^{\text{J}} = \lim_{\epsilon \to 0^+} \int_{\Gamma - e^{\text{i}}} q^* \delta J p \; \mathrm{d}\Gamma \text{ is regular } \because \underbrace{q^*}_{O(r^0)} \underbrace{\delta J}_{O(r^0)} = O\left(r^0\right) \tag{3.71}$$

Therefore, δH^{N} and δH^{R} require further treatment. δH^{N} can be regularized by substracting and adding the limit when $r \to 0$ of a part of the integrand:

$$\delta H^{\text{N}} = \frac{1}{2\pi} \lim_{\epsilon \to 0^+} \int_{\Gamma - e^{\text{i}}} \frac{1}{r} r_{,j} t_j n_m v_{m,k} t_k p \; \mathrm{d}\Gamma = \frac{1}{2\pi} \lim_{\epsilon \to 0^+} \int_{\Gamma - e^{\text{i}}} \frac{1}{r} \frac{\partial r}{\partial \Gamma} n_m v_{m,k} t_k p \; \mathrm{d}\Gamma$$

$$= \frac{1}{2\pi} \left[\lim_{\epsilon \to 0^+} \int_{\Gamma - e^{\text{i}}} \frac{1}{r} \frac{\partial r}{\partial \Gamma} \left(n_m v_{m,k} t_k p - n^{\text{i}}_m v^{\text{i}}_{m,k} t^{\text{i}}_k p^{\text{i}} \right) \; \mathrm{d}\Gamma + n^{\text{i}}_m v^{\text{i}}_{m,k} t^{\text{i}}_k p^{\text{i}} \lim_{\epsilon \to 0^+} \int_{\Gamma - e^{\text{i}}} \frac{1}{r} \; \mathrm{d}r \right] \tag{3.72}$$

leading to one regular integral and another integral $\int 1/r \; \mathrm{d}r$ that can be solved analytically. For δH^{R}, first, it is necessary to expand the integrand:

$$\delta H^{\text{R}} = -\frac{1}{2\pi} \lim_{\epsilon \to 0^+} \int_{\Gamma - e^{\text{i}}} \frac{1}{r^2} \left(\delta_{jm} - 2 r_{,j} r_{,m} \right) \left(v_m - v^{\text{i}}_m \right) n_j p \; \mathrm{d}\Gamma$$

$$= \frac{1}{2\pi} \left[\lim_{\epsilon \to 0^+} \int_{\Gamma - e^{\text{i}}} \frac{2}{r^2} \frac{\partial r}{\partial n} \left(v_m - v^{\text{i}}_m \right) r_{,m} p \; \mathrm{d}\Gamma - \lim_{\epsilon \to 0^+} \int_{\Gamma - e^{\text{i}}} \frac{1}{r^2} \left(v_m - v^{\text{i}}_m \right) n_m p \; \mathrm{d}\Gamma \right] \tag{3.73}$$

which gives one regular integral and another strongly singular integral. Then, taking into account that:

$$v_m = v^{\text{i}}_m + v^{\text{i}}_{m,j} r_j + O\left(r^2\right) \implies v_m - v^{\text{i}}_m - v^{\text{i}}_{m,j} r_j = O\left(r^2\right) \tag{3.74}$$

39

and adding and substracting $v^{\mathrm{i}}_{m,j} r_j$:

$$
\delta H^{\mathrm{R}} = \frac{1}{2\pi} \left[\lim_{\epsilon \to 0^+} \int_{\Gamma - e^{\mathrm{i}}} \frac{2}{r^2} \frac{\partial r}{\partial n} \left(v_m - v^{\mathrm{i}}_m \right) r_{,m} p \; \mathrm{d}\Gamma - \lim_{\epsilon \to 0^+} \int_{\Gamma - e^{\mathrm{i}}} \frac{1}{r^2} \left(v_m - v^{\mathrm{i}}_m - v^{\mathrm{i}}_{m,j} r_j \right) n_m p \; \mathrm{d}\Gamma \right.
$$

$$
\left. - \lim_{\epsilon \to 0^+} \int_{\Gamma - e^{\mathrm{i}}} \frac{1}{r} v^{\mathrm{i}}_{m,j} r_j n_m p \; \mathrm{d}\Gamma \right] \quad (3.75)
$$

a new regular integral and a new strongly singular integral appear. By checking out Figure 3.3, it is easy to see that:

$$
r_j = \left(\frac{\partial r}{\partial \Gamma} \right)^{\mathrm{i}} t^{\mathrm{i}}_j + O(r) \tag{3.76}
$$

which can be used to add and substract a part of the integrand of the strongly singular integral:

$$
\delta H^{\mathrm{R}} = \frac{1}{2\pi} \left[\lim_{\epsilon \to 0^+} \int_{\Gamma - e^{\mathrm{i}}} \frac{2}{r^2} \frac{\partial r}{\partial n} \left(v_m - v^{\mathrm{i}}_m \right) r_{,m} p \; \mathrm{d}\Gamma - \lim_{\epsilon \to 0^+} \int_{\Gamma - e^{\mathrm{i}}} \frac{1}{r^2} \left(v_m - v^{\mathrm{i}}_m - v^{\mathrm{i}}_{m,j} r_j \right) n_m p \; \mathrm{d}\Gamma \right.
$$

$$
\left. - \lim_{\epsilon \to 0^+} \int_{\Gamma - e^{\mathrm{i}}} \frac{1}{r} \left(v^{\mathrm{i}}_{m,j} r_j n_m p - v^{\mathrm{i}}_{m,j} \left(\frac{\partial r}{\partial \Gamma} \right)^{\mathrm{i}} t^{\mathrm{i}}_j n^{\mathrm{i}}_m p^{\mathrm{i}} \right) \mathrm{d}\Gamma - n^{\mathrm{i}}_m v^{\mathrm{i}}_{m,j} t^{\mathrm{i}}_j p^{\mathrm{i}} \lim_{\epsilon \to 0^+} \int_{\Gamma - e^{\mathrm{i}}} \frac{1}{r} \left(\frac{\partial r}{\partial \Gamma} \right)^{\mathrm{i}} \mathrm{d}\Gamma \right]
$$

$$
\tag{3.77}
$$

leading to a new regular integral and another strongly singular integral. Finally, by adding and substracting the limit of $\partial r / \partial \Gamma$ when $r \to 0$ leads to:

$$
\delta H^{\mathrm{R}} = \frac{1}{2\pi} \left[\lim_{\epsilon \to 0^+} \int_{\Gamma - e^{\mathrm{i}}} \frac{2}{r^2} \frac{\partial r}{\partial n} \left(v_m - v^{\mathrm{i}}_m \right) r_{,m} p \; \mathrm{d}\Gamma - \lim_{\epsilon \to 0^+} \int_{\Gamma - e^{\mathrm{i}}} \frac{1}{r^2} \left(v_m - v^{\mathrm{i}}_m - v^{\mathrm{i}}_{m,j} r_j \right) n_m p \; \mathrm{d}\Gamma \right.
$$

$$
- \lim_{\epsilon \to 0^+} \int_{\Gamma - e^{\mathrm{i}}} \frac{1}{r} \left(v^{\mathrm{i}}_{m,j} r_j n_m p - v^{\mathrm{i}}_{m,j} \left(\frac{\partial r}{\partial \Gamma} \right)^{\mathrm{i}} t^{\mathrm{i}}_j n^{\mathrm{i}}_m p^{\mathrm{i}} \right) \mathrm{d}\Gamma - n^{\mathrm{i}}_m v^{\mathrm{i}}_{m,j} t^{\mathrm{i}}_j p^{\mathrm{i}} \lim_{\epsilon \to 0^+} \int_{\Gamma - e^{\mathrm{i}}} \frac{1}{r} \left(\left(\frac{\partial r}{\partial \Gamma} \right)^{\mathrm{i}} - \frac{\partial r}{\partial \Gamma} \right) \mathrm{d}\Gamma
$$

$$
\left. - n^{\mathrm{i}}_m v^{\mathrm{i}}_{m,j} t^{\mathrm{i}}_j p^{\mathrm{i}} \lim_{\epsilon \to 0^+} \int_{\Gamma - e^{\mathrm{i}}} \frac{1}{r} \; \mathrm{d}r \right] \quad (3.78)
$$

which is a set of regular integrals and an integral $\int 1/r \; \mathrm{d}r$ analytically solvable. It must be noticed that terms involving the integral $\int 1/r \; \mathrm{d}r$ cancel out when δH is evaluated using Equation (3.68).

3.3.3 Discretization, collocation, numerical integration and solution

The boundary Γ is discretized using a set of N_{be} boundary elements: $\Gamma = \cup_{i=1}^{i=N_{\mathrm{be}}} \Phi_i$ where $\Phi_i \cap \Phi_j = \varnothing$ when $i \neq j$. As explained above, the discretization is performed using
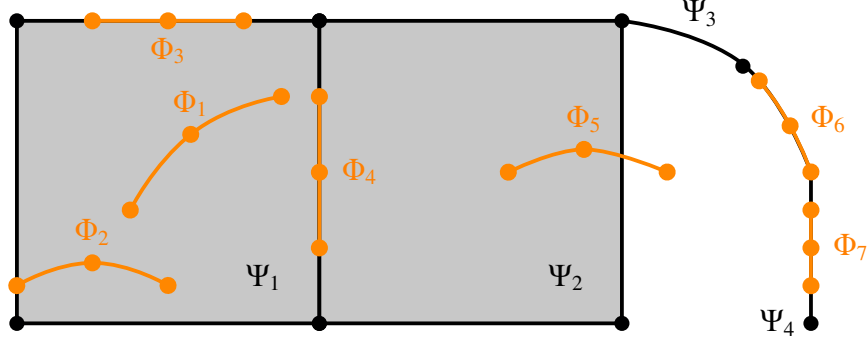
Figure 3.4: Possible positions of a boundary element throughout a design mesh

isoparametric elements. For a given boundary element Φ with N_{n}^{Φ} nodes:

$$
\begin{aligned}
\text{Geometry:} \quad & x_j = \phi_p x_{jp}^{\Phi} \\
\text{Variables:} \quad & p = \phi_p p_p^{\Phi}, \ q = \phi_p q_p^{\Phi}, \ \delta p = \phi_p \delta p_p^{\Phi}, \ \delta q = \phi_p \delta q_p^{\Phi}
\end{aligned}
\tag{3.79}
$$

where $p = 1, \ldots, N_{\mathrm{n}}^{\Phi}$ is the node index of the boundary element. The design domain is discretized using a set of N_{de} design elements: $\Upsilon = \cup_{i=1}^{i=N_{\mathrm{de}}} \Psi_i$ where $\Psi_i \cap \Psi_j = \varnothing$ when $i \neq j$. For a given design element Ψ with N_{n}^{Ψ} nodes:

$$
\begin{aligned}
\text{Geometry:} \quad & x_j = \psi_q x_{jq}^{\Psi} \\
\text{Design velocity field:} \quad & v_j = \psi_q v_{jq}^{\Psi}
\end{aligned}
\tag{3.80}
$$

where $q = 1, \ldots, N_{\mathrm{n}}^{\Psi}$ is the node index of the design element. In the following, the indices p and q are exclusively related to node indices of boundary and design elements, respectively, and any other index is related to a coordinate index.

It was shown in the previous section that the collocation point $\mathbf{x}^i$ must be in a point where $\mathbf{v}(\mathbf{x}^i) \in C^1$. Figure 3.4 shows a design mesh consisting of two two-dimensional design elements (Ψ_1 and Ψ_2) with a common edge, and two one-dimensional design elements (Ψ_3 and Ψ_4) with a common node. Design elements Ψ_2 (two-dimensional) and Ψ_3 (one-dimensional) share a common node. By defining the values of the design velocity field at each node, a C^{∞} design velocity field is built throughout the design mesh except at some locations where it is guaranteed only to be C^0. These locations are the edges and nodes shared by two or more design elements. The existence of these locations conditions the collocation procedure of the BIEs in the sensitivity analysis (and the required zero-order analysis). There are two ways of dealing with it:

Fully isoparametric approach The design velocity field is interpolated also with the shape functions of the boundary element Φ:

$$
\begin{aligned}
\text{Geometry:} \quad & x_j = \phi_p x_{jp}^{\Phi} \\
\text{Variables:} \quad & p = \phi_p p_p^{\Phi}, \ q = \phi_p q_p^{\Phi}, \ \delta p = \phi_p \delta p_p^{\Phi}, \ \delta q = \phi_p \delta q_p^{\Phi} \\
\text{Design velocity field:} \quad & v_j = \phi_q v_{jq}^{\Phi}
\end{aligned}
\tag{3.81}
$$

where $p, q = 1, \dots, N_n^{\Phi}$ is the node index of the boundary element. The design velocity field at nodes v_{jq}^{Φ} are calculated from the design mesh. This interpolation guarantees differentiability along the boundary element except at the end nodes. Hence, a Multiple Collocation Approach (MCA) is used [31], where the collocation is performed only inside the boundary element. This fully isoparametric approach using the MCA is simple and applicable to all possible positions of the boundary elements shown in Figure 3.4. It is even possible to consider the boundary element Φ_5 if a null design velocity field is assigned to the node located outside the design mesh. Despite its versatility, it comes with a big disadvantage: its computational cost.

Mixed approach Nodal collocation is used for boundary elements whose nodes are located at points where $\mathbf{v}(\mathbf{x}^i) \in C^1$. For boundary elements where at least one node violates this condition, the full isoparametric approach is used. This approach is versatile and, at the same time, as computationally cheap as possible. The only disadvantage is the implementation effort needed to automatically distinguise between both situations. In Figure 3.4, nodal collocation is used on boundary elements Φ_1, Φ_2, Φ_3 and Φ_7, while the full isoparametric approach is used on boundary elements Φ_4, Φ_5 and Φ_6.

Once discretization and collocation procedures have been described, it is possible to present the discretized form of Boundary Integral Equations (3.40) and (3.62). For any collocation point $\mathbf{x}^i$, both can be written in a generic way as:

$$
c^i \delta p^i + b_{mj}^i v_{m,j}^i p^i + \sum_{e=1}^{N_{be}} \left(H_p \delta p_p \right)^{\Phi_e} + \sum_{e=1}^{N_{be}} \left(\delta H_p p_p \right)^{\Phi_e} = \sum_{e=1}^{N_{be}} \left(G_p \delta q_p \right)^{\Phi_e} + \sum_{e=1}^{N_{be}} \left(\delta G_p q_p \right)^{\Phi_e}
$$

$$
(3.82)
$$

where:

- If $\mathbf{x}^i \in \Gamma$, then:

$$
\Phi^i = \left\{ \Phi_e, e = 1, \dots, N_{be} : \mathbf{x}^i \in \Phi_e \right\}
$$

$$
\Psi^i = \left\{ \Psi_d, d = 1, \dots, N_{de} : \mathbf{x}^i \in \Psi_d \right\}
$$

$$
p^i = \left(\phi_p^i p_p \right)^{\Phi^i}
$$

$$
\delta p^i = \left(\phi_p^i \delta p_p \right)^{\Phi^i}
$$

$$
v_{m,j}^i = \left(\psi_{q,j}^i v_{mq} \right)^{\Psi^i}
$$

and c^i and b_{mj}^i are calculated as shown previously according to the local geometry of the boundary at the collocation point.

- If $\mathbf{x}^i \notin \Gamma$, then $c^i = \delta_{\Omega}^i$ and $b_{mj}^i = 0$.

For a boundary element Φ associated with a design element Ψ, two different situations must be considered:

Exterior integration, $\mathbf{x}^i \notin \Phi$. All integrals are strictly regular, and standard Gauss-Legendre quadrature is able to approximate them numerically. The quadrature order mainly depends on the normalized distance $d = r_{\min}/D$, where $r_{\min}$ is the minimum distance between $\mathbf{x}^i$ and Φ, and D is the diameter of the bounding ball of Φ. As Figure 3.5 shows, the number of integration points increase as d decrease, becoming prohibitive for $d \ll 1$. For this reason, they are called nearly- or quasi-singular integrals. In order to reduce the number of integration points for a given integration error, several strategies have been proposed. Two of the most relevant non-linear transformations that smooth the integrands are the Telles transformation [56, 57] and the sinh transformation [36]. A combination of subdivision of the integration path [37] and Telles transformation is used in this work.
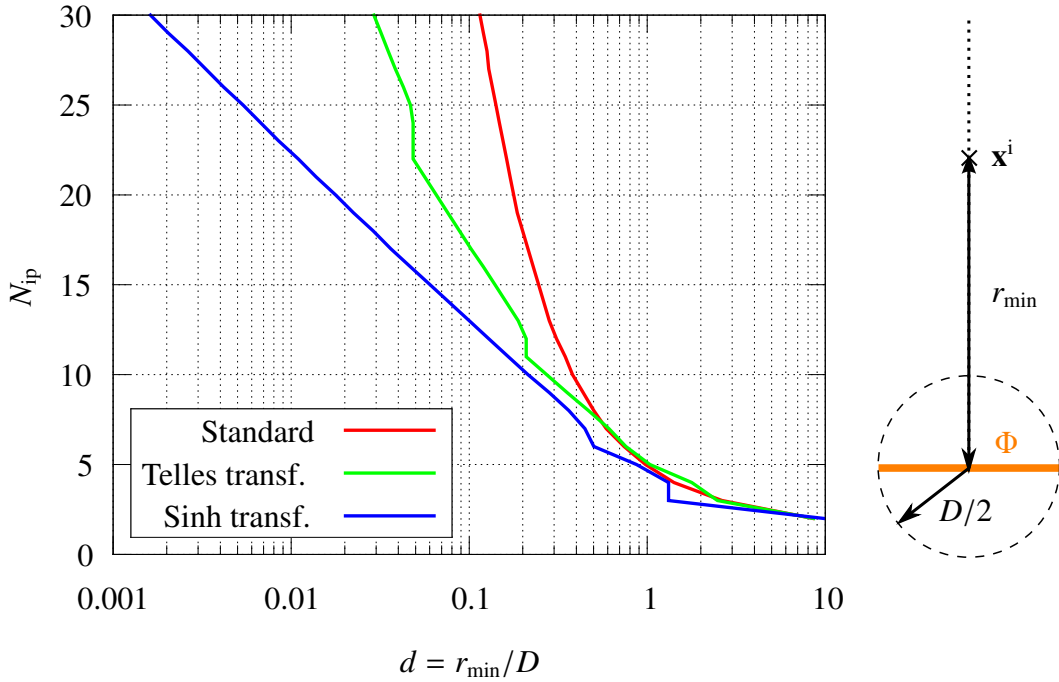

Figure 3.5: Number of integration points vs. normalized distance for integrand $I = 1/r^2$ and relative error $\epsilon = 10^{-6}$

When $\mathbf{x}^i \notin \Phi$, the contributions of a boundary element Φ similar to those of the SBIE are:

$$H_p = \int_\Phi q^* \phi_p \, \mathrm{d}\Gamma \tag{3.83}$$

$$G_p = \int_\Phi p^* \phi_p \, \mathrm{d}\Gamma \tag{3.84}$$

The contributions of the new integrals arising in the δSBIE consider separately the design velocity field along the boundary element (through the design element Ψ) and the design

velocity field at the collocation point:

$$\delta H_p = \delta H_{mqp}^{T1} v_{mq}^{\Psi} - \delta H_{mp}^{T2} v_m^{i} = \left(\delta H_{mqp}^{N1} + \delta H_{mqp}^{R1} + \delta H_{mqp}^{J1} \right) v_{mq}^{\Psi} - \delta H_{mp}^{R2} v_m^{i} \tag{3.85}$$

$$\delta G_p = \delta G_{mqp}^{T1} v_{mq}^{\Psi} - \delta G_{mp}^{T2} v_m^{i} = \left(\delta G_{mqp}^{R1} + \delta G_{mqp}^{J1} \right) v_{mq}^{\Psi} - \delta G_{mp}^{R2} v_m^{i} \tag{3.86}$$

where:

$$\delta H_{mqp}^{N1} = - \int_{\Phi} p_{,j}^{*} t_j n_m \psi_{q,k} t_k \phi_p \; \mathrm{d}\Gamma \tag{3.87}$$

$$\delta H_{mqp}^{R1} = \int_{\Phi} p_{,jm}^{*} n_j \psi_q \phi_p \; \mathrm{d}\Gamma \tag{3.88}$$

$$\delta H_{mp}^{R2} = \int_{\Phi} p_{,jm}^{*} n_j \phi_p \; \mathrm{d}\Gamma \tag{3.89}$$

$$\delta H_{mqp}^{J1} = \int_{\Phi} q^{*} t_m \psi_{q,k} t_k \phi_p \; \mathrm{d}\Gamma \tag{3.90}$$

$$\delta G_{mqp}^{R1} = \int_{\Phi} p_{,m}^{*} \psi_q \phi_p \; \mathrm{d}\Gamma \tag{3.91}$$

$$\delta G_{mp}^{R2} = \int_{\Phi} p_{,m}^{*} \phi_p \; \mathrm{d}\Gamma \tag{3.92}$$

$$\delta G_{mqp}^{J1} = \int_{\Phi} p^{*} t_m \psi_{q,k} t_k \phi_p \; \mathrm{d}\Gamma \tag{3.93}$$

Interior integration, $\mathbf{x}^i \in \Phi$. The integrals contain a singularity, which can be integrable in the Riemann sense (regular or weakly singular) or in the more general Finite Part sense. The regularization performed in the previous section leads to a set of integrals integrable in the Riemann sense, making explicit the Finite Part of the original integral. In any case, the integrand is unbounded at the collocation point, and hence no integration point can lie at it. A way to achieve this is to split the integration domain at the collocation point, and then make use of a gaussian quadrature for each subdivision. In the case of weakly singular integrals, a gaussian quadrature with weighting function $w = \ln x$ can be used in order to have a reduced number of integration points [29]. Another alternative is using the Telles transformation with a null transformation Jacobian at the singularity. The latter is used in this work.

When $\mathbf{x}^i \in \Phi$, the contributions of Φ similar to those of the SBIE are:

$$H_p = \lim_{\epsilon \to 0^{+}} \int_{\Phi - e^{i}} q^{*} \phi_p \; \mathrm{d}\Gamma \tag{3.94}$$

$$G_p = \lim_{\epsilon \to 0^{+}} \int_{\Phi - e^{i}} p^{*} \phi_p \; \mathrm{d}\Gamma \tag{3.95}$$

Since $\mathbf{x}^i \in \Phi$, the contributions of the new integrals arising in the δSBIE consider only the design velocity field along the boundary element (through the design element Ψ):

$$\delta H_p = \delta H_{mqp}^{T1} v_{mq}^{\Psi} = \left(\delta H_{mqp}^{N1} + \delta H_{mqp}^{R1} + \delta H_{mqp}^{J1}\right) v_{mq}^{\Psi} \tag{3.96}$$

$$\delta G_p = \delta G_{mqp}^{T1} v_{mq}^{\Psi} = \left(\delta G_{mqp}^{R1} + \delta G_{mqp}^{J1}\right) v_{mq}^{\Psi} \tag{3.97}$$

where:

$$\delta H_{mqp}^{N1} = \frac{1}{2\pi} \lim_{\epsilon \to 0^+} \int_{\Phi - e^i} \frac{1}{r} \frac{\partial r}{\partial \Gamma} \left(n_m \psi_{q,k} t_k \phi_p - n_m^i \psi_{q,k}^i t_k^i \phi_p^i\right)\, d\Gamma \tag{3.98}$$

$$\delta H_{mqp}^{R1} = \frac{1}{2\pi} \left\{ \int_{\Phi - e^i} \frac{2 r_{,m}}{r^2} \frac{\partial r}{\partial n} \left(\psi_q - \psi_q^i\right) \phi_p\, d\Gamma - \int_{\Phi - e^i} \frac{n_m}{r^2} \left(\psi_q - \psi_q^i - \psi_{q,j}^i r_j\right) \phi_p\, d\Gamma \right.$$
$$\left. - \int_{\Phi - e^i} \frac{1}{r} \left[n_m \phi_p \psi_{q,j}^i r_{,j} - \left(\frac{\partial r}{\partial \Gamma}\right)^i n_m^i \phi_p^i \psi_{q,j}^i t_j^i \right] d\Gamma - n_m^i \phi_p^i \psi_{q,j}^i t_j^i \int_{\Phi - e^i} \frac{1}{r} \left(\left(\frac{\partial r}{\partial \Gamma}\right)^i - \frac{\partial r}{\partial \Gamma} \right) d\Gamma \right\} \tag{3.99}$$

$$\delta H_{mqp}^{J1} = \lim_{\epsilon \to 0^+} \int_{\Phi - e^i} q^* t_m \psi_{q,k} t_k \phi_p\, d\Gamma \tag{3.100}$$

$$\delta G_{mqp}^{R1} = \lim_{\epsilon \to 0^+} \int_{\Phi - e^i} p_{,m}^* \left(\psi_q - \psi_q^i\right) \phi_p\, d\Gamma \tag{3.101}$$

$$\delta G_{mqp}^{J1} = \lim_{\epsilon \to 0^+} \int_{\Phi - e^i} p^* t_m \psi_{q,k} t_k \phi_p\, d\Gamma \tag{3.102}$$

where the limit notation $\lim_{\epsilon \to 0^+}$ before some integrals has been omitted for brevity. Note that terms involving the integral $\int 1/r\, d\Gamma$ has been removed from δH_{mqp}^{N1} and δH_{mqp}^{R1} since they cancel out when evaluating δH_{mqp}^{T1}.

The solution of the sensitivity problem requires the solution of the zero-order solution. As it is well known, the discretized form of the SBIE is:

$$c^i p^i + \sum_{e=1}^{N_{be}} \left(H_p p_p\right)^{\Phi_e} = \sum_{e=1}^{N_{be}} \left(G_p q_p\right)^{\Phi_e} \tag{3.103}$$

which is somewhat a simplified version of the δSBIE (3.82). Performing a suitable collocation of the SBIE throughout the discretization leads to the influence matrices $\mathbf{H}$ and $\mathbf{G}$, which are built by assembling free-terms and H_p integrals into $\mathbf{H}$, and G_p integrals into $\mathbf{G}$. The discretized system is transformed into a system of linear equations once the boundary conditions are applied:

$$\mathbf{H}\mathbf{p} = \mathbf{G}\mathbf{q} \quad \xrightarrow{\text{boundary conditions}} \quad \mathbf{A}\mathbf{x} = \mathbf{B}\bar{\mathbf{x}} = \mathbf{b} \tag{3.104}$$

where **A** is composed of components of **H** and **G** related to the unknown components of **p** and **q** (gathered into **x**), and **B** is composed of components of **H** and **G** related to the known components of **p** and **q** (gathered into x̄). Following a similar procedure but using the δSBIE (3.82), the first-order discretized system is:

$$\mathbf{H}\delta\mathbf{p} + \delta\mathbf{H}\mathbf{p} = \mathbf{G}\delta\mathbf{q} + \delta\mathbf{G}\mathbf{q} \xrightarrow{\text{boundary conditions}} \mathbf{A}\delta\mathbf{x} = \mathbf{B}\delta\bar{\mathbf{x}} + \delta\mathbf{G}\mathbf{q} - \delta\mathbf{H}\mathbf{p} = \mathbf{b}^\delta \quad (3.105)$$

where **A** and **B** is similar to that of the zero-order system (if the same discretization and collocation is used), and the components of $\delta\bar{\mathbf{x}}$ are related to the sensitivities of the boundary conditions. Note the parallelism between the obtained Equation (3.105) and Equation (2.3) related to the sensitivity analysis using the FEM.

3.4   Helmholtz problem

The previous section deals with the Laplace problem, which, despite being the simplest case, it is very useful to explain, discuss and understand in detail all the steps to obtain a BEM formulation for sensitivity analysis. Furthermore, the crucial part already solved for the Laplace problem is applicable with small modifications to other problems. A simple change of flux variable $f = -kq$, where f is the physical flux and k is the conductivity, make possible to use the already developed formulation for heat transfer or electrostatics problems. By expanding the fundamental solution, it is also possible to obtain the BEM formulation for the Helmholtz problem, which with simple change of flux variables allows the study of wave propagation within inviscid fluids or the anti-plane wave motion in two-dimensional elastodynamics. In the present section, the BEM formulation (SBIE and δSBIE) for sensitivity analysis for the Helmholtz problem is developed.

Concerning the BIEs, the only formal difference between the Laplace problem and the Helmholtz problem is the fundamental solution [29], which represents a dynamic event with a propagation speed c in the frequency domain ω. Being $k = \omega/c$ the wavenumber, the fundamental solution p^* and its derivatives are:

$$p^* = \frac{1}{2\pi}\text{K}_0\left(ikr\right) = \frac{1}{2\pi}P \quad (3.106)$$

$$p^*_j = \frac{1}{2\pi}\frac{\partial P}{\partial r}r_{,j} = \frac{1}{2\pi}Qr_{,j} \quad (3.107)$$

$$p^*_{jm} = \frac{1}{2\pi}\left[\frac{1}{r}\frac{\partial P}{\partial r}\delta_{jm} + \left(\frac{\partial^2 P}{\partial r^2} - \frac{1}{r}\frac{\partial P}{\partial r}\right)r_{,j}r_{,m}\right] = \frac{1}{2\pi}\left(R_1\delta_{jm} + R_2r_{,j}r_{,m}\right) \quad (3.108)$$

$$q^* = p^*_j n_j = \frac{1}{2\pi}\frac{\partial P}{\partial r}\frac{\partial r}{\partial n} = \frac{1}{2\pi}Q\frac{\partial r}{\partial n} \quad (3.109)$$

where i is the imaginary unit, and $\text{K}_n\left(z\right)$ is the modified Bessel function of the second kind of order n and argument z. Terms Q, R_1 and R_2 depend exclusively on r and k:

$$Q = -ik\text{K}_1\left(ikr\right) \quad (3.110)$$

$$R_1 = \frac{1}{r}Q \quad (3.111)$$

$$R_2 = (ik)^2\text{K}_2\left(ikr\right) \quad (3.112)$$

Bessel functions $K_n(z)$ can be decomposed in the following manner [1, Equation (9.6.11)]:

$$K_0(z) = -\ln\frac{z}{2} - \gamma + K_0^R(z)$$

$$K_1(z) = \frac{1}{z} + \frac{z}{2}\left(\ln\frac{z}{2} + \gamma - \frac{1}{2}\right) + K_1^R(z)$$

$$K_2(z) = \frac{2}{z^2} - \frac{1}{2} - \frac{z^2}{8}\left(\ln\frac{z}{2} + \gamma - \frac{3}{4}\right) + K_2^R(z)$$

(3.113)

where $\gamma = 0.5772156649\ldots$ is the Euler-Mascheroni constant. These decompositions come from extracting some terms from the infinite series that define $K_n(z)$, and gathering the rest of the terms in the residue and $K_n^R(z)$ which is of order $O(z^{n+2}\ln z)$. The ascending series are computationally competitive only for moderate values of the argument ($|z| < 7$ for double precision), whereas an asymptotic expansion [1, Equation 9.7.2] is required for larger values of the argument. By using this decomposition, P, Q, R_1 and R_2 can be written is such a way that a part depending only on r is segregated from another parts depending on r and k:

$$P = -\ln r - \ln\frac{ik}{2} - \gamma + K_0^R(ikr) = -\ln r + O\left(r^0\right)$$

(3.114)

$$Q = -\frac{1}{r} + \frac{k^2}{2}r\ln r + \frac{k^2}{2}\left(\ln\frac{ik}{2} + \gamma - \frac{1}{2}\right)r - ikK_1^R(ikr) = -\frac{1}{r} + O(r\ln r)$$

(3.115)

$$R_1 = -\frac{1}{r^2} + \frac{k^2}{2}\ln r + \frac{k^2}{2}\left(\ln\frac{ik}{2} + \gamma - \frac{1}{2}\right) - \frac{ik}{r}K_1^R(ikr) = -\frac{1}{r^2} + O(\ln r)$$

(3.116)

$$R_2 = \frac{2}{r^2} + \frac{k^2}{2} - \frac{k^4}{8}r^2\ln r - \frac{k^4}{8}\left(\ln\frac{ik}{2} + \gamma - \frac{3}{4}\right)r^2 - k^2K_2^R(ikr) = \frac{2}{r^2} + O\left(r^0\right)$$

(3.117)

Therefore, the fundamental solution and its derivatives can be written as:

$$p^* = \left(p^*\right)^{\text{static}} + \left(p^*\right)^{\text{dynamic}}$$

(3.118)

$$p_j^* = \left(p_j^*\right)^{\text{static}} + \left(p_j^*\right)^{\text{dynamic}}$$

(3.119)

$$p_{jm}^* = \left(p_{jm}^*\right)^{\text{static}} + \left(p_{jm}^*\right)^{\text{dynamic}}$$

(3.120)

$$q^* = \left(q^*\right)^{\text{static}} + \left(q^*\right)^{\text{dynamic}}$$

(3.121)

where the static parts correspond to the Laplace problem. Dynamic parts lead to at most weakly singular integrals, hence neither produce additional free-terms nor require further treatment.

3.4.1 Inviscid fluid

Consider an inviscid fluid with density ρ and bulk modulus K. The wave propagation speed is then $c = \sqrt{K/\rho}$. Within the small perturbation hypothesis, the wave propagation in this medium follows the Helmholtz equation with the dynamic pressure p as the primary variable [29]. The flux variable (secondary variable) is the fluid normal displacement u_n:

$$u_n = \frac{1}{\rho\omega^2}\frac{\partial p}{\partial n} = \frac{1}{\rho\omega^2}q$$

(3.122)

Thus, simply by making the change of variable $q = \rho\omega^2 u_n$, the formulation can be used to study this problem.

3.4.2 Anti-plane elastodynamics

Consider an elastic solid with density ρ and shear modulus μ. The shear wave propagation speed is then $c_2 = \sqrt{\mu/\rho}$. The two-dimensional analysis of the anti-plane motion is governed by the Helmholtz equation with the anti-plane displacement $u_3 = p$ as the primary variable, and $c_2 = c$ as the wave propagation speed [29]. The flux variable is now the anti-plane traction:

$$t_3 = \sigma_{3\alpha} n_\alpha = \mu u_{3,\alpha} n_\alpha = \mu q \tag{3.123}$$

where $\alpha = 1, 2$, and summation convention is implied. Hence, by making the change of variable $q = t_3/\mu$, the formulation can be used to study this problem.

3.5 Elastostatics

Consider the static analysis of an elastic solid with Poisson's ratio ν and shear modulus (or Lamé's second parameter) μ. Lamé's first parameter is then $\lambda = 2\mu\nu/(1 - 2\nu)$. The primary variable of the governing differential equations for the in-plane problem are the displacements u_k, and the secondary variables are the tractions $t_k = \sigma_{kj} n_j$, where the stress tensor is $\sigma_{kj} = \lambda u_{m,m} \delta_{kj} + \mu(u_{k,j} + u_{j,k})$, and $k, j, m = 1, 2$. In the present work, the plane strain problem is considered, although the plane stress problem can be obtained easily from it [24].

3.5.1 δSBIE for non-boundary collocation points

The Singular BIE (SBIE) for an interior or exterior collocation point with respect to the reference domain Ω can be written as [24]:

$$\delta_\Omega^i u_l^i + \int_\Gamma t_{lk}^* u_k \, \mathrm{d}\Gamma = \int_\Gamma u_{lk}^* t_k \, \mathrm{d}\Gamma, \quad \delta_\Omega^i = \begin{cases} 1, & \mathbf{x}^i \in \Omega \\ 0, & \mathbf{x}^i \notin \Omega \cup \Gamma \end{cases} \tag{3.124}$$

where the body loads have been discarded, $l = 1, 2$ is the live index related to the load direction, $k = 1, 2$ is the dummy index related to the observation direction, and:

$$u_{lk}^* = \frac{1}{8\pi\mu(1-\nu)} \left[-\delta_{lk}(3 - 4\nu) \ln r + r_{,l} r_{,k} \right] \tag{3.125}$$

$$u_{lk,j}^* = \frac{1}{8\pi\mu(1-\nu)} \frac{1}{r} \left[-\delta_{lk}(3 - 4\nu) r_{,j} + \delta_{jl} r_{,k} + \delta_{kj} r_{,l} - 2r_{,l} r_{,k} r_{,j} \right] \tag{3.126}$$

$$\sigma_{lkm}^* = \lambda u_{lj,j}^* \delta_{km} + \mu \left(u_{lk,m}^* + u_{lm,k}^* \right) \tag{3.127}$$

$$\sigma_{lkm}^* = -\frac{1}{4\pi(1-\nu)} \frac{1}{r} \left[2r_{,l} r_{,k} r_{,m} + (1 - 2\nu)\left(\delta_{lk} r_{,m} + \delta_{lm} r_{,k} - \delta_{km} r_{,l} \right) \right] \tag{3.128}$$

$$t_{lk}^* = \sigma_{lkm}^* n_m \tag{3.129}$$

$$t_{lk}^* = -\frac{1}{4\pi(1-\nu)} \frac{1}{r} \left\{ \frac{\partial r}{\partial n} \left[\delta_{lk}(1 - 2\nu) + 2r_{,l} r_{,k} \right] + (1 - 2\nu)\left(n_l r_{,k} - n_k r_{,l} \right) \right\} \tag{3.130}$$

Likewise, for the perturbed domain $\tilde{\Omega}$:

$$\delta_{\tilde{\Omega}}^{\mathrm{i}}\tilde{u}_l^{\mathrm{i}} + \int_{\Gamma} \tilde{t}_{lk}^* \tilde{u}_k \, \mathrm{d}\tilde{\Gamma} = \int_{\Gamma} \tilde{u}_{lk}^* \tilde{t}_k \, \mathrm{d}\tilde{\Gamma}, \quad \delta_{\tilde{\Omega}}^{\mathrm{i}} = \begin{cases} 1, & \mathbf{x}^{\mathrm{i}} \in \tilde{\Omega} \\ 0, & \mathbf{x}^{\mathrm{i}} \notin \tilde{\Omega} \cup \tilde{\Gamma} \end{cases} \tag{3.131}$$

As seen in previous sections, the relationships of geometrical objects and variables between the reference domain Ω and the perturbed domain $\tilde{\Omega}$ are given by linear mappings:

$$\tilde{u}_k^{\mathrm{i}} = u_k^{\mathrm{i}} + \delta u_k^{\mathrm{i}}\left(a - a^0\right) \tag{3.132}$$

$$\tilde{u}_k = u_k + \delta u_k\left(a - a^0\right) \tag{3.133}$$

$$\tilde{u}_{k,j} = u_{k,j} + \delta u_{k,j}\left(a - a^0\right) \tag{3.134}$$

$$\tilde{n}_j = n_j + \delta n_j\left(a - a^0\right) \tag{3.135}$$

$$\tilde{\sigma}_{kj} = \lambda\tilde{u}_{m,m}\delta_{kj} + \mu(\tilde{u}_{k,j} + \tilde{u}_{j,k}) = \sigma_{kj} + \delta\tilde{\sigma}_{kj}\left(a - a^0\right) \tag{3.136}$$

$$\tilde{t}_k = \tilde{\sigma}_{kj}\tilde{n}_j = \sigma_{kj}n_j + \left(\sigma_{kj}\delta n_j + \delta\sigma_{kj}n_j\right)\left(a - a^0\right) = t_k + \delta t_k\left(a - a^0\right) \tag{3.137}$$

$$\mathrm{d}\tilde{\Gamma} = \left[1 + \delta J\left(a - a^0\right)\right] \, \mathrm{d}\Gamma \tag{3.138}$$

where only linear terms $(a - a^0)$ are kept. The fundamental solution u_{lk}^* depends on the observation and collocation points $u_{lk}^* = u_{lk}^*(\mathbf{x}, \mathbf{x}^{\mathrm{i}})$, hence its linear mapping must be built from the Taylor's expansion with respect to both points. As seen with the Laplace problem, this means that the linear mapping can be written as:

$$\tilde{u}_{lk}^* = u_{lk}^* + u_{lk,j}^*\delta r_j\left(a - a^0\right) = u_{lk}^* + \delta u_{lk}^*\left(a - a^0\right) \tag{3.139}$$

The linear mapping of $\tilde{t}_{lk}^*$ is built by using the linear mapping of its components:

$$\begin{aligned}
\tilde{t}_{lk}^* = \tilde{\sigma}_{lkm}^*\tilde{n}_m &= \left[\sigma_{lkm}^* + \sigma_{lkm,j}^*\delta r_j\left(a - a^0\right)\right]\left[n_m + \delta n_m\left(a - a^0\right)\right] \\
&= \sigma_{lkm}^*n_m + \left(\sigma_{lkm}^*\delta n_m + \sigma_{lkm,j}^*\delta r_j n_m\right)\left(a - a^0\right) \\
&= t_{lk}^* + \delta t_{lk}^*\left(a - a^0\right)
\end{aligned} \tag{3.140}$$

and keeping only linear terms $(a - a^0)$. Note that $\sigma_{lkm,j}^*$ is obtained by differentiation of Equation (3.128):

$$\begin{aligned}
\sigma_{lkm,j}^* = -\frac{1}{4\pi\left(1 - \nu\right)}\frac{1}{r^2}\Big[&- 8r_{,l}r_{,k}r_{,m}r_{,j} - 2\left(1 - 2\nu\right)\left(\delta_{lk}r_{,m}r_{,j} + \delta_{lm}r_{,k}r_{,j} - \delta_{km}r_{,l}r_{,j}\right) \\
&+ 2\left(\delta_{lj}r_{,k}r_{,m} + \delta_{kj}r_{,l}r_{,m} + \delta_{mj}r_{,l}r_{,k}\right) + \left(1 - 2\nu\right)\left(\delta_{lk}\delta_{mj} + \delta_{lm}\delta_{kj} - \delta_{km}\delta_{lj}\right)\Big]
\end{aligned} \tag{3.141}$$

Finally, substituting all these linear mappings into Equation (3.131), keeping only linear terms $(a - a^0)$, substracting Equation (3.124) from it, and dropping out $(a - a^0)$ terms, give the sensitivity SBIE (or δSBIE):

$$\delta_{\Omega}^{\mathrm{i}}\delta u_l^{\mathrm{i}} + \int_{\Gamma} t_{lk}^*\delta u_k \, \mathrm{d}\Gamma + \int_{\Gamma} \left(\delta t_{lk}^* + t_{lk}^*\delta J\right) u_k \, \mathrm{d}\Gamma = \int_{\Gamma} u_{lk}^*\delta t_k \, \mathrm{d}\Gamma + \int_{\Gamma} \left(\delta u_{lk}^* + u_{lk}^*\delta J\right) t_k \, \mathrm{d}\Gamma \tag{3.142}$$

The first and third integrals are similar to the integrals of the SBIE, except that now the sensitivities δu_k and δt_k appear. The second and fourth integrals are new integrals that depend on u_k and t_k, thus they can be evaluated only once the zero-order solution is known.

3.5.2 δSBIE for boundary collocation points

The process to obtain the δSBIE for boundary collocation points is analogous to the process performed for the Laplace problem, so many aspects are skipped and assumed similar here. The limiting process is also done from an interior collocation point ($\delta_\Omega^i = 1$). The integration path of the integrals of Equation (3.142) is modified according to Equation (3.41), then:

$$\int_\Gamma (\dots)\ \mathrm{d}\Gamma = \lim_{\epsilon \to 0^+} \int_{\Gamma^i} (\dots)\ \mathrm{d}\Gamma + \lim_{\epsilon \to 0^+} \int_{\Gamma - e^i} (\dots)\ \mathrm{d}\Gamma \tag{3.143}$$

Integration over Γ^i In order to perform the integration over the arc Γ^i, a polar system of coordinates centered at the collocation point is used, see Section 3.3.2. Assuming that the displacement sensitivity is continuous, i.e. $\delta u_k = \delta u_k^i + O(\epsilon)$, the evaluation of the first integral of Equation (3.142) leads to:

$$\delta u_l^i + \lim_{\epsilon \to 0^+} \int_{\Gamma^i} t_{lk}^* \delta u_k\ \mathrm{d}\Gamma = \left[\delta_{lk} - \frac{1}{4\pi(1-\nu)} \left((1-2\nu)\delta_{lk}\Delta\theta^{\mathrm{ext}} + 2\int_{\theta_1}^{\theta_2} n_l n_k\ \mathrm{d}\theta \right) \right] \delta u_k^i \tag{3.144}$$
$$= c_{lk}^i \delta u_k^i$$

where c_{lk}^i is the well-known elastic free-term:

$$\left(c_{lk}^i \right) = \frac{\Delta\theta^{\mathrm{ext}}}{2\pi}\left(\delta_{lk} \right) - \frac{1}{8\pi(1-\nu)} \begin{pmatrix} \sin 2\theta_2 - \sin 2\theta_1 & -(\cos 2\theta_2 - \cos 2\theta_1) \\ -(\cos 2\theta_2 - \cos 2\theta_1) & -(\sin 2\theta_2 - \sin 2\theta_1) \end{pmatrix} \tag{3.145}$$

Given that the displacement is continuous: $u_k = u_k^i + O(\epsilon)$; and the design velocity field is differentiable: $v_m = v_m^i + v_{m,j}^i r_j \epsilon + O(\epsilon^2)$; the second integral of Equation (3.142) can be written as:

$$\lim_{\epsilon \to 0^+} \int_{\Gamma^i} \left(\delta t_{lk}^* + t_{lk}^* \delta J \right) u_k\ \mathrm{d}\Gamma = \lim_{\epsilon \to 0^+} \int_{\Gamma^i} \left(\sigma_{lkm}^* \delta n_m + \sigma_{lkm,j}^* \delta r_j n_m + t_{lk}^* \delta J \right) u_k\ \mathrm{d}\Gamma = b_{lkjm}^i v_{j,m}^i u_k^i$$
$$\tag{3.146}$$

where b_{lkjm}^i is:

$$b_{lkjm}^i = -\frac{1}{4\pi(1-\nu)} \left[-6\int_{\theta_1}^{\theta_2} n_l n_k n_j n_m\ \mathrm{d}\theta - (1-2\nu)\delta_{lk}\int_{\theta_1}^{\theta_2} n_j n_m\ \mathrm{d}\theta \right.$$

$$+ (1+2\nu)\delta_{lj}\int_{\theta_1}^{\theta_2} n_k n_m\ \mathrm{d}\theta + (3-2\nu)\delta_{kj}\int_{\theta_1}^{\theta_2} n_l n_m\ \mathrm{d}\theta - (1-2\nu)\int_{\theta_1}^{\theta_2} t_l n_k n_j t_m\ \mathrm{d}\theta$$

$$\left. + (1-2\nu)\int_{\theta_1}^{\theta_2} n_l t_k n_j t_m\ \mathrm{d}\theta + 2\int_{\theta_1}^{\theta_2} n_l n_k t_j t_m\ \mathrm{d}\theta + (1-2\nu)\delta_{lk}\int_{\theta_1}^{\theta_2} t_j t_m\ \mathrm{d}\theta \right] \tag{3.147}$$

50

and its evaluation can be found in Appendix A. The new free-term b^{i}_{lkjm} is null if the collocation point is located at a smooth boundary point. Assuming that traction t_k and traction sensitivity δt_k are bounded, the third and fourth integrals of Equation (3.142) are null:

$$\lim_{\epsilon \to 0^+} \int_{\Gamma^{\mathrm{i}}} u^*_{lk}\delta t_k \ \mathrm{d}\Gamma = 0 \tag{3.148}$$

$$\lim_{\epsilon \to 0^+} \int_{\Gamma^{\mathrm{i}}} \left(\delta u^*_{lk} + u^*_{lk}\delta J\right) t_k \ \mathrm{d}\Gamma = 0 \tag{3.149}$$

Therefore, after performing the integration over Γ^{i}, the δSBIE for boundary collocation points can be written as:

$$c^{\mathrm{i}}_{lk}\delta u^{\mathrm{i}}_k + b^{\mathrm{i}}_{lkjm}v^{\mathrm{i}}_{j,m}u^{\mathrm{i}}_k + \lim_{\epsilon \to 0^+} \int_{\Gamma - e^{\mathrm{i}}} t^*_{lk}\delta u_k \ \mathrm{d}\Gamma + \lim_{\epsilon \to 0^+} \int_{\Gamma - e^{\mathrm{i}}} \left(\delta t^*_{lk} + t^*_{lk}\delta J\right) u_k \ \mathrm{d}\Gamma$$

$$= \lim_{\epsilon \to 0^+} \int_{\Gamma - e^{\mathrm{i}}} u^*_{lk}\delta t_k \ \mathrm{d}\Gamma + \lim_{\epsilon \to 0^+} \int_{\Gamma - e^{\mathrm{i}}} \left(\delta u^*_{lk} + u^*_{lk}\delta J\right) t_k \ \mathrm{d}\Gamma \tag{3.150}$$

Integration over $\Gamma - e^{\mathrm{i}}$ The first integral of Equation (3.150) is clearly strongly singular:

$$H_l = \lim_{\epsilon \to 0^+} \int_{\Gamma - e^{\mathrm{i}}} t^*_{lk}\delta u_k \ \mathrm{d}\Gamma \ \text{is strongly singular} \ \because \ t^*_{lk} = O\left(r^{-1}\right) \tag{3.151}$$

The term leading to the strongly singular part can be segregated:

$$H_l = -\frac{1}{4\pi\left(1-v\right)}\left\{\lim_{\epsilon \to 0^+} \int_{\Gamma - e^{\mathrm{i}}} \frac{1}{r}\frac{\partial r}{\partial n}\left[\delta_{lk}\left(1-2v\right) + 2r_{,l}r_{,k}\right]\delta u_k \ \mathrm{d}\Gamma \right.$$

$$\left. + \left(1-2v\right)\lim_{\epsilon \to 0^+} \int_{\Gamma - e^{\mathrm{i}}} \frac{1}{r}\left(n_l r_{,k} - n_k r_{,l}\right)\delta u_k \ \mathrm{d}\Gamma\right\} \tag{3.152}$$

Because the displacement sensitivity is continuous, one can add and substract δu^{i}_k from δu_k in order to further segregate the strongly singular term:

$$H_l = -\frac{1}{4\pi\left(1-v\right)}\left\{\lim_{\epsilon \to 0^+} \int_{\Gamma - e^{\mathrm{i}}} \frac{1}{r}\frac{\partial r}{\partial n}\left[\delta_{lk}\left(1-2v\right) + 2r_{,l}r_{,k}\right]\delta u_k \ \mathrm{d}\Gamma \right.$$

$$\left. + \left(1-2v\right)\left[\lim_{\epsilon \to 0^+} \int_{\Gamma - e^{\mathrm{i}}} \frac{1}{r}\left(n_l r_{,k} - n_k r_{,l}\right)\left(\delta u_k - \delta u^{\mathrm{i}}_k\right) \ \mathrm{d}\Gamma + \delta u^{\mathrm{i}}_k\lim_{\epsilon \to 0^+} \int_{\Gamma - e^{\mathrm{i}}} \frac{1}{r}\left(n_l r_{,k} - n_k r_{,l}\right) \ \mathrm{d}\Gamma\right]\right\}$$

$$\tag{3.153}$$

It is easy to see that:

$$\frac{\partial r}{\partial \Gamma} = r_{,1}t_{,1} + r_{,2}t_{,2} = -r_{,1}n_2 + r_{,2}n_1 = n_1 r_{,2} - n_2 r_{,1} \Rightarrow n_l r_{,k} - n_k r_{,l} = \epsilon_{lk}\frac{\partial r}{\partial \Gamma} \quad (3.154)$$

Hence, the regularized integral can be written as:

$$H_l = -\frac{1}{4\pi(1-\nu)}\left\{\lim_{\epsilon\to 0^+}\int_{\Gamma-e^i}\frac{1}{r}\frac{\partial r}{\partial n}\Big[\delta_{lk}(1-2\nu) + 2r_{,l}r_{,k}\Big]\delta u_k \ \mathrm{d}\Gamma\right.$$

$$\left. + (1-2\nu)\left[\lim_{\epsilon\to 0^+}\int_{\Gamma-e^i}\frac{1}{r}(n_l r_{,k} - n_k r_{,l})\left(\delta u_k - \delta u_k^i\right) \ \mathrm{d}\Gamma + \epsilon_{lk}\delta u_k^i \lim_{\epsilon\to 0^+}\int_{\Gamma-e^i}\frac{1}{r} \ \mathrm{d}r\right]\right\}$$
$$(3.155)$$

where $\int 1/r \ \mathrm{d}r$ is analytically solvable. The second integral of Equation (3.150) can be split into three integrals:

$$\delta H_l = \lim_{\epsilon\to 0^+}\int_{\Gamma-e^i}\left(\delta t_{lk}^* + t_{lk}^*\delta J\right)u_k \ \mathrm{d}\Gamma = \lim_{\epsilon\to 0^+}\int_{\Gamma^i}\left(\sigma_{lkm}^*\delta n_m + \sigma_{lkm,j}^*\delta r_j n_m + t_{lk}^*\delta J\right)u_k \ \mathrm{d}\Gamma$$
$$(3.156)$$
$$= \delta H_l^N + \delta H_l^R + \delta H_l^J$$

δH_l^N is a strongly singular integral:

$$\delta H_l^N = \lim_{\epsilon\to 0^+}\int_{\Gamma-e^i}\sigma_{lkm}^*\delta n_m u_k \ \mathrm{d}\Gamma \text{ is strongly singular } \because \sigma_{lkm}^* = O\left(r^{-1}\right) \quad (3.157)$$

If its integrand is expanded, two integrals are obtained:

$$\delta H_l^N = -\lim_{\epsilon\to 0^+}\int_{\Gamma-e^i}\sigma_{lkm}^* t_m n_r v_{r,s} t_s u_k \ \mathrm{d}\Gamma$$

$$= \frac{1}{4\pi(1-\nu)}\lim_{\epsilon\to 0^+}\int_{\Gamma-e^i}\frac{1}{r}\left[2r_{,l}r_{,k}\frac{\partial r}{\partial \Gamma} + (1-2\nu)\left(\delta_{lk}\frac{\partial r}{\partial \Gamma} + t_l r_{,k} - t_k r_{,l}\right)\right]n_r v_{r,s} t_s u_k \ \mathrm{d}\Gamma$$

$$= \frac{1}{4\pi(1-\nu)}\left\{(1-2\nu)\lim_{\epsilon\to 0^+}\int_{\Gamma-e^i}\frac{1}{r}(t_l r_{,k} - t_k r_{,l})n_r v_{r,s} t_s u_k \ \mathrm{d}\Gamma\right.$$

$$\left. + \lim_{\epsilon\to 0^+}\int_{\Gamma-e^i}\frac{1}{r}\frac{\partial r}{\partial \Gamma}\Big[2r_{,l}r_{,k} + (1-2\nu)\delta_{lk}\Big]n_r v_{r,s} t_s u_k \ \mathrm{d}\Gamma\right\} \quad (3.158)$$

where the first integral is regular because $t_l r_{,k} - t_k r_{,l} = O(r)$. In the second integral, it is possible to add and substract $n_r^i v_{r,s}^i t_s^i$ from $n_r v_{r,s} t_s u_k$:

$$\delta H_l^N = \frac{1}{4\pi(1-\nu)}\left\{(1-2\nu)\lim_{\epsilon\to 0^+}\int_{\Gamma-e^i}\frac{1}{r}(t_l r_{,k} - t_k r_{,l})\,n_r v_{r,s} t_s u_k\,\mathrm{d}\Gamma\right.$$

$$+\lim_{\epsilon\to 0^+}\int_{\Gamma-e^i}\frac{1}{r}\frac{\partial r}{\partial \Gamma}\left[2r_{,l}r_{,k}+(1-2\nu)\delta_{lk}\right]\left(n_r v_{r,s} t_s u_k - n_r^i v_{r,s}^i t_s^i u_k^i\right)\,\mathrm{d}\Gamma$$

$$\left.+n_r^i v_{r,s}^i t_s^i u_k^i \lim_{\epsilon\to 0^+}\int_{\Gamma-e^i}\frac{1}{r}\frac{\partial r}{\partial \Gamma}\left[2r_{,l}r_{,k}+(1-2\nu)\delta_{lk}\right]\,\mathrm{d}\Gamma\right\} \quad (3.159)$$

where new regular and strongly singular integrals are obtained. In the new strongly singular integral, one of its terms lead to an integral $\int 1/r\,\mathrm{d}r$:

$$\delta H_l^N = \frac{1}{4\pi(1-\nu)}\left\{(1-2\nu)\lim_{\epsilon\to 0^+}\int_{\Gamma-e^i}\frac{1}{r}(t_l r_{,k} - t_k r_{,l})\,n_r v_{r,s} t_s u_k\,\mathrm{d}\Gamma\right.$$

$$+\lim_{\epsilon\to 0^+}\int_{\Gamma-e^i}\frac{1}{r}\frac{\partial r}{\partial \Gamma}\left[2r_{,l}r_{,k}+(1-2\nu)\delta_{lk}\right]\left(n_r v_{r,s} t_s u_k - n_r^i v_{r,s}^i t_s^i u_k^i\right)\,\mathrm{d}\Gamma$$

$$\left.+n_r^i v_{r,s}^i t_s^i u_k^i\left[(1-2\nu)\delta_{lk}\lim_{\epsilon\to 0^+}\int_{\Gamma-e^i}\frac{1}{r}\,\mathrm{d}r+2\lim_{\epsilon\to 0^+}\int_{\Gamma-e^i}\frac{1}{r}\frac{\partial r}{\partial \Gamma}r_{,l}r_{,k}\,\mathrm{d}\Gamma\right]\right\} \quad (3.160)$$

and the other term can be expanded as:

$$r_{,l}r_{,k}=\left(\frac{\partial r}{\partial \Gamma}\right)^i t_l^i\left(\frac{\partial r}{\partial \Gamma}\right)^i t_k^i + O(r) = t_l^i t_k^i + O(r) \quad (3.161)$$

which leads to:

$$\delta H_l^N = \frac{1}{4\pi(1-\nu)}\left\{(1-2\nu)\lim_{\epsilon\to 0^+}\int_{\Gamma-e^i}\frac{1}{r}(t_l r_{,k} - t_k r_{,l})\,n_r v_{r,s} t_s u_k\,\mathrm{d}\Gamma\right.$$

$$+\lim_{\epsilon\to 0^+}\int_{\Gamma-e^i}\frac{1}{r}\frac{\partial r}{\partial \Gamma}\left[2r_{,l}r_{,k}+(1-2\nu)\delta_{lk}\right]\left(n_r v_{r,s} t_s u_k - n_r^i v_{r,s}^i t_s^i u_k^i\right)\,\mathrm{d}\Gamma$$

$$\left.+n_r^i v_{r,s}^i t_s^i u_k^i\left[2\lim_{\epsilon\to 0^+}\int_{\Gamma-e^i}\frac{1}{r}\frac{\partial r}{\partial \Gamma}\left(r_{,l}r_{,k}-t_l^i t_k^i\right)\,\mathrm{d}\Gamma+\left[(1-2\nu)\delta_{lk}+2t_l^i t_k^i\right]\lim_{\epsilon\to 0^+}\int_{\Gamma-e^i}\frac{1}{r}\,\mathrm{d}r\right]\right\}$$

$$(3.162)$$

Hence, δH_l^N can be written as a set of regular integrals and one integral $\int 1/r\,\mathrm{d}r$. The integral δH_l^R is also strongly singular:

$$\delta H_l^R = \lim_{\epsilon\to 0^+}\int_{\Gamma-e^i}\sigma_{lkm,j}^* \delta r_j n_m u_k\,\mathrm{d}\Gamma \text{ is strongly singular } \because \underbrace{\sigma_{lkm,j}^*}_{O(r^{-2})}\underbrace{\delta r_j}_{O(r)} = O\left(r^{-1}\right) \quad (3.163)$$

If the following part of the integrand is expanded:

$$\sigma^*_{lkm,j} n_m = -\frac{1}{4\pi\left(1-v\right)} \left\{ \frac{1}{r^2}\frac{\partial r}{\partial n}\left[-8r_{,l}r_{,k}r_{,j} - 2\left(1-2v\right)\delta_{lk}r_{,j} + 2\left(\delta_{lj}r_{,k} + \delta_{kj}r_{,l}\right)\right] \right.$$

$$\left. + \frac{1}{r^2}\left[-2\left(1-2v\right)r_{,j}\left(n_l r_{,k} - n_k r_{,l}\right) + 2n_j r_{,l}r_{,k} + \left(1-2v\right)\left(\delta_{lk}n_j + \delta_{kj}n_l - \delta_{lj}n_k\right)\right]\right\}$$

$$= \underbrace{\tilde{\sigma}^a_{lkj}}_{O(r^{-1})} + \underbrace{\tilde{\sigma}^b_{lkj}}_{O(r^{-2})} \quad (3.164)$$

It is easy to see that $\tilde{\sigma}^a_{lkj}$ leads to a regular integral while $\tilde{\sigma}^b_{lkj}$ leads to a strongly singular integral:

$$\delta H^R_l = \lim_{\epsilon\to0^+}\int_{\Gamma-e^i}\tilde{\sigma}^a_{lkj}\left(v_j - v^i_j\right)u_k\,\mathrm{d}\Gamma + \lim_{\epsilon\to0^+}\int_{\Gamma-e^i}\tilde{\sigma}^b_{lkj}\left(v_j - v^i_j\right)u_k\,\mathrm{d}\Gamma \quad (3.165)$$

Given that the design velocity field is differentiable, i.e. $v_j - v^i_j - v^i_{j,s}r_s = O\left(r^2\right)$, one can add and substract $v^i_{j,s}r_s$ from δr_j leading to new regular and strongly singular integrals:

$$\delta H^R_l = \lim_{\epsilon\to0^+}\int_{\Gamma-e^i}\tilde{\sigma}^a_{lkj}\left(v_j - v^i_j\right)u_k\,\mathrm{d}\Gamma + \lim_{\epsilon\to0^+}\int_{\Gamma-e^i}\tilde{\sigma}^b_{lkj}\left(v_j - v^i_j - v^i_{j,s}r_s\right)u_k\,\mathrm{d}\Gamma$$

$$+ \lim_{\epsilon\to0^+}\int_{\Gamma-e^i} r\tilde{\sigma}^b_{lkj}v^i_{j,s}r_s u_k\,\mathrm{d}\Gamma \quad (3.166)$$

This new strongly singular integral can be further reduced by adding and substracting $\lim_{r\to0}\left(r_{,s}u_k\right) = \left(\partial r/\partial\Gamma\right)^i t^i_s u^i_k$ to $r_{,s}u_k$:

$$\delta H^R_l = \lim_{\epsilon\to0^+}\int_{\Gamma-e^i}\tilde{\sigma}^a_{lkj}\left(v_j - v^i_j\right)u_k\,\mathrm{d}\Gamma + \lim_{\epsilon\to0^+}\int_{\Gamma-e^i}\tilde{\sigma}^b_{lkj}\left(v_j - v^i_j - v^i_{j,s}r_s\right)u_k\,\mathrm{d}\Gamma$$

$$+ \lim_{\epsilon\to0^+}\int_{\Gamma-e^i} r\tilde{\sigma}^b_{lkj}\left(v^i_{j,s}r_s u_k - v^i_{j,s}\left(\frac{\partial r}{\partial\Gamma}\right)^i t^i_s u^i_k\right)\,\mathrm{d}\Gamma + v^i_{j,s}t^i_s u^i_k \lim_{\epsilon\to0^+}\int_{\Gamma-e^i} r\tilde{\sigma}^b_{lkj}\left(\frac{\partial r}{\partial\Gamma}\right)^i\,\mathrm{d}\Gamma$$

$$(3.167)$$

The latter integral can be expanded and written as:

$$A = \lim_{\epsilon\to0^+}\int_{\Gamma-e^i} r\tilde{\sigma}^b_{lkj}\left(\frac{\partial r}{\partial\Gamma}\right)^i\,\mathrm{d}\Gamma = -\frac{1}{4\pi\left(1-v\right)}\lim_{\epsilon\to0^+}\int_{\Gamma-e^i}\frac{1}{r}\left(\frac{\partial r}{\partial\Gamma}\right)^i\left[-2\left(1-2v\right)r_{,j}\left(n_l r_{,k} - n_k r_{,l}\right)\right.$$

$$\left. + 2n_j r_{,l}r_{,k} + \left(1-2v\right)\left(\delta_{lk}n_j + \delta_{kj}n_l - \delta_{lj}n_k\right)\right]\,\mathrm{d}\Gamma \quad (3.168)$$

54

By adding and substracting the following, already used, expansions: $r_{,j} = (\partial r/\partial\Gamma)^{\mathrm{i}}\, t^{\mathrm{i}}_j +$ $O(r)$, $r_{,l}r_{,k} = t^{\mathrm{i}}_l t^{\mathrm{i}}_k + O(r)$ and $n_j = n^{\mathrm{i}}_j + O(r)$; it can be written as:

$$
\begin{aligned}
A = -\frac{1}{4\pi(1-v)} \Bigg\{ &\lim_{\epsilon\to 0^+} \int\limits_{\Gamma-e^{\mathrm{i}}} \frac{1}{r}\left(\frac{\partial r}{\partial\Gamma}\right)^{\mathrm{i}} \Bigg[-2(1-2v)\left(r_{,j} - \left(\frac{\partial r}{\partial\Gamma}\right)^{\mathrm{i}} t^{\mathrm{i}}_j\right)(n_l r_{,k} - n_k r_{,l}) \\
&+ 2\left(n_j r_{,l} r_{,k} - n^{\mathrm{i}}_j t^{\mathrm{i}}_l t^{\mathrm{i}}_k\right) + (1-2v)\left(\delta_{lk}\left(n_j - n^{\mathrm{i}}_j\right) + \delta_{kj}\left(n_l - n^{\mathrm{i}}_l\right) - \delta_{lj}\left(n_k - n^{\mathrm{i}}_k\right)\right) \Bigg]\,\mathrm{d}\Gamma \\
&- 2(1-2v)\, t^{\mathrm{i}}_j \lim_{\epsilon\to 0^+} \int\limits_{\Gamma-e^{\mathrm{i}}} \frac{1}{r}\,(n_l r_{,k} - n_k r_{,l})\ \mathrm{d}\Gamma \\
&+ \left[2n^{\mathrm{i}}_j t^{\mathrm{i}}_l t^{\mathrm{i}}_k + (1-2v)\left(\delta_{lk}n^{\mathrm{i}}_j + \delta_{kj}n^{\mathrm{i}}_l - \delta_{lj}n^{\mathrm{i}}_k\right)\right] \lim_{\epsilon\to 0^+} \int\limits_{\Gamma-e^{\mathrm{i}}} \frac{1}{r}\left(\frac{\partial r}{\partial\Gamma}\right)^{\mathrm{i}}\,\mathrm{d}\Gamma \Bigg\} \quad (3.169)
\end{aligned}
$$

where the second integral is similar to the strongly singular integral appearing in the regularization process of H_l. Also, it is easy to see by inspection that $\delta_{kj}n^{\mathrm{i}}_l - \delta_{lj}n^{\mathrm{i}}_k = \epsilon_{lk}t^{\mathrm{i}}_j$. The third integral can be regularized by adding and substracting $\partial r/\partial\Gamma$ to $(\partial r/\partial\Gamma)^{\mathrm{i}}$:

$$
\begin{aligned}
A = -\frac{1}{4\pi(1-v)} \Bigg\{ &\lim_{\epsilon\to 0^+} \int\limits_{\Gamma-e^{\mathrm{i}}} \frac{1}{r}\left(\frac{\partial r}{\partial\Gamma}\right)^{\mathrm{i}} \Bigg[-2(1-2v)\left(r_{,j} - \left(\frac{\partial r}{\partial\Gamma}\right)^{\mathrm{i}} t^{\mathrm{i}}_j\right)(n_l r_{,k} - n_k r_{,l}) \\
&+ 2\left(n_j r_{,l} r_{,k} - n^{\mathrm{i}}_j t^{\mathrm{i}}_l t^{\mathrm{i}}_k\right) + (1-2v)\left(\delta_{lk}\left(n_j - n^{\mathrm{i}}_j\right) + \delta_{kj}\left(n_l - n^{\mathrm{i}}_l\right) - \delta_{lj}\left(n_k - n^{\mathrm{i}}_k\right)\right) \Bigg]\,\mathrm{d}\Gamma \\
&+ \left[2n^{\mathrm{i}}_j t^{\mathrm{i}}_l t^{\mathrm{i}}_k + (1-2v)\left(\delta_{lk}n^{\mathrm{i}}_j + \epsilon_{lk}t^{\mathrm{i}}_j\right)\right] \lim_{\epsilon\to 0^+} \int\limits_{\Gamma-e^{\mathrm{i}}} \frac{1}{r}\left(\left(\frac{\partial r}{\partial\Gamma}\right)^{\mathrm{i}} - \frac{\partial r}{\partial\Gamma}\right)\,\mathrm{d}\Gamma \\
&+ \left[n^{\mathrm{i}}_j\left(2t^{\mathrm{i}}_l t^{\mathrm{i}}_k + (1-2v)\delta_{lk}\right) - (1-2v)\epsilon_{lk}t^{\mathrm{i}}_j\right] \lim_{\epsilon\to 0^+} \int\limits_{\Gamma-e^{\mathrm{i}}} \frac{1}{r}\,\mathrm{d}r \Bigg\} \quad (3.170)
\end{aligned}
$$

Therefore, δH^{R}_l can be written as a set of regular integrals and an integral $\int 1/r\ \mathrm{d}r$. The integral δH^{J}_l can be easily regularized. If, in the first place, the expansion of $\delta J = t^*_{lk}t_j v_{j,s}t_s = t^{\mathrm{i}}_j v^{\mathrm{i}}_{j,s}t^{\mathrm{i}}_s + O(r)$ is considered:

$$
\begin{aligned}
\delta H^{\mathrm{J}}_l &= \lim_{\epsilon\to 0^+} \int\limits_{\Gamma-e^{\mathrm{i}}} t^*_{lk}\delta J u_k\ \mathrm{d}\Gamma = \lim_{\epsilon\to 0^+} \int\limits_{\Gamma-e^{\mathrm{i}}} t^*_{lk}t_j v_{j,s}t_s u_k\ \mathrm{d}\Gamma \\
&= \lim_{\epsilon\to 0^+} \int\limits_{\Gamma-e^{\mathrm{i}}} t^*_{lk}\left(t_j v_{j,s}t_s - t^{\mathrm{i}}_j v^{\mathrm{i}}_{j,s}t^{\mathrm{i}}_s\right)u_k\ \mathrm{d}\Gamma + t^{\mathrm{i}}_j v^{\mathrm{i}}_{j,s}t^{\mathrm{i}}_s \lim_{\epsilon\to 0^+} \int\limits_{\Gamma-e^{\mathrm{i}}} t^*_{lk}u_k\ \mathrm{d}\Gamma \quad (3.171)
\end{aligned}
$$

then the resulting strongly singular integral is similar to H_l. Hence, the regularized form of δH_l^J can be written as:

$$\delta H_l^J = \lim_{\epsilon \to 0^+} \int_{\Gamma - e^i} t_{lk}^* \left(t_j v_{j,s} t_s - t_j^i v_{j,s}^i t_s^i \right) u_k \, d\Gamma$$

$$- \frac{1}{4\pi(1-\nu)} t_j^i v_{j,s}^i t_s^i \left\{ \lim_{\epsilon \to 0^+} \int_{\Gamma - e^i} \frac{1}{r} \frac{\partial r}{\partial n} \left[\delta_{lk}(1-2\nu) + 2r_{,l} r_{,k} \right] u_k \, d\Gamma \right.$$

$$\left. + (1-2\nu) \left[\lim_{\epsilon \to 0^+} \int_{\Gamma - e^i} \frac{1}{r} (n_l r_{,k} - n_k r_{,l})\left(u_k - u_k^i \right) d\Gamma + \epsilon_{lk} u_k^i \lim_{\epsilon \to 0^+} \int_{\Gamma - e^i} \frac{1}{r} \, dr \right] \right\} \quad (3.172)$$

Eventually, we are in the position to evaluate $\delta H_l = \delta H_l^N + \delta H_l^R + \delta H_l^J$ by simply adding the three contributions. It is easy to see that all terms related to the integral $\int 1/r \, dr$ cancel out when adding all the contributions.

The third integral of Equation (3.150) is weakly singular:

$$G_l = \lim_{\epsilon \to 0^+} \int_{\Gamma - e^i} u_{lk}^* \delta t_k \, d\Gamma \text{ is weakly singular } \because u_{lk}^* = O(\ln r) \quad (3.173)$$

The fourth integral of Equation (3.150) can be split into two integrals:

$$\delta G_l = \lim_{\epsilon \to 0^+} \int_{\Gamma - e^i} (\delta u_{lk}^* + u_{lk}^* \delta J) t_k \, d\Gamma = \delta G_l^R + \delta G_l^J \quad (3.174)$$

where:

$$\delta G_l^R = \lim_{\epsilon \to 0^+} \int_{\Gamma - e^i} u_{lk,j}^* \delta r_j t_k \, d\Gamma \text{ is regular } \because \underbrace{u_{lk,j}^*}_{O(r^{-1})} \underbrace{\delta r_j}_{O(r)} = O\left(r^0\right) \quad (3.175)$$

$$\delta G_l^J = \lim_{\epsilon \to 0^+} \int_{\Gamma - e^i} u_{lk}^* \delta J t_k \, d\Gamma \text{ is weakly singular } \because \underbrace{u_{lk}^*}_{O(\ln r)} \underbrace{\delta J}_{O(r^0)} = O(\ln r) \quad (3.176)$$

3.5.3   Discretization and solution

The discussion done in Section 3.3.3 about discretization, collocation, numerical integration and solution of the Laplace BEM sensitivity problem holds for the elastostatic case. The difference is in the length of the formulation, which is also more involved as it has been shown in the previous section.

The discretized form of Boundary Integral Equations (3.142) and (3.150) for any collocation point $\mathbf{x}^i$ can be written in a generic way as:

$$c_{lk}^i \delta u_k^i + b_{lkjm}^i v_{j,m}^i u_k^i + \sum_{e=1}^{N_{be}} \left(H_{lkp} \delta u_{kp} \right)^{\Phi_e} + \sum_{e=1}^{N_{be}} \left(\delta H_{lkp} u_{kp} \right)^{\Phi_e} = \sum_{e=1}^{N_{be}} \left(G_{lkp} \delta t_{kp} \right)^{\Phi_e} + \sum_{e=1}^{N_{be}} \left(\delta G_{lkp} t_{kp} \right)^{\Phi_e}$$

$$(3.177)$$

where:

- If $\mathbf{x}^{\mathrm{i}} \in \Gamma$, then:

$$\Phi^{\mathrm{i}} = \left\{\Phi_e, e = 1, \ldots, N_{\mathrm{be}} : \mathbf{x}^{\mathrm{i}} \in \Phi_e\right\}$$

$$\Psi^{\mathrm{i}} = \left\{\Psi_d, d = 1, \ldots, N_{\mathrm{de}} : \mathbf{x}^{\mathrm{i}} \in \Psi_d\right\}$$

$$u_k^{\mathrm{i}} = \left(\phi_p^{\mathrm{i}} u_{kp}\right)^{\Phi^{\mathrm{i}}}$$

$$\delta u_k^{\mathrm{i}} = \left(\phi_p^{\mathrm{i}} \delta u_{kp}\right)^{\Phi^{\mathrm{i}}}$$

$$v_{j,m}^{\mathrm{i}} = \left(\psi_{q,m}^{\mathrm{i}} v_{jq}\right)^{\Psi^{\mathrm{i}}}$$

and c_{lk}^{i} and b_{lkjm}^{i} are calculated as shown previously according to the local geometry of the boundary at the collocation point.

- If $\mathbf{x}^{\mathrm{i}} \notin \Gamma$, then $c_{lk}^{\mathrm{i}} = \delta_{lk} \delta_{\Omega}^{\mathrm{i}}$ and $b_{lkjm}^{\mathrm{i}} = 0$.

For a boundary element Φ associated with a design element Ψ, two different situations must be considered:

Exterior integration, $\mathbf{x}^{\mathrm{i}} \notin \Phi$. When $\mathbf{x}^{\mathrm{i}} \notin \Phi$, the contributions of a boundary element Φ similar to those of the SBIE are:

$$H_{lkp} = \int_{\Phi} t_{lk}^* \phi_p \, \mathrm{d}\Gamma \tag{3.178}$$

$$G_{lkp} = \int_{\Phi} u_{lk}^* \phi_p \, \mathrm{d}\Gamma \tag{3.179}$$

The contributions of the new integrals arising in the δSBIE consider separately the design velocity field along the boundary element (through the design element Ψ) and the design velocity field at the collocation point:

$$\delta H_{lkp} = \delta H_{lkmqp}^{T1} v_{mq}^{\Psi} - \delta H_{lkmp}^{T2} v_m^{\mathrm{i}} = \left(\delta H_{lkmqp}^{N1} + \delta H_{lkmqp}^{R1} + \delta H_{lkmqp}^{J1}\right) v_{mq}^{\Psi} - \delta H_{lkmp}^{R2} v_m^{\mathrm{i}} \tag{3.180}$$

$$\delta G_{lkp} = \delta G_{lkmqp}^{T1} v_{mq}^{\Psi} - \delta G_{lkmp}^{T2} v_m^{\mathrm{i}} = \left(\delta G_{lkmqp}^{R1} + \delta G_{lkmqp}^{J1}\right) v_{mq}^{\Psi} - \delta G_{lkmp}^{R2} v_m^{\mathrm{i}} \tag{3.181}$$

where:

$$\delta H_{lkmqp}^{\mathrm{N1}} = -\int_{\Phi} \sigma_{lkj}^* t_j n_m \psi_{q,s} t_s \phi_p \, \mathrm{d}\Gamma \tag{3.182}$$

$$\delta H_{lkmqp}^{\mathrm{R1}} = \int_{\Phi} \sigma_{lkj,m}^* n_j \psi_q \phi_p \, \mathrm{d}\Gamma \tag{3.183}$$

$$\delta H_{lkmp}^{\mathrm{R2}} = \int_{\Phi} \sigma_{lkj,m}^* n_j \phi_p \, \mathrm{d}\Gamma \tag{3.184}$$

$$\delta H_{lkmqp}^{\mathrm{J1}} = \int_{\Phi} t_{lk}^* t_m \psi_{q,s} t_s \phi_p \, \mathrm{d}\Gamma \tag{3.185}$$

$$\delta G_{lkmqp}^{\text{R1}} = \int\limits_{\Phi} u_{lk,m}^{*} \psi_q \phi_p \ \mathrm{d}\Gamma \tag{3.186}$$

$$\delta G_{lkmp}^{\text{R2}} = \int\limits_{\Phi} u_{lk,m}^{*} \phi_p \ \mathrm{d}\Gamma \tag{3.187}$$

$$\delta G_{lkmqp}^{\text{J1}} = \int\limits_{\Phi} u_{lk}^{*} t_m \psi_{q,s} t_s \phi_p \ \mathrm{d}\Gamma \tag{3.188}$$

Interior integration, $\mathbf{x}^{\text{i}} \in \Phi$. When $\mathbf{x}^{\text{i}} \in \Phi$, the contributions of Φ similar to those of the SBIE are:

$$H_{lkp} = -\frac{1}{4\pi(1-\nu)} \left\{ \lim_{\epsilon \to 0^+} \int\limits_{\Phi - e^{\text{i}}} \frac{1}{r} \frac{\partial r}{\partial n} \Big[\delta_{lk}(1-2\nu) + 2 r_{,l} r_{,k} \Big] \phi_p \ \mathrm{d}\Gamma \right.$$

$$\left. + (1-2\nu) \left[\lim_{\epsilon \to 0^+} \int\limits_{\Phi - e^{\text{i}}} \frac{1}{r} (n_l r_{,k} - n_k r_{,l}) \left(\phi_p - \phi_p^{\text{i}} \right) \ \mathrm{d}\Gamma + \epsilon_{lk} \phi_p^{\text{i}} \lim_{\epsilon \to 0^+} \int\limits_{\Phi - e^{\text{i}}} \frac{1}{r} \ \mathrm{d}r \right] \right\} \tag{3.189}$$

$$G_{lkp} = \lim_{\epsilon \to 0^+} \int\limits_{\Phi - e^{\text{i}}} u_{lk}^{*} \phi_p \ \mathrm{d}\Gamma \tag{3.190}$$

Since $\mathbf{x}^{\text{i}} \in \Phi$, the contributions of the new integrals arising in the δSBIE consider only the design velocity field along the boundary element (through the design element Ψ):

$$\delta H_{lkp} = \delta H_{lkmqp}^{T1} v_{mq}^{\Psi} = \left(\delta H_{lkmqp}^{N1} + \delta H_{lkmqp}^{R1} + \delta H_{lkmqp}^{J1} \right) v_{mq}^{\Psi} \tag{3.191}$$

$$\delta G_{lkp} = \delta G_{lkmqp}^{T1} v_{mq}^{\Psi} = \left(\delta G_{lkmqp}^{R1} + \delta G_{lkmqp}^{J1} \right) v_{mq}^{\Psi} \tag{3.192}$$

where:

$$\delta H_{lkmqp}^{\text{N1}} = \frac{1}{4\pi(1-\nu)} \left\{ (1-2\nu) \int\limits_{\Phi - e^{\text{i}}} \frac{1}{r} (t_l r_{,k} - t_k r_{,l}) n_m \psi_{q,s} t_s \phi_p \ \mathrm{d}\Gamma \right.$$

$$+ \int\limits_{\Phi - e^{\text{i}}} \frac{1}{r} \frac{\partial r}{\partial \Gamma} \Big[2 r_{,l} r_{,k} + (1-2\nu) \delta_{lk} \Big] \left(n_m \psi_{q,s} t_s \phi_p - n_m^{\text{i}} \psi_{q,s}^{\text{i}} t_s^{\text{i}} \phi_p^{\text{i}} \right) \ \mathrm{d}\Gamma$$

$$\left. + 2 n_m^{\text{i}} \psi_{q,s}^{\text{i}} t_s^{\text{i}} \phi_p^{\text{i}} \int\limits_{\Phi - e^{\text{i}}} \frac{1}{r} \frac{\partial r}{\partial \Gamma} \left(r_{,l} r_{,k} - t_l^{\text{i}} t_k^{\text{i}} \right) \ \mathrm{d}\Gamma \right\} \tag{3.193}$$

$$\delta H_{lkmqp}^{\text{R1}} = \int\limits_{\Gamma-e^{\text{i}}} \tilde{\sigma}_{lkm}^{\text{a}} \left(\psi_q - \psi_q^{\text{i}} \right) \phi_p \, \mathrm{d}\Gamma + \int\limits_{\Gamma-e^{\text{i}}} \tilde{\sigma}_{lkm}^{\text{b}} \left(\psi_q - \psi_q^{\text{i}} - \psi_{q,s}^{\text{i}} r_s \right) \phi_p \, \mathrm{d}\Gamma$$

$$+ \int\limits_{\Gamma-e^{\text{i}}} r\tilde{\sigma}_{lkm}^{\text{b}} \left(\psi_{q,s}^{\text{i}} r_{,s} \phi_p - \psi_{q,s}^{\text{i}} \left(\frac{\partial r}{\partial \Gamma} \right)^{\text{i}} t_s^{\text{i}} \phi_p^{\text{i}} \right) \mathrm{d}\Gamma$$

$$- \frac{1}{4\pi(1-\nu)} \psi_{q,s}^{\text{i}} t_s^{\text{i}} \phi_p^{\text{i}} \left\{ \int\limits_{\Gamma-e^{\text{i}}} \frac{1}{r} \left(\frac{\partial r}{\partial \Gamma} \right)^{\text{i}} \left[-2(1-2\nu) \left(r_{,m} - \left(\frac{\partial r}{\partial \Gamma} \right)^{\text{i}} t_m^{\text{i}} \right)(n_l r_{,k} - n_k r_{,l}) \right. \right.$$

$$\left. + 2 \left(n_m r_{,l} r_{,k} - n_m^{\text{i}} t_l^{\text{i}} t_k^{\text{i}} \right) + (1-2\nu) \left(\delta_{lk} \left(n_m - n_m^{\text{i}} \right) + \delta_{km} \left(n_l - n_l^{\text{i}} \right) - \delta_{lm} \left(n_k - n_k^{\text{i}} \right) \right) \right] \mathrm{d}\Gamma$$

$$\left. + \left[2n_m^{\text{i}} t_l^{\text{i}} t_k^{\text{i}} + (1-2\nu) \left(\delta_{lk} n_m^{\text{i}} + \epsilon_{lk} t_m^{\text{i}} \right) \right] \int\limits_{\Gamma-e^{\text{i}}} \frac{1}{r} \left(\left(\frac{\partial r}{\partial \Gamma} \right)^{\text{i}} - \frac{\partial r}{\partial \Gamma} \right) \mathrm{d}\Gamma \right\} \quad (3.194)$$

$$\delta H_{lkmqp}^{\text{J1}} = \int\limits_{\Phi-e^{\text{i}}} t_{lk}^{*} \left(t_m \psi_{q,s} t_s - t_m^{\text{i}} \psi_{q,s}^{\text{i}} t_s^{\text{i}} \right) \phi_p \, \mathrm{d}\Gamma$$

$$- \frac{1}{4\pi(1-\nu)} t_m^{\text{i}} \psi_{q,s}^{\text{i}} t_s^{\text{i}} \left\{ \int\limits_{\Phi-e^{\text{i}}} \frac{1}{r} \frac{\partial r}{\partial n} \left[\delta_{lk}(1-2\nu) + 2r_{,l} r_{,k} \right] \phi_p \, \mathrm{d}\Gamma \right.$$

$$\left. + (1-2\nu) \int\limits_{\Phi-e^{\text{i}}} \frac{1}{r} (n_l r_{,k} - n_k r_{,l}) \left(\phi_p - \phi_p^{\text{i}} \right) \mathrm{d}\Gamma \right\} \quad (3.195)$$

$$\delta G_{lkmqp}^{\text{R1}} = \lim_{\epsilon \to 0^+} \int\limits_{\Phi-e^{\text{i}}} u_{lk,m}^{*} \left(\psi_q - \psi_q^{\text{i}} \right) \phi_p \, \mathrm{d}\Gamma \quad (3.196)$$

$$\delta G_{lkmqp}^{\text{J1}} = \lim_{\epsilon \to 0^+} \int\limits_{\Phi-e^{\text{i}}} u_{lk}^{*} t_m \psi_{q,s} t_s \phi_p \, \mathrm{d}\Gamma \quad (3.197)$$

where the limit notation $\lim_{\epsilon \to 0^+}$ before some integrals has been omitted for brevity. Note that terms involving the integral $\int 1/r \, \mathrm{d}\Gamma$ has been removed from $\delta H_{lkmqp}^{\text{N1}}$, $\delta H_{lkmqp}^{\text{R1}}$ and $\delta H_{lkmqp}^{\text{J1}}$ since they cancel out when evaluating $\delta H_{lkmqp}^{\text{T1}}$.

The solution of the sensitivity problem requires the solution of the zero-order solution. As it is well known, the discretized form of the SBIE is:

$$c_{lk}^{\text{i}} u_k^{\text{i}} + \sum_{e=1}^{N_{\text{be}}} \left(H_{lkp} u_{kp} \right)^{\Phi_e} = \sum_{e=1}^{N_{\text{be}}} \left(G_{lkp} t_{kp} \right)^{\Phi_e} \quad (3.198)$$

Performing a suitable collocation of the SBIE throughout the discretization leads to the influence matrices **H** and **G**, which are built by assembling free-terms and H_{lkp} integrals into **H**, and G_{lkp} integrals into **G**. The discretized system is transformed into a system of linear equations once the boundary conditions are applied:

$$\mathbf{Hu} = \mathbf{Gt} \quad \xrightarrow{\text{boundary conditions}} \quad \mathbf{Ax} = \mathbf{B\bar{x}} = \mathbf{b} \quad (3.199)$$

where **A** is composed of components of **H** and **G** related to the unknown components of **u** and **t** (gathered into **x**), and **B** is composed of components of **H** and **G** related to the known components of **u** and **t** (gathered into **x̄**). Following a similar procedure but using the δSBIE (3.177), the first-order discretized system is:

$$\mathbf{H}\delta\mathbf{u} + \delta\mathbf{H}\mathbf{u} = \mathbf{G}\delta\mathbf{t} + \delta\mathbf{G}\mathbf{t} \quad \xrightarrow{\text{boundary conditions}} \quad \mathbf{A}\delta\mathbf{x} = \mathbf{B}\delta\bar{\mathbf{x}} + \delta\mathbf{G}\mathbf{t} - \delta\mathbf{H}\mathbf{u} = \mathbf{b}^{\delta} \quad (3.200)$$

where **A** and **B** is similar to that of the zero-order system, and the components of $\delta\bar{\mathbf{x}}$ are related to the sensitivities of the boundary conditions.

3.6 Elastodynamics

In the present section, the time harmonic counterpart of the elastostatic problem is studied. The formulation is completely analogous to the elastostatic problem, except that the fundamental solution is more involved. However, it can be split into a part similar to the elastostatic one, and another part that leads to at most weakly singular integrals. This splitting process was also applied to the Helmholtz problem in Section 3.4.

Consider the time harmonic analysis of an elastic solid with density ρ, Poisson's ratio ν and shear modulus μ. Lamé's first parameter is then $\lambda = 2\mu\nu/(1 - 2\nu)$. As it is well known [29], two body modes exist: the longitudinal mode (primary wave or P-wave) with a propagation speed $c_1 = \sqrt{(\lambda + 2\mu)/\rho}$, and the transversal mode (secondary wave or S-wave) with a propagation speed $c_2 = \sqrt{\mu/\rho}$. The P and S wavenumbers are denoted as $k_1 = \omega/c_1$ and $k_2 = \omega/c_2$, respectively, where ω is the circular frequency.

The fundamental solution and its derivatives can be written as [29]:

$$\begin{aligned}
u^*_{lk} &= \frac{1}{2\pi\mu}\left[U_1\delta_{lk} - U_2 r_{,l}r_{,k}\right] \\
U_1 &= K_0\left(ik_2 r\right) + \frac{1}{ik_2 r}\left[K_1\left(ik_2 r\right) - \frac{k_1}{k_2}K_1\left(ik_1 r\right)\right] \\
U_2 &= K_2\left(ik_2 r\right) - \frac{k_1^2}{k_2^2}K_2\left(ik_1 r\right)
\end{aligned} \quad (3.201)$$

$$\begin{aligned}
u^*_{lk,m} &= \frac{1}{2\pi\mu}\left[V_1\delta_{lk}r_{,m} + V_2 r_{,l}r_{,j}r_{,m} + V_3\left(\delta_{lm}r_{,k} + \delta_{km}r_{,l}\right)\right] \\
V_1 &= \frac{\partial U_1}{\partial r} \\
V_2 &= \frac{2}{r}U_2 - \frac{\partial U_2}{\partial r} \\
V_3 &= -\frac{1}{r}U_2
\end{aligned} \quad (3.202)$$

$$\sigma^*_{lkm} = \frac{1}{2\pi}\left[T_1 r_{,l} r_{,k} r_{,m} + T_2\left(\delta_{lk} r_{,m} + \delta_{lm} r_{,k}\right) + T_3 \delta_{km} r_{,l}\right]$$

$$T_1 = 2\left(\frac{2}{r}U_2 - \frac{\partial U_2}{\partial r}\right)$$

$$T_2 = \frac{\partial U_1}{\partial r} - \frac{1}{r}U_2 \tag{3.203}$$

$$T_3 = \frac{\lambda}{\mu}\left(\frac{\partial U_1}{\partial r} - \frac{\partial U_2}{\partial r} - \frac{1}{r}U_2\right) - \frac{2}{r}U_2$$

$$t^*_{lk} = \sigma^*_{lkm} n_m = \frac{1}{2\pi}\left[T_1 r_{,l} r_{,k}\frac{\partial r}{\partial n} + T_2\left(\delta_{lk}\frac{\partial r}{\partial n} + \delta_{lm} r_{,k}\right) + T_3 n_k r_{,l}\right] \tag{3.204}$$

$$\sigma^*_{lkm,j} = \frac{1}{2\pi}\Bigg[R_1\left(\delta_{lj} r_{,m} r_{,k} + \delta_{kj} r_{,l} r_{,m} + \delta_{mj} r_{,l} r_{,k}\right) + R_2 r_{,j}\left(\delta_{lk} r_{,m} + \delta_{lm} r_{,k}\right)$$

$$+ R_3 r_{,l} r_{,k} r_{,m} r_{,j} + R_4 \delta_{km}\delta_{lj} + R_5 \delta_{km} r_{,l} r_{,j} + R_6\left(\delta_{lk}\delta_{mj} + \delta_{lm}\delta_{kj}\right)\Bigg]$$

$$R_1 = \frac{1}{r}T_1$$

$$R_2 = \frac{\partial^2 U_1}{\partial r^2} - \frac{1}{r}\left(\frac{\partial U_1}{\partial r} + \frac{\partial U_2}{\partial r} - \frac{2}{r}U_2\right)$$

$$R_3 = 2\left[-\frac{\partial^2 U_2}{\partial r^2} + \frac{1}{r}\left(5\frac{\partial U_2}{\partial r} - \frac{8}{r}U_2\right)\right] \tag{3.205}$$

$$R_4 = \frac{1}{r}T_3$$

$$R_5 = \frac{\lambda}{\mu}\left(\frac{\partial^2 U_1}{\partial r^2} - \frac{\partial^2 U_2}{\partial r^2} - \frac{1}{r}\frac{\partial U_1}{\partial r} + \frac{2}{r^2}U_2\right) - \frac{2}{r}\frac{\partial U_2}{\partial r} + \frac{4}{r^2}U_2$$

$$R_6 = \frac{1}{r}T_2$$

where terms U_i, V_i, T_i and R_i depend on distance r, frequency ω and material properties. By using the decomposition of Bessel functions presented in Equation (3.113), the non-frequency dependant part (static) of each term can be segregated. Their full decomposition can be found in Appendix B. Terms U_i, V_i, T_i and R_i can be written as:

$$U_1 = -\frac{3-4\nu}{4(1-\nu)}\ln r + O\left(r^0\right)$$

$$U_2 = -\frac{1}{4(1-\nu)} + O\left(r^2\ln r\right) \tag{3.206}$$

$$V_1 = -\frac{3-4\nu}{4(1-\nu)}\frac{1}{r} + O\left(r\ln r\right)$$

$$V_2 = -\frac{1}{2(1-\nu)}\frac{1}{r} + O\left(r\right) \tag{3.207}$$

$$T_1 = -\frac{1}{1-\nu}\frac{1}{r} + O\left(r\right)$$

$$T_2 = -\frac{1-2\nu}{2(1-\nu)}\frac{1}{r} + O\left(r\ln r\right) \tag{3.208}$$

$$T_3 = \frac{1-2\nu}{2(1-\nu)}\frac{1}{r} + O\left(r\ln r\right)$$

$$R_2 = \frac{1 - 2\nu}{1 - \nu} \frac{1}{r^2} + O\left(r^0\right)$$

$$R_3 = \frac{4}{1 - \nu} \frac{1}{r^2} + O\left(r^0\right) \tag{3.209}$$

$$R_5 = -\frac{1 - 2\nu}{1 - \nu} \frac{1}{r^2} + O\left(r^0\right)$$

where terms V_3, R_1, R_4 and R_6 have been omitted for brevity, see Equations (3.202) and (3.205). Also, in order to be able to verify that the static parts lead to the elastostatic fundamental solution, the following relationships have been used:

$$\frac{c_2^2}{c_1^2} = \frac{1 - 2\nu}{2(1 - \nu)} \tag{3.210}$$

$$\frac{\lambda}{\mu} = \frac{c_1^2}{c_2^2} - 2 \tag{3.211}$$

By substituting these decompositions into Equations (3.201-3.205), it is very easy to see that the static parts lead to the elastostatic fundamental solution and its derivatives, and that the "dynamic residues" lead to at most weakly singular integrals:

$$u_{lk}^* = \left(u_{lk}^*\right)^{\text{static}} + \left(u_{lk}^*\right)^{\text{dynamic}} \tag{3.212}$$

$$u_{lk,m}^* = \left(u_{lk,m}^*\right)^{\text{static}} + \left(u_{lk,m}^*\right)^{\text{dynamic}} \tag{3.213}$$

$$t_{lk}^* = \left(t_{lk}^*\right)^{\text{static}} + \left(t_{lk}^*\right)^{\text{dynamic}} \tag{3.214}$$

$$\sigma_{lkm}^* = \left(\sigma_{lkm}^*\right)^{\text{static}} + \left(\sigma_{lkm}^*\right)^{\text{dynamic}} \tag{3.215}$$

$$\sigma_{lkm,j}^* = \left(\sigma_{lkm,j}^*\right)^{\text{static}} + \left(\sigma_{lkm,j}^*\right)^{\text{dynamic}} \tag{3.216}$$

3.7 Validation examples

In this section, some examples with analytical solution are used to validate the formulation and its implementation. Only dynamic problems are considered since their static counterparts can be checked by simply making $\omega \to 0$. In the same line as in the previous chapter, the example is a square domain with boundary conditions such that a one-dimensional wave phenomenon occurs. However, in order to validate the formulation for curved geometries, the domain is divided into two regions with the same material properties but with curved interfaces. Details about coupling between BEM regions are given in Chapter 4.

3.7.1 Inviscid fluid problem

Analytical solution

Consider a rectangular domain Ω with the geometry and boundary conditions shown in Figure 3.6. The domain Ω contain an inviscid fluid with density ρ, and bulk modulus K. The solution of the related Helmholtz equation consists of two pressure waves travelling
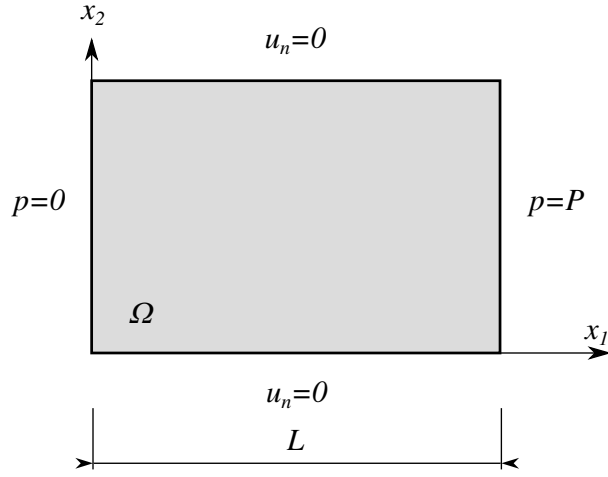
Design velocity field: $v_1(x)=x/L$, $v_2(x)=0$

Figure 3.6: Problem layout (inviscid fluid problem)

in opposite directions along x_1:

$$p(x_1) = Ae^{-ikx_1} + Be^{ikx_1} \tag{3.217}$$

where A and B are the amplitudes of the waves, $k = \omega/c$ is the wavenumber, ω is the circular frequency, and $c = \sqrt{K/\rho}$ is the wave propagation speed. Once boundary conditions are considered, the pressure p and fluid displacement in the x_1 direction ($u_1 = 1/(\rho\omega^2)p_{,1}$) can be written as:

$$p(x_1) = \frac{P}{\sin kL} \sin kx_1 \tag{3.218}$$

$$u_1(x_1) = \frac{Pk}{\rho\omega^2 \sin kL} \cos kx_1 \tag{3.219}$$

If L is taken as the shape design variable with a design velocity field $\mathbf{v} = (x/L, 0)$, then the sensitivities are:

$$\delta p(x_1) = \frac{Pk}{\sin kL} \left(-\frac{\cos kL}{\sin kL} \sin kx_1 + \frac{x_1}{L} \cos kx_1 \right) \tag{3.220}$$

$$\delta u_1(x_1) = -\frac{Pk^2}{\rho\omega^2 \sin kL} \left(\frac{\cos kL}{\sin kL} \cos kx_1 + \frac{x_1}{L} \sin kx_1 \right) \tag{3.221}$$

BEM solution

The problem is solved numerically by using the BEM sensitivity analysis with the δSBIE developed in this chapter. The domain is a square with side length L, and is meshed using different element sizes ($L/4$, $L/10$) and different element order (linear, quadratic). By doing so, h and p convergence can be tested. Also, a fictitious circular inclusion filled with the same material is considered in order to demonstrate that the formulation works well also for curved elements. All meshes used here are shown in Figure 3.7. Dimensionless frequency $a_0 = \omega L/c$ is used, which is in the range $(0, 6]$.
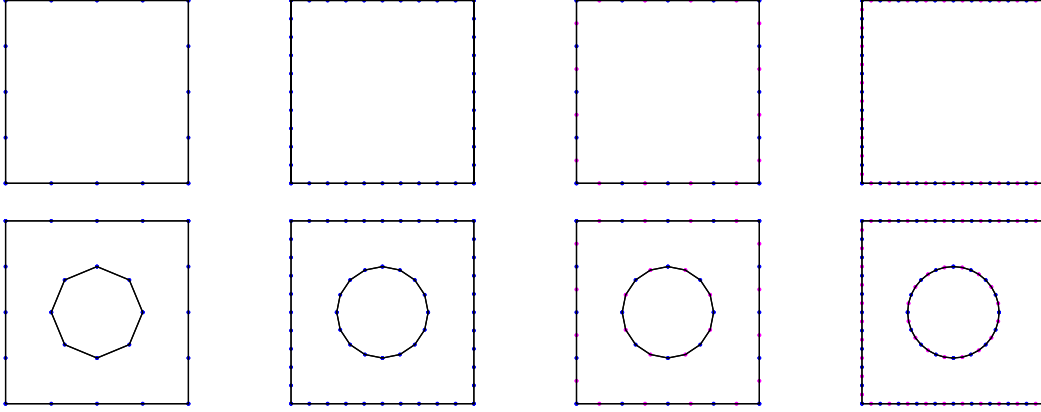
Figure 3.7: Linear and quadratic meshes with $L/4$ and $L/10$ element sizes, and with and without a fictitious circular inclusion.

The design velocity field is defined in the same way as it is described in Section 2.3. It is done by defining a design mesh containing one 4-node quadrilateral element covering the domain Ω, and appropriate values of $\mathbf{v}$ are assigned to the four nodes in order to define $\mathbf{v} = \partial\mathbf{x}/\partial L = (x_1/L, 0)$, see Figure 2.3 (Left).

Figure 3.8 shows the normalized displacement u_1 and sensitivity δu_1 at $x_1 = L$, and their relative errors with respect to the analytical solution. These results are obtained for the upper meshes in Figure 3.7. Figure 3.9 shows the same results but using the meshes with the fictitious circular inclusion, i.e. the lower meshes in Figure 3.7. In all cases, error levels are so small that the differences between numerical and analytical solutions can only be seen in the relative error graphs. These graphs clearly demonstrate the h and p convergence of the developed BEM sensitivity analysis for plane and curved boundary elements. The error levels at low frequencies are higher when using the meshes with the fictitious circular inclusion. However, the same phenomenon is seen in both the displacement and the displacement sentitivity, and hence it seems to be related to the discretization itself.

3.7.2 Elastodynamic problem

The analytical solution of this example can be found in Section 2.3. The numerical solution is obtained using the same configuration and the same set of meshes as in the previous section. Poisson's ratio is assumed to be $\nu = 1/4$. In this case, the dimensionless frequency is $a_0 = \omega L/c_1$, where c_1 is the P-wave propagation speed.

Figure 3.10 shows the normalized displacement u_1 and sensitivity δu_1 at $x_1 = L$, and their relative errors with respect to the analytical solution. Figure 3.11 shows the same results but using the meshes with the fictitious circular inclusion. As in the previous section, h and p convergence can be seen in these graphs for straight and curved boundary elements.
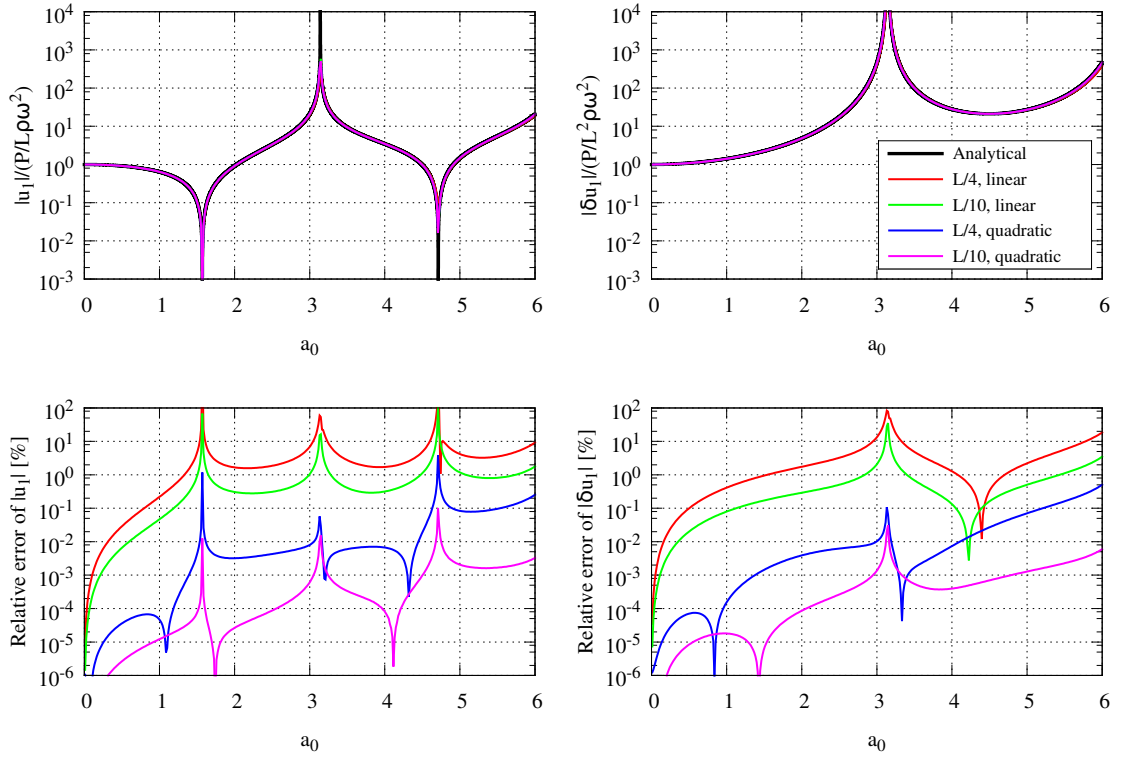
Figure 3.8: Convergence of $u_1(L)$ and $\delta u_1(L)$ for the inviscid fluid problem
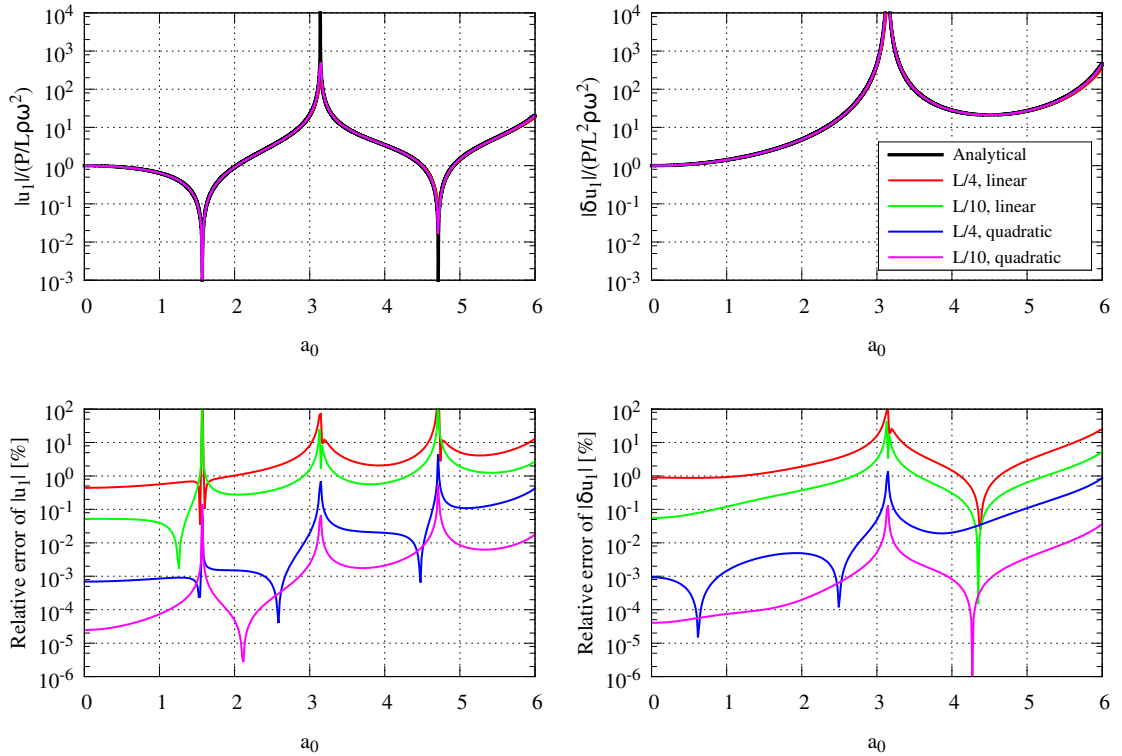

Figure 3.9: Convergence of $u_1(L)$ and $\delta u_1(L)$ for the inviscid fluid problem (meshes with a fictitious circular inclusion)
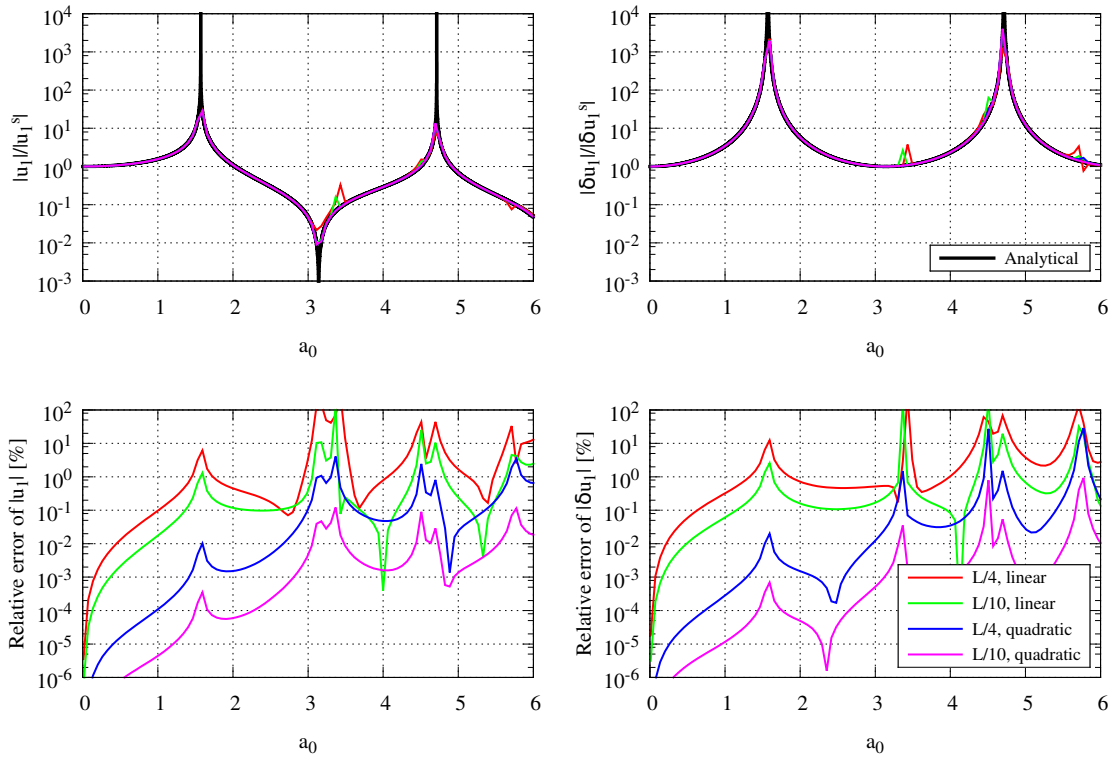
Figure 3.10: Convergence of $u_1(L)$ and $\delta u_1(L)$ for the elastodynamic problem
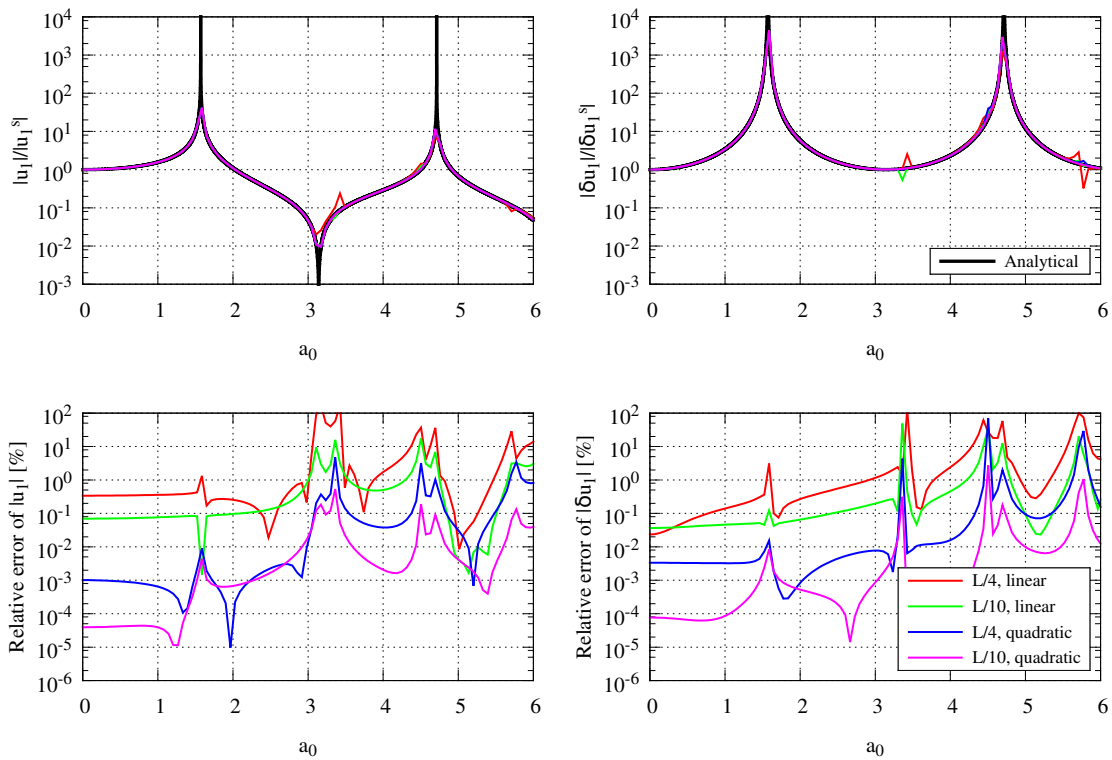

Figure 3.11: Convergence of $u_1(L)$ and $\delta u_1(L)$ for the elastodynamic problem (meshes with a fictitious circular inclusion)

Chapter 4

Shape sensitivities in multi-region problems

4.1 Introduction

Formulations developed in Chapter 2 (DDM–FEM) and Chapter 3 (DDM–BEM) can be combined for solving multi-region problems in an advantageous way. Each region is managed either by the BEM or by the FEM, whichever is more appropriate. Unbounded regions are handled very naturally by the BEM, but they require special formulations if treated by the FEM. The BEM also works very well when analysing regions with cracks or where accurate stresses are needed. The FEM is intrinsically well-adapted to manage structural members and inhomogeneities.

In this chapter, BEM–BEM and BEM–FEM coupling between regions are considered. BEM–BEM coupling between regions of the same or different type is relatively straightforward, and not too many variations exist. On the other hand, several coupling strategies can be used to build a BEM–FEM interaction [8]. The most direct and simple approach consists in establishing compatibility and equilibrium conditions along the interfaces at the level of discretizated equations. Depending on the relative number of degrees of freedom of FEM and BEM regions, it may be also convenient to symmetrize the BEM matrices and treat BEM regions as macro finite elements. A more advanced method is that of Belytschko et al. [14, 41, 15]. This approach uses a single variational statement for the whole domain, which is then discretized using appropriate continuous test and trial functions throughout the domain. Using the patch test and solving several problems, they found that this method is far superior to the direct approach [41]. However, it requires doing some modifications to the standard formulations, and is more expansive computationally. Therefore, the direct approach is used in this work.

The rest of the chapter is organized as follows. In Section 4.2, discretization and collocation procedures in multi-region problems are described. The coupling conditions for the cases considered in this work are described in Section 4.3.
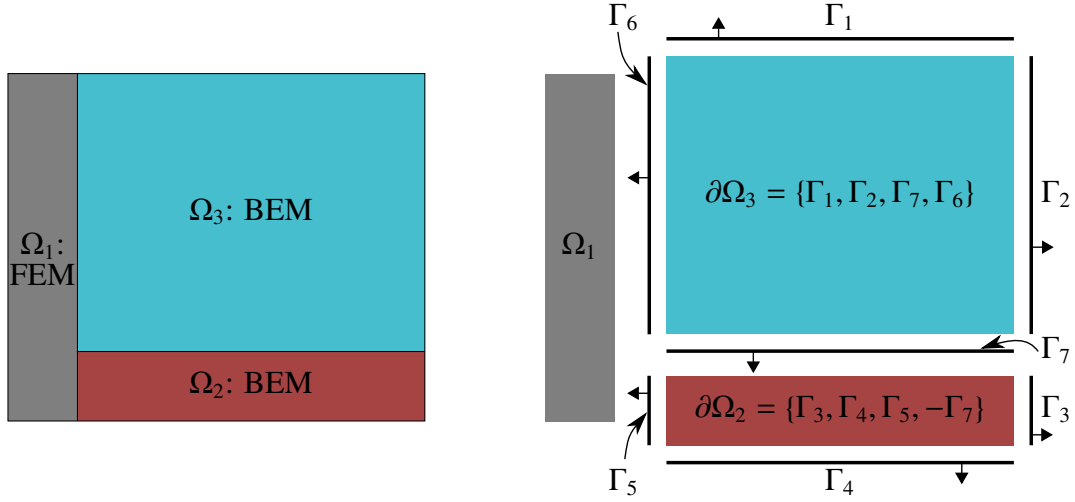
Figure 4.1: Multi-region problem example (geometry)

4.2 Discretization and collocation in multi-region problems

The domain Ω of a multi-region problem consists of N_r regions Ω_i, i.e. $\Omega = \cup_{i=1}^{i=N_r} \Omega_i$. A region Ω_i can be treated using either the BEM or the FEM. If a region Ω_i is treated using the BEM, then is necessary to explicitly define its boundary $\partial\Omega_i$ as a set of oriented boundaries Γ_j, i.e. $\partial\Omega_i = \left\{\pm\Gamma_j,\ j \in \mathcal{B}_i\right\}$. Each boundary Γ_j is discretized into boundary elements Φ_k, $\Gamma_j = \cup_{k\in C_j}\Phi_k$, where nodes are unique, i.e. each boundary is a piece of mesh with unique nodes and elements. If a region Ω_i is treated using the FEM, then it is directly discretized into finite elements Υ_k, $\Omega_i = \cup_{k\in\mathcal{D}_i}\Upsilon_k$, where nodes can be shared by several finite elements of different regions. Figure 4.1 shows an example of a multi-region problem with BEM and FEM regions.

The boundary of a region $\partial\Omega_i$ is split into several boundaries Γ_k in order to assign a different boundary or interface condition to each one of them. Also, it is split at sharp corners in order to have a better representation of tractions there. Since it has been established that each boundary has its own nodes, double nodes appear at points where different boundaries meet. If standard nodal collocation is applied at these nodes, then a singular system of linear equations could be obtained. There are several ways to overcome this difficulty, for example using discontinuous elements, special corner elements, alternative BIEs, or additional equations. In the present work, non-nodal collocation is used at these nodes, where the collocation points are located inside the elements but near the nodes. This approach not only solves the degeneracy problem with an acceptable error, but is also quite simple. The meshes obtained from standard pre-processors do not require modifications. Furthermore, it can be fully automated without much difficulty. Figure 4.2 shows a detail of discretization and collocation in a multi-region problem example.

As shown in Figure 4.2, a BEM–BEM interface is intrinsically conforming because of the way it is discretized. On the other hand, in order to have a conforming BEM–FEM interface, the corresponding boundary of the FEM mesh must match the BEM boundary mesh.
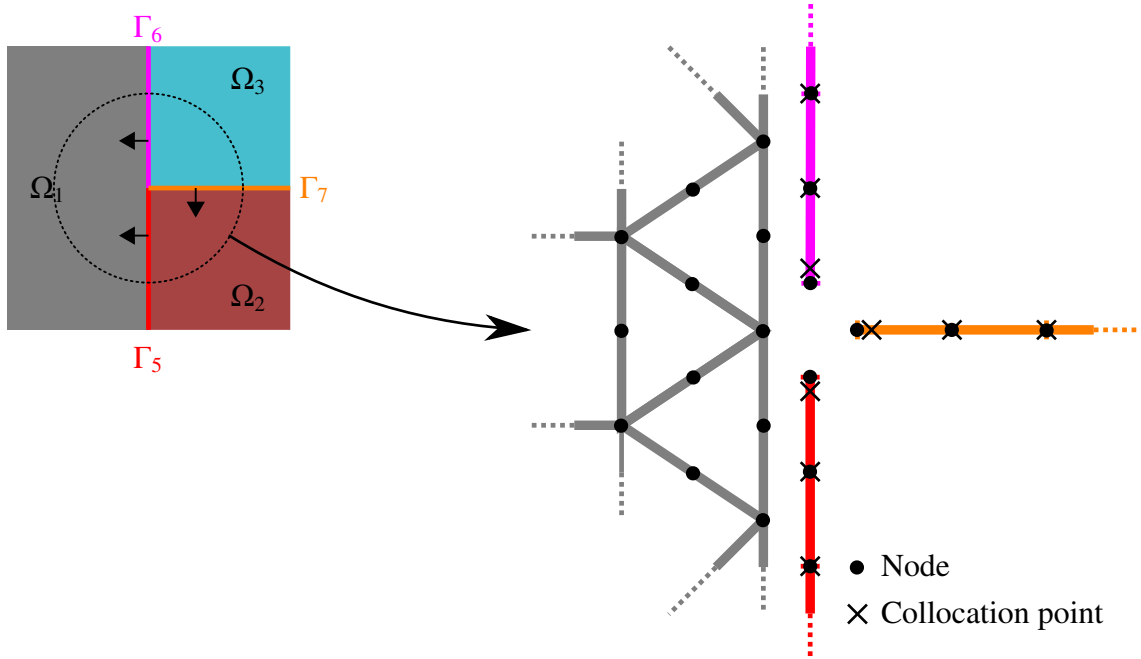
Figure 4.2: Multi-region problem example (exploded mesh and collocation)

4.3 Coupling conditions

Coupling is directly performed by establishing compatibility and equilibrium along both faces of the interface at the level of discretized equations.

4.3.1 BEM–BEM

Consider two BEM regions Ω_i and Ω_j ($i \neq j$) connected through an interface boundary Γ_k with orientation defined by its unit normal $\mathbf{n}$, see Figure 4.3. Relative to region Ω_i, Γ_k has positive orientation, hence $\mathbf{n}^{(i)} = \mathbf{n}$. However, relative to region Ω_j, Γ_k has negative orientation, and thus $\mathbf{n}^{(j)} = -\mathbf{n}$. Following this notation, coupling conditions between BEM regions are described next.
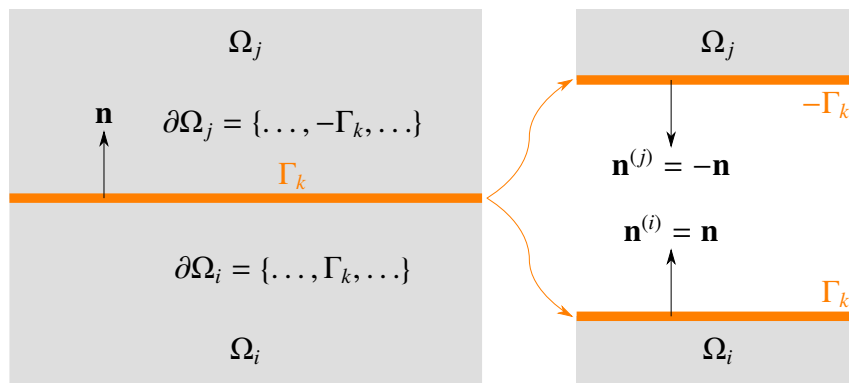

Figure 4.3: Boundary Γ_k acting as an interface between BEM regions Ω_i and Ω_j

BEM (Ω_i: elastic solid) – BEM (Ω_j: elastic solid)   The compatibility and equilibrium at the interface in a nodal fashion can be written as:

$$
\begin{aligned}
\mathbf{u}^{(i)} &= \mathbf{u}^{(j)} \\
\mathbf{t}^{(i)} + \mathbf{t}^{(j)} &= \mathbf{0}
\end{aligned}
\tag{4.1}
$$

$$
\begin{aligned}
\delta\mathbf{u}^{(i)} &= \delta\mathbf{u}^{(j)} \\
\delta\mathbf{t}^{(i)} + \delta\mathbf{t}^{(j)} &= \mathbf{0}
\end{aligned}
\tag{4.2}
$$

where it must be noticed that displacements and tractions and their sensitivities have the same coupling equations. In the following, we denote $\mathbf{u}_i$ and $\mathbf{t}_i$ as vectors of displacements and tractions in all boundaries of Ω_i except Γ_k, and $\mathbf{u}_k^{(i)}$ and $\mathbf{t}_k^{(i)}$ as vectors of displacements and tractions of Γ_k with respect to Ω_i. Also, we denote $\mathbf{u}_j$ and $\mathbf{t}_j$ as vectors of displacements and tractions in all boundaries of Ω_j except Γ_k, and $\mathbf{u}_k^{(j)}$ and $\mathbf{t}_k^{(j)}$ as vectors of displacements and tractions of Γ_k with respect to Ω_j. The equations obtained after collocating the SBIE for both regions are:

$$
\begin{pmatrix} \mathbf{H}_{ii} & \mathbf{H}_{ik} \\ \mathbf{H}_{ki} & \mathbf{H}_{kk}^{(i)} \end{pmatrix}
\begin{Bmatrix} \mathbf{u}_i \\ \mathbf{u}_k^{(i)} \end{Bmatrix}
-
\begin{pmatrix} \mathbf{G}_{ii} & \mathbf{G}_{ik} \\ \mathbf{G}_{ki} & \mathbf{G}_{kk}^{(i)} \end{pmatrix}
\begin{Bmatrix} \mathbf{t}_i \\ \mathbf{t}_k^{(i)} \end{Bmatrix}
=
\begin{Bmatrix} \mathbf{0}_i \\ \mathbf{0}_k \end{Bmatrix}
\tag{4.3}
$$

$$
\begin{pmatrix} \mathbf{H}_{jj} & \mathbf{H}_{jk} \\ \mathbf{H}_{kj} & \mathbf{H}_{kk}^{(j)} \end{pmatrix}
\begin{Bmatrix} \mathbf{u}_j \\ \mathbf{u}_k^{(j)} \end{Bmatrix}
-
\begin{pmatrix} \mathbf{G}_{jj} & \mathbf{G}_{jk} \\ \mathbf{G}_{kj} & \mathbf{G}_{kk}^{(j)} \end{pmatrix}
\begin{Bmatrix} \mathbf{t}_j \\ \mathbf{t}_k^{(j)} \end{Bmatrix}
=
\begin{Bmatrix} \mathbf{0}_j \\ \mathbf{0}_k \end{Bmatrix}
\tag{4.4}
$$

which reduce to:

$$
\begin{pmatrix}
\mathbf{H}_{ii} & \mathbf{H}_{ik} & \mathbf{G}_{ik} & \mathbf{0}_{ij} \\
\mathbf{H}_{ki} & \mathbf{H}_{kk}^{(i)} & \mathbf{G}_{kk}^{(i)} & \mathbf{0}_{kj} \\
\mathbf{0}_{ki} & \mathbf{H}_{kk}^{(j)} & -\mathbf{G}_{kk}^{(j)} & \mathbf{H}_{kj} \\
\mathbf{0}_{ji} & \mathbf{H}_{jk} & \mathbf{G}_{jk} & \mathbf{H}_{jj}
\end{pmatrix}
\begin{Bmatrix} \mathbf{u}_i \\ \mathbf{u}_k^{(i)} \\ \mathbf{t}_k^{(j)} \\ \mathbf{u}_j \end{Bmatrix}
-
\begin{pmatrix}
\mathbf{G}_{ii} & \mathbf{0}_{ij} \\
\mathbf{G}_{ki} & \mathbf{0}_{kj} \\
\mathbf{0}_{ki} & \mathbf{G}_{kj} \\
\mathbf{0}_{ji} & \mathbf{G}_{jj}
\end{pmatrix}
\begin{Bmatrix} \mathbf{t}_i \\ \mathbf{t}_j \end{Bmatrix}
=
\begin{Bmatrix} \mathbf{0}_i \\ \mathbf{0}_k \\ \mathbf{0}_k \\ \mathbf{0}_j \end{Bmatrix}
\tag{4.5}
$$

once coupling conditions are applied maintaining $\mathbf{u}_k^{(i)}$ and $\mathbf{t}_k^{(i)}$ as active degrees of freedom along the interface. The final system of linear equations is obtained after applying the boundary conditions:

$$
\begin{pmatrix}
\mathbf{A}_{ii} & \mathbf{H}_{ik} & \mathbf{G}_{ik} & \mathbf{0}_{ij} \\
\mathbf{A}_{ki} & \mathbf{H}_{kk}^{(i)} & \mathbf{G}_{kk}^{(i)} & \mathbf{0}_{kj} \\
\mathbf{0}_{ki} & \mathbf{H}_{kk}^{(j)} & -\mathbf{G}_{kk}^{(j)} & \mathbf{A}_{kj} \\
\mathbf{0}_{ji} & \mathbf{H}_{jk} & \mathbf{G}_{jk} & \mathbf{A}_{jj}
\end{pmatrix}
\begin{Bmatrix} \mathbf{x}_i \\ \mathbf{u}_k^{(i)} \\ \mathbf{t}_k^{(j)} \\ \mathbf{x}_j \end{Bmatrix}
=
\begin{pmatrix}
\mathbf{B}_{ii} & \mathbf{0}_{ij} \\
\mathbf{B}_{ki} & \mathbf{0}_{kj} \\
\mathbf{0}_{ki} & \mathbf{B}_{kj} \\
\mathbf{0}_{ji} & \mathbf{B}_{jj}
\end{pmatrix}
\begin{Bmatrix} \tilde{\mathbf{x}}_i \\ \tilde{\mathbf{x}}_j \end{Bmatrix}
=
\begin{Bmatrix} \mathbf{b}_i \\ \mathbf{b}_k^{(i)} \\ \mathbf{b}_k^{(j)} \\ \mathbf{b}_j \end{Bmatrix}
\tag{4.6}
$$

where $\mathbf{x}_i$ and $\mathbf{x}_j$ gather unknown displacements and tractions, and $\tilde{\mathbf{x}}_i$ and $\tilde{\mathbf{x}}_j$ gather known displacements and tractions. Matrices $\mathbf{A}$ and $\mathbf{B}$ combine terms of $\mathbf{H}$ and $\mathbf{G}$ matrices according the known and unknown displacements and tractions. Once this system of equations is solved, all displacements and tractions are known.

70

Therefore, in order to solve the sensitivity problem, we proceed following a similar process but collocating the δSBIE instead of the SBIE:

$$
\begin{Bmatrix}
\begin{bmatrix}
\mathbf{A}_{ii} & \mathbf{H}_{ik} & \mathbf{G}_{ik} & \mathbf{0}_{ij} \\
\mathbf{A}_{ki} & \mathbf{H}_{kk}^{(i)} & \mathbf{G}_{kk}^{(i)} & \mathbf{0}_{kj} \\
\mathbf{0}_{ki} & \mathbf{H}_{kk}^{(j)} & -\mathbf{G}_{kk}^{(j)} & \mathbf{A}_{kj} \\
\mathbf{0}_{ji} & \mathbf{H}_{jk} & \mathbf{G}_{jk} & \mathbf{A}_{jj}
\end{bmatrix}
\begin{Bmatrix}
\delta\mathbf{x}_i \\
\delta\mathbf{u}_k^{(i)} \\
\delta\mathbf{t}_k^{(j)} \\
\delta\mathbf{x}_j
\end{Bmatrix}
\end{Bmatrix}
=
\begin{bmatrix}
\mathbf{B}_{ii} & \mathbf{0}_{ij} \\
\mathbf{B}_{ki} & \mathbf{0}_{kj} \\
\mathbf{0}_{ki} & \mathbf{B}_{kj} \\
\mathbf{0}_{ji} & \mathbf{B}_{jj}
\end{bmatrix}
\begin{Bmatrix}
\delta\tilde{\mathbf{x}}_i \\
\delta\tilde{\mathbf{x}}_j
\end{Bmatrix}
$$
$$
-
\begin{bmatrix}
\delta\mathbf{H}_{ii} & \delta\mathbf{H}_{ik} & \mathbf{0}_{ik} & \mathbf{0}_{ij} \\
\delta\mathbf{H}_{ki} & \delta\mathbf{H}_{kk}^{(i)} & \mathbf{0}_{kk} & \mathbf{0}_{kj} \\
\mathbf{0}_{ki} & \mathbf{0}_{kk} & \delta\mathbf{H}_{kk}^{(j)} & \delta\mathbf{H}_{kj} \\
\mathbf{0}_{ji} & \mathbf{0}_{jk} & \delta\mathbf{H}_{jk} & \delta\mathbf{H}_{jj}
\end{bmatrix}
\begin{Bmatrix}
\mathbf{u}_i \\
\mathbf{u}_k^{(i)} \\
\mathbf{u}_k^{(j)} \\
\mathbf{u}_j
\end{Bmatrix}
+
\begin{bmatrix}
\delta\mathbf{G}_{ii} & \delta\mathbf{G}_{ik} & \mathbf{0}_{ik} & \mathbf{0}_{ij} \\
\delta\mathbf{G}_{ki} & \delta\mathbf{G}_{kk}^{(i)} & \mathbf{0}_{kk} & \mathbf{0}_{kj} \\
\mathbf{0}_{ki} & \mathbf{0}_{kk} & \delta\mathbf{G}_{kk}^{(j)} & \delta\mathbf{G}_{kj} \\
\mathbf{0}_{ji} & \mathbf{0}_{jk} & \delta\mathbf{G}_{jk} & \delta\mathbf{G}_{jj}
\end{bmatrix}
\begin{Bmatrix}
\mathbf{t}_i \\
\mathbf{t}_k^{(i)} \\
\mathbf{t}_k^{(j)} \\
\mathbf{t}_j
\end{Bmatrix}
\tag{4.7}
$$

where the left hand side matrix is exactly the same as before.

BEM (Ω_i: inviscid fluid) – BEM (Ω_j: inviscid fluid)   The nodal compatibility and equilibrium at the interface can be written as:

$$
\begin{aligned}
u_n^{(i)}\mathbf{n}^{(i)} = u_n^{(j)}\mathbf{n}^{(j)} &\quad\Rightarrow\quad u_n^{(i)} = -u_n^{(j)} \\
-p^{(i)}\mathbf{n}^{(i)} - p^{(j)}\mathbf{n}^{(j)} = \mathbf{0} &\quad\Rightarrow\quad p^{(i)} = p^{(j)}
\end{aligned}
\tag{4.8}
$$

$$
\begin{aligned}
\delta u_n^{(i)} &= -\delta u_n^{(j)} \\
\delta p^{(i)} &= \delta p^{(j)}
\end{aligned}
\tag{4.9}
$$

where, as in the previous case, normal displacements and pressures and their sensitivities have the same coupling equations. The procedure to obtain the final system of equations is analogous to the process followed in the previous case.

BEM (Ω_i: inviscid fluid) – BEM (Ω_j: elastic solid)   In this case, the nodal compatibility and equilibrium is:

$$
\begin{aligned}
u_n^{(i)}\mathbf{n}^{(i)} = \mathbf{u}^{(j)} &\quad\Rightarrow\quad u_n^{(i)} = -\mathbf{u}^{(j)} \cdot \mathbf{n}^{(j)} \\
-p^{(i)}\mathbf{n}^{(i)} + \mathbf{t}^{(j)} = \mathbf{0} &\quad\Rightarrow\quad \mathbf{t}^{(j)} = p^{(i)}\mathbf{n}^{(i)}
\end{aligned}
\tag{4.10}
$$

$$
\begin{aligned}
\delta u_n^{(i)} &= -\delta\mathbf{u}^{(j)} \cdot \mathbf{n}^{(j)} - \mathbf{u}^{(j)} \cdot \delta\mathbf{n}^{(j)} \\
\delta\mathbf{t}^{(j)} &= \delta p^{(i)}\mathbf{n}^{(i)} + p^{(i)}\delta\mathbf{n}^{(i)}
\end{aligned}
\tag{4.11}
$$

where, unlike the previous cases, the sensitivities do not follow exactly the same coupling equations due to an additional term that takes into account the variation of the unit normal. This, however, does not lead to difficulties. The only difference with respect to the previous cases is a new term in the right hand side of the system of equations.

4.3.2   BEM–FEM

Consider a BEM region Ω_i (elastic solid) and a FEM region Ω_j (elastic solid) connected through a BEM boundary Γ_k with orientation defined by its unit normal $\mathbf{n}$, see Figure 4.4.
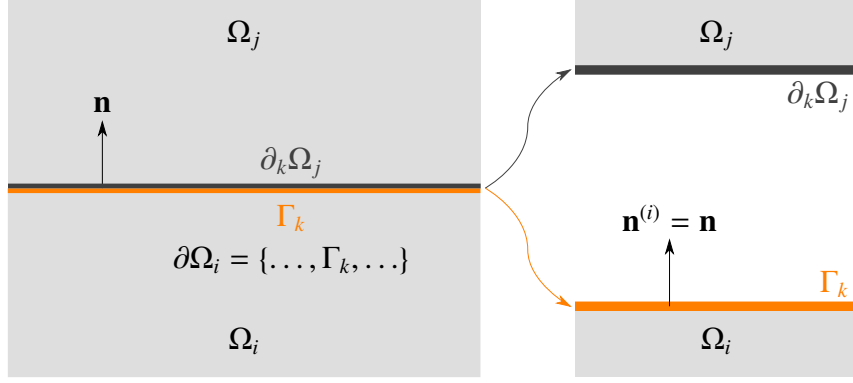
Figure 4.4: Coupling between a BEM boundary Γ_k and a FEM boundary $\partial_k\Omega_j$

The FEM boundary $\partial_k\Omega_j$ is not explicitly defined, but defined implicitly by its coincidence in position with Γ_k.

Let $\mathbf{u}_k^{(i)}$ and $\mathbf{t}_k^{(i)}$ be vectors of displacements and tractions along the boundary Γ_k belonging to the BEM region Ω_i. The displacements and tractions of the remaining boundary of Ω_i are denoted as $\mathbf{u}_i$ and $\mathbf{t}_i$. Vectors $\mathbf{u}_k^{(j)}$ and $\mathbf{t}_k^{(j)}$ are displacements and tractions (as surface distributed loads) along the FEM boundary $\partial_k\Omega_j$. The displacements of the remaining region Ω_j are denoted as $\mathbf{u}_j$. Compatibility and equilibrium conditions along both faces of the interface are established by imposing:

$$
\begin{aligned}
\mathbf{u}_k^{(i)} &= \mathbf{u}_k^{(j)} \\
\mathbf{t}_k^{(i)} + \mathbf{t}_k^{(j)} &= \mathbf{0}_k
\end{aligned}
\tag{4.12}
$$

$$
\begin{aligned}
\delta\mathbf{u}_k^{(i)} &= \delta\mathbf{u}_k^{(j)} \\
\delta\mathbf{t}_k^{(i)} + \delta\mathbf{t}_k^{(j)} &= \mathbf{0}_k
\end{aligned}
\tag{4.13}
$$

where it must be noticed that displacements and tractions and their sensitivities have the same coupling equations. The equations obtained after collocating the SBIE throughout the boundaries of Ω_i can be written as:

$$
\begin{pmatrix} \mathbf{H}_{ii} & \mathbf{H}_{ik} \\ \mathbf{H}_{ki} & \mathbf{H}_{kk} \end{pmatrix} \begin{Bmatrix} \mathbf{u}_i \\ \mathbf{u}_k^{(i)} \end{Bmatrix} - \begin{pmatrix} \mathbf{G}_{ii} & \mathbf{G}_{ik} \\ \mathbf{G}_{ki} & \mathbf{G}_{kk} \end{pmatrix} \begin{Bmatrix} \mathbf{t}_i \\ \mathbf{t}_k^{(i)} \end{Bmatrix} = \begin{Bmatrix} \mathbf{0}_i \\ \mathbf{0}_k \end{Bmatrix}
\tag{4.14}
$$

Moreover, the global FEM equilibrium equation of the region Ω_i is:

$$
\begin{pmatrix} \mathbf{K}_{jj} & \mathbf{K}_{jk} \\ \mathbf{K}_{kj} & \mathbf{K}_{kk} \end{pmatrix} \begin{Bmatrix} \mathbf{u}_j \\ \mathbf{u}_k^{(j)} \end{Bmatrix} - \begin{pmatrix} \mathbf{0}_{ik} \\ \mathbf{Q}_{kk} \end{pmatrix} \begin{Bmatrix} \mathbf{t}_k^{(j)} \end{Bmatrix} = \begin{Bmatrix} \mathbf{f}_j \\ \mathbf{0}_k \end{Bmatrix}
\tag{4.15}
$$

where $\mathbf{Q}_{kk}$ is the matrix that transforms boundary distributed loads along the FEM boundary $\partial_k\Omega_j$ into nodal loads. It is built by assembling the boundary distributed load matrices $\mathbf{Q}_t$ along $\partial_k\Omega_j$, see Equation (2.21). Loads in the rest of the region can be included through $\mathbf{f}_j$. Once coupling conditions are applied maintaining $\mathbf{u}_k^{(j)}$ and $\mathbf{t}_k^{(i)}$ as active degrees

of freedom along the interface, the coupled system can be written as:

$$
\begin{pmatrix}
\mathbf{H}_{ii} & \mathbf{H}_{ik} & -\mathbf{G}_{ik} & \mathbf{0}_{ij} \\
\mathbf{H}_{ki} & \mathbf{H}_{kk} & -\mathbf{G}_{kk} & \mathbf{0}_{kj} \\
\mathbf{0}_{ki} & \mathbf{K}_{kk} & \mathbf{Q}_{kk} & \mathbf{K}_{kj} \\
\mathbf{0}_{ji} & \mathbf{K}_{jk} & \mathbf{0}_{jk} & \mathbf{K}_{jj}
\end{pmatrix}
\begin{Bmatrix}
\mathbf{u}_i \\
\mathbf{u}_k^{(j)} \\
\mathbf{t}_k^{(i)} \\
\mathbf{u}_j
\end{Bmatrix}
-
\begin{pmatrix}
\mathbf{G}_{ii} \\
\mathbf{G}_{ki} \\
\mathbf{0}_{ki} \\
\mathbf{0}_{ji}
\end{pmatrix}
\{\ \mathbf{t}_i\ \}
=
\begin{Bmatrix}
\mathbf{0}_i \\
\mathbf{0}_k \\
\mathbf{0}_k \\
\mathbf{f}_j
\end{Bmatrix}
\tag{4.16}
$$

Finally, the boundary conditions are applied:

$$
\begin{pmatrix}
\mathbf{A}_{ii} & \mathbf{H}_{ik} & -\mathbf{G}_{ik} & \mathbf{0}_{im} \\
\mathbf{A}_{ki} & \mathbf{H}_{kk} & -\mathbf{G}_{kk} & \mathbf{0}_{km} \\
\mathbf{0}_{ki} & \mathbf{K}_{kk} & \mathbf{Q}_{kk} & \mathbf{K}_{km} \\
\mathbf{0}_{mi} & \mathbf{K}_{mk} & \mathbf{0}_{mk} & \mathbf{K}_{mm}
\end{pmatrix}
\begin{Bmatrix}
\mathbf{x}_i \\
\mathbf{u}_k^{(j)} \\
\mathbf{t}_k^{(i)} \\
\mathbf{u}_m
\end{Bmatrix}
=
\begin{Bmatrix}
\mathbf{B}_{ii}\tilde{\mathbf{x}}_i \\
\mathbf{B}_{ki}\tilde{\mathbf{x}}_i \\
-\mathbf{K}_{kn}\tilde{\mathbf{u}}_n \\
\mathbf{f}_m - \mathbf{K}_{mn}\tilde{\mathbf{u}}_n
\end{Bmatrix}
\tag{4.17}
$$

where $\mathbf{x}_i$ and $\tilde{\mathbf{x}}_i$ are vectors of unknown and known field variables, respectively, related to the BEM region, and $\mathbf{u}_m$ and $\tilde{\mathbf{u}}_n$ are unknown and known displacements, respectively, related to the FEM region. Once this system of equations is solved, displacements and tractions are known throughout the domain.

In order to solve the sensitivity problem, we proceed similarly to what has been done so far, but collocating the δSBIE instead of the SBIE for the BEM region, and using Equation (2.3) for the FEM region:

$$
\begin{pmatrix}
\mathbf{A}_{ii} & \mathbf{H}_{ik} & -\mathbf{G}_{ik} & \mathbf{0}_{im} \\
\mathbf{A}_{ki} & \mathbf{H}_{kk} & -\mathbf{G}_{kk} & \mathbf{0}_{km} \\
\mathbf{0}_{ki} & \mathbf{K}_{kk} & \mathbf{Q}_{kk} & \mathbf{K}_{km} \\
\mathbf{0}_{mi} & \mathbf{K}_{mk} & \mathbf{0}_{mk} & \mathbf{K}_{mm}
\end{pmatrix}
\begin{Bmatrix}
\delta\mathbf{x}_i \\
\delta\mathbf{u}_k^{(j)} \\
\delta\mathbf{t}_k^{(i)} \\
\delta\mathbf{u}_m
\end{Bmatrix}
=
\begin{Bmatrix}
\mathbf{B}_{ii}\delta\tilde{\mathbf{x}}_i \\
\mathbf{B}_{ki}\delta\tilde{\mathbf{x}}_i \\
-\mathbf{K}_{kn}\delta\tilde{\mathbf{u}}_n \\
\delta\mathbf{f}_m - \mathbf{K}_{mn}\delta\tilde{\mathbf{u}}_n
\end{Bmatrix}
$$
$$
-
\begin{pmatrix}
\delta\mathbf{H}_{ii} & \delta\mathbf{H}_{ik} & \mathbf{0}_{im} & \mathbf{0}_{in} \\
\delta\mathbf{H}_{ki} & \delta\mathbf{H}_{kk} & \mathbf{0}_{km} & \mathbf{0}_{kn} \\
\mathbf{0}_{ki} & \delta\mathbf{K}_{kk} & \delta\mathbf{K}_{km} & \delta\mathbf{K}_{kn} \\
\mathbf{0}_{mi} & \delta\mathbf{K}_{mk} & \delta\mathbf{K}_{mm} & \delta\mathbf{K}_{mn}
\end{pmatrix}
\begin{Bmatrix}
\mathbf{u}_i \\
\mathbf{u}_k^{(i)} \\
\mathbf{u}_m \\
\tilde{\mathbf{u}}_n
\end{Bmatrix}
+
\begin{pmatrix}
\delta\mathbf{G}_{ii} & \delta\mathbf{G}_{ik} \\
\delta\mathbf{G}_{ki} & \delta\mathbf{G}_{kk} \\
\mathbf{0}_{ki} & -\delta\mathbf{Q}_{kk} \\
\mathbf{0}_{mi} & \mathbf{0}_{mk}
\end{pmatrix}
\begin{Bmatrix}
\mathbf{t}_i \\
\mathbf{t}_k^{(i)}
\end{Bmatrix}
\tag{4.18}
$$

where the δ notation is used instead of $\partial/\partial a$ for the FEM part. Note that all FEM matrices can be calculated analytically (except for the numerical integration) as shown in Chapter 2. In particular, $\delta\mathbf{Q}_{kk}$ is calculated with the help of Equations (2.33) and (2.49).

Chapter 5

Shape optimization of a simple wave barrier

5.1 Introduction

Almost all the ingredients needed to perform the shape optimization of a wave barrier have been described in the previous chapters. In this chapter, they are put together in order to optimize a simple wave barrier.

The rest of the chapter is organized as follows. In Section 5.2, the simple wave barrier problem is studied. Finally, Section 5.3 closes this report by giving the main conclusions, and recommendations for further research.
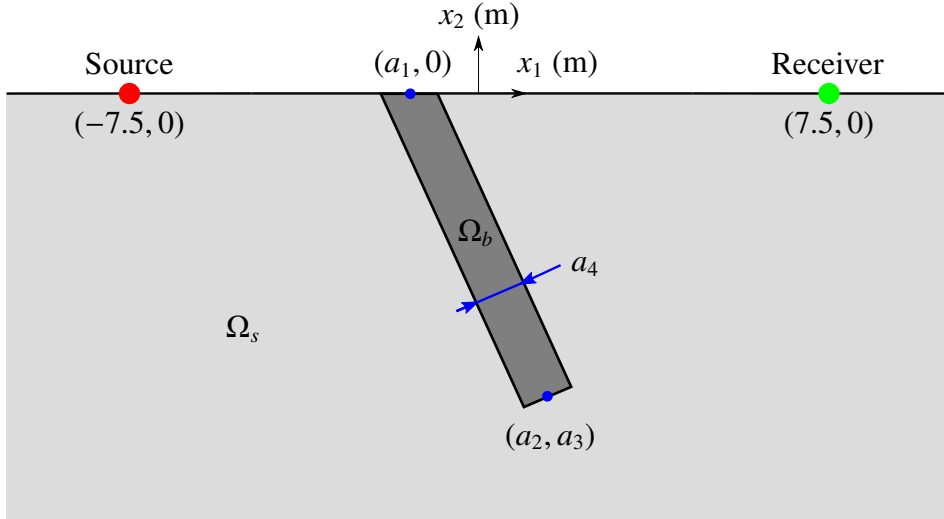
5.2 Simple wave barrier

5.2.1 Definition

The design optimization of a simple straight wave barrier is considered. Figure 5.1 shows a layout of the considered system, including the material properties of the soil region Ω_s and barrier region Ω_b, and the design variables a_1, a_2, a_3 and a_4. A point source and a point receiver are considered, which are spaced 15 meters. The point source oscillates at 25 Hz. The design space of the barrier is located in between. The design variable a_1 is the horizontal coordinate of the top of the barrier, which can vary from -5 to 5 meters. The design variable a_2 is the horizontal coordinate of the bottom of the barrier, which can also vary from -5 to 5 meters. The third design variable a_3 is the vertical coordinate of the bottom of the barrier, which can also vary from -8 to -1 meters. The fourth design variable a_4 is the thickness of the barrier, which is assumed to vary from 0.3 to 1.5 meters. According to Figure 5.1, the area of Ω_b is simply $a_4 \sqrt{(a_1 - a_2)^2 + (a_3)^2}$.

The design optimization is defined as:

$$\min_{a_1,a_2,a_3,a_4} \psi, \quad \psi = 20 \log_{10} \left(\frac{|\mathbf{u}^{\text{with barrier}}(7.5, 0)|}{|\mathbf{u}^{\text{without barrier}}(7.5, 0)|} \right) \tag{5.1}$$

Ω_b: $\mu = 605$ MPa, $\nu = 1/4$, $\rho = 2000$ kg/m³, $\xi = 0.05$
Ω_s: $\mu = 80$ MPa, $\nu = 1/3$, $\rho = 2000$ kg/m³, $\xi = 0.05$

Figure 5.1: Layout of the studied simple wave barrier

such that:

$$a_1 = [-5, 5]$$
$$a_2 = [-5, 5]$$
$$a_3 = [-8, -1] \quad \quad (5.2)$$
$$a_4 = [0.3, 1.5]$$
$$A_{\max} \geq a_4 \sqrt{(a_1 - a_2)^2 + (a_3)^2}$$

Therefore, the objective function is a measure of the amplification of the displacement $|\mathbf{u}|$ at the receiver due to the barrier, and hence it has to be minimized. The design space allows any barrier within a rectangle between source and receiver, where the barrier always emerges at the soil surface. A simple economic constraint is defined by setting a maximum barrier area $A_{\max}$.

5.2.2 Sensitivity test

Before performing the design optimization, a sensitivity test is done in this section. This test consists in calculating the sensitivities of the objective function with respect to all the design variables using different methodologies and models. It allows us to verify that almost every aspect of the methodology is correctly executed. Also, this test implicitly validates the coupling conditions presented in Chapter 4.

The methodologies we are referring to are the Global Finite Difference (GFD) and the Direct Differentiation Method (DDM) to calculate the sensitivities. Three models of the problem are considered:

- BEM–BEM. All regions are BEM regions.

- BEM–FEM 1. The half-plane is a BEM region, and the design space and the barrier are FEM regions.

- BEM–FEM 2. The half-plane (including the design space) is a BEM region, and the barrier is a FEM region.

GFD are calculated using a 2-point central finite difference formula. Note that each mesh that GFD requires is generated by the pre-processor once the perturbation is defined, hence the meshes are not necessarily topologically identical. The design velocity field that DDM requires is defined by a 4-node quadrilateral design element that cover the barrier. Additionally, for "BEM–BEM" and "BEM–FEM 2" models, the design mesh requires two line design elements from the top of the barrier to the ends of the design space along the soil surface. The four corners of the barrier are defined by the following points:

$$\theta = \arctan \frac{a_2 - a_1}{-a_3} \tag{5.3}$$

$$\mathbf{p}_1 = \left(a_1 + \frac{a_4/2}{\cos \theta}, 0 \right) \tag{5.4}$$

$$\mathbf{p}_2 = \left(a_2 + \frac{a_4}{2} \cos \theta, a_3 + \frac{a_4}{2} \sin \theta \right) \tag{5.5}$$

$$\mathbf{p}_3 = \left(a_2 - \frac{a_4}{2} \cos \theta, a_3 - \frac{a_4}{2} \sin \theta \right) \tag{5.6}$$

$$\mathbf{p}_4 = \left(a_1 - \frac{a_4/2}{\cos \theta}, 0 \right) \tag{5.7}$$

Taking into account this, the design velocity field at each one of the nodes of the quadrilateral design element is obtained by simply doing $\mathbf{v}^{(i)} = \partial \mathbf{p}_i / \partial a_j$. The two additional line design elements have design velocity fields $\mathbf{v}^{(1)}$ and $\mathbf{v}^{(4)}$ at their start nodes, and a null design velocity field at their ends.

In all the models, quadratic elements are used. The half-plane mesh is truncated at $x_1 = -50$ and $x_1 = 50$ meters. The element sizes are 2.5 meters for elements outside the design space (aprox. 3 elements per wavelenth), and a_4 meters for elements inside the design space (more than 5 elements per wavelenth). This sensitivity test is done over two designs: a vertical barrier with $\mathbf{a} = (0, 0, -8, 0.5$, and a inclined barrier with $\mathbf{a} = (-4, 4, -8, 1)$. Figure 5.2 shows the meshes used in this section.

The results of this test are shown in Tables 5.1 and 5.2. These results demonstrate the lack of robustness of GFD, especially for models that include a FEM region. However, its simplicity allows us to validate the models using DDM. Results obtained from GFD converge to the results obtained from DDM as the perturbation decreases. Generally, the results obtained from different models and methodologies agree, except in the case of the "BEM–FEM 1" model for the design variable a_3 (vertical coordinate of the bottom part of the barrier). Nonetheless, the discrepancy seems to be acceptable ($\approx 10\%$).

5.2.3 Design optimization

The optimization function used in MATLAB is `fmincon` with the interior-point algorithm. The objective function and its gradient is supplied by an user-defined function, where the analysis model is launched and its results are processed in order to calculate the objective
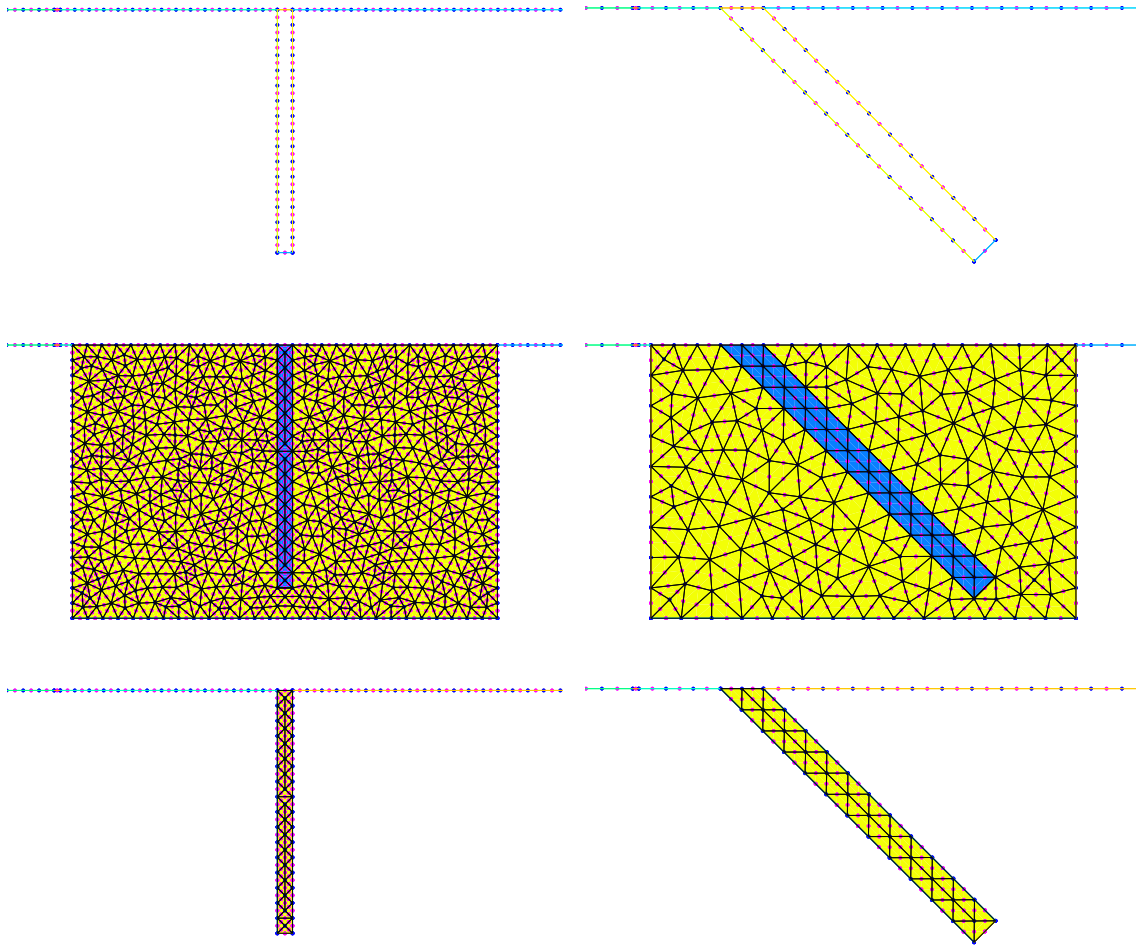
Figure 5.2: Meshes used in the sensitivity test: BEM–BEM (top), BEM–FEM 1 (middle), BEM–FEM 2 (bottom); vertical barrier (left), inclined barrier (right)

Methodology / Model	Δa_j	$\dfrac{\mathrm{d}\psi}{\mathrm{d}a_1}$	$\dfrac{\mathrm{d}\psi}{\mathrm{d}a_2}$	$\dfrac{\mathrm{d}\psi}{\mathrm{d}a_3}$	$\dfrac{\mathrm{d}\psi}{\mathrm{d}a_4}$
GFD / BEM–BEM	10^{-1}	-0.272123	-0.025787	0.047936	-2.730099
	10^{-2}	-0.272620	-0.025949	0.045517	-2.742033
	10^{-3}	-0.272535	-0.025951	0.048044	-2.727737
	10^{-4}	-0.272548	-0.025972	0.048062	-2.697366
DDM / BEM–BEM	-	-0.272383	-0.025988	0.0480537	-2.716126
GFD / BEM–FEM 1	10^{-1}	-0.272386	-0.027116	0.038623	-2.738707
	10^{-2}	-0.265332	-0.034423	0.014281	-2.701757
	10^{-3}	-0.182082	-0.112729	0.012887	-2.832151
	10^{-4}	0.655976	-0.965777	-0.179035	-2.763377
DDM / BEM–FEM 1	-	-0.270422	-0.024804	0.040647	-2.721775
GFD / BEM–FEM 2	10^{-1}	-0.273811	-0.024663	0.046720	-2.732175
	10^{-2}	-0.272441	-0.026763	0.043196	-2.743785
	10^{-3}	-0.253422	-0.045722	0.045168	-2.741105
	10^{-4}	-0.067677	-0.231990	0.030587	-2.714976
DDM / BEM–FEM 1	-	-0.274320	-0.024530	0.046884	-2.717310

Table 5.1: Sensitivities for a vertical barrier ($\mathbf{a} = (0, 0, -8, 0.5)$)

Methodology / Model	Δa_j	$\dfrac{\mathrm{d}\psi}{\mathrm{d}a_1}$	$\dfrac{\mathrm{d}\psi}{\mathrm{d}a_2}$	$\dfrac{\mathrm{d}\psi}{\mathrm{d}a_3}$	$\dfrac{\mathrm{d}\psi}{\mathrm{d}a_4}$
GFD / BEM–BEM	10^{-1}	0.918170	0.315681	-0.091428	-2.763727
	10^{-2}	0.918818	0.315490	-0.092140	-2.701609
	10^{-3}	0.918724	0.315770	-0.092117	-2.738099
	10^{-4}	0.918735	0.315631	-0.092111	-2.740870
DDM / BEM–BEM	-	0.918243	0.315682	-0.092150	-2.754934
GFD / BEM–FEM 1	10^{-1}	0.918748	0.313146	-0.099214	-2.691929
	10^{-2}	0.907295	0.367585	-0.095097	-2.568600
	10^{-3}	0.904674	0.316097	-0.073474	-2.557267
	10^{-4}	0.855978	0.385557	-0.199216	-2.821976
DDM / BEM–FEM 1	-	0.915422	0.309543	-0.079929	-2.706064
GFD / BEM–FEM 2	10^{-1}	0.922270	0.306479	-0.095655	-2.744842
	10^{-2}	0.912900	0.315847	-0.091904	-2.686637
	10^{-3}	0.913033	0.316588	-0.091738	-2.723225
	10^{-4}	0.912735	0.321061	-0.091038	-2.721601
DDM / BEM–FEM 1	-	0.912321	0.316000	-0.091886	-2.739976

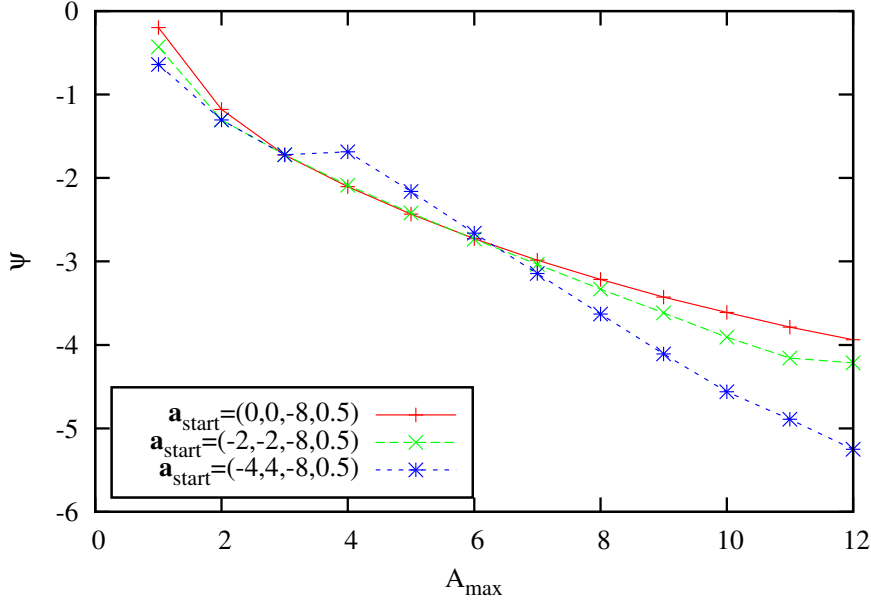Table 5.2: Sensitivities for a inclined barrier ($\mathbf{a} = (-4, 4, -8, 1)$)

Figure 5.3: ψ versus A_{max}

function and its gradient. Here, the BEM–BEM model is used as the analysis model. The upper and lower bounds of the design variables are defined explicitly before calling `fmincon`. The non-linear constraint is implemented by an user-defined function where it is evaluated.

The shape optimization has been performed for a range of maximum areas $A_{\mathrm{max}} = [1, 12]$. By doing so, an approximation of the Pareto front is obtained for the conflicting constraint A_{max} and objective function ψ. Three local minima have been observed when starting from three different designs: $\mathbf{a}_{\mathrm{start}} = (0, 0, -8, 0.5)$, $\mathbf{a}_{\mathrm{start}} = (-2, -2, -8, 0.5)$ and $\mathbf{a}_{\mathrm{start}} = (-4, 4, -8, 0.5)$. The results are shown in Tables 5.3, 5.4 and 5.5, and Figures 5.4, 5.5 and 5.6. The approximation of the Pareto front is shown in Figure 5.3.

5.3 Conclusions and further research

This report collects the results obtained during the research stay, which has been the first contact of the author with FEM or BEM sensitivity analysis. It also contains some developments done during the month after the stay.

The FEM sensitivity formulation, despite being relatively simple if the semianalytical approach is used, is not trouble-free. For this reason, it was decided to take a step forward and search for an analytical solution to the matrices differentiation. Among others, Olhoff et al. [49] had offered a tractable solution. We have developed their formulation for two-dimensional solid elements, and excellent results have been obtained. Their formulation is more simple than it looks, and it is adviceable to make the effort for the sake of robustness.

The BEM sensitivity formulation is, however, much more involved. Almost one third of this report is concerned to this formulation. The Variation Singular Boundary Integral Equation for interior and boundary points have been developed for Laplace, Helmholtz, elastostatics and elastodynamics problems. The corresponding chapter has been written

A_{max}	a_1	a_2	a_3	a_4	ψ
1	1.175	2.273	-3.147	0.300	-0.198
2	1.034	1.526	-6.648	0.300	-1.177
3	0.951	1.275	-7.633	0.393	-1.725
4	0.963	1.250	-7.799	0.513	-2.102
5	0.977	1.233	-7.923	0.631	-2.433
6	0.988	1.224	-8.000	0.750	-2.728
7	1.006	1.240	-8.000	0.875	-2.985
8	1.024	1.252	-8.000	1.000	-3.216
9	1.038	1.257	-8.000	1.125	-3.428
10	1.057	1.265	-8.000	1.250	-3.612
11	1.072	1.264	-8.000	1.375	-3.788
12	1.096	1.265	-8.000	1.500	-3.938

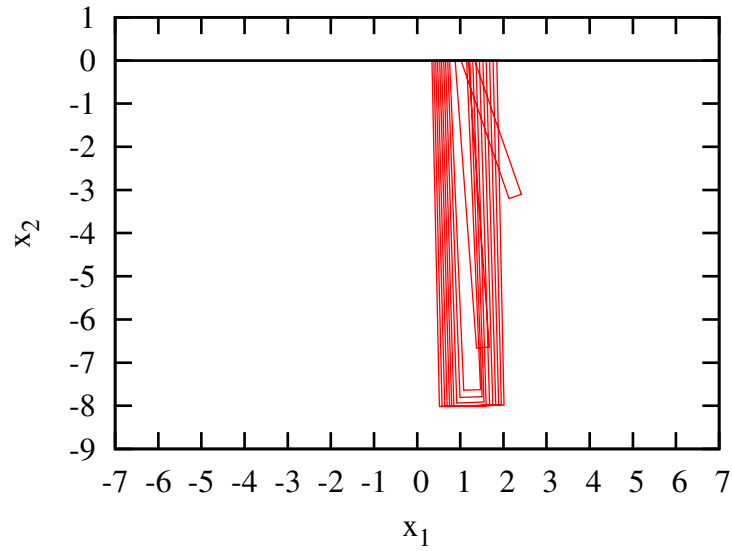Table 5.3: Optimization results when $\mathbf{a}_{start} = (0, 0, -8, 0.5)$

Figure 5.4: Layout of the optimized wave barrier varying A_{max}, $\mathbf{a}_{start} = (0, 0, -8, 0.5)$.

A_{max}	a_1	a_2	a_3	a_4	ψ
1	-3.646	-5.000	-3.046	0.300	-0.429
2	-1.983	-3.827	-6.118	0.313	-1.304
3	-1.856	-3.807	-6.360	0.451	-1.722
4	-1.755	-3.800	-6.510	0.586	-2.087
5	-1.668	-3.808	-6.595	0.721	-2.421
6	-1.590	-3.835	-6.625	0.858	-2.734
7	-1.513	-3.881	-6.604	0.998	-3.034
8	-1.441	-3.941	-6.542	1.142	-3.330
9	-1.375	-3.999	-6.475	1.288	-3.616
10	-1.304	-4.043	-6.410	1.435	-3.906
11	-1.221	-3.961	-6.802	1.500	-4.156
12	-1.200	-3.709	-7.440	1.500	-4.216

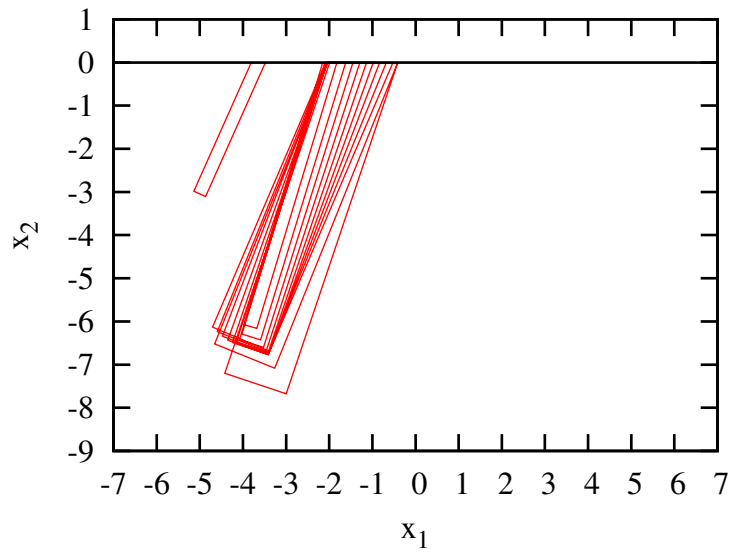Table 5.4: Optimization results when $\mathbf{a}_{start} = (-2, -2, -8, 0.5)$

Figure 5.5: Layout of the optimized wave barrier varying A_{max}, $\mathbf{a}_{start} = (-2, -2, -8, 0.5)$.

A_{max}	a_1	a_2	a_3	a_4	ψ
1	5.000	1.820	-1.000	0.300	-0.641
2	-1.983	-3.827	-6.118	0.313	-1.304
3	-1.856	-3.807	-6.360	0.451	-1.722
4	-5.000	-2.376	-5.018	0.706	-1.687
5	-5.000	-2.410	-5.123	0.871	-2.161
6	-5.000	-2.417	-5.228	1.029	-2.661
7	-5.000	-2.410	-5.334	1.180	-3.144
8	-5.000	-2.375	-5.443	1.324	-3.631
9	-4.995	-2.272	-5.580	1.448	-4.108
10	-5.000	-1.847	-5.874	1.500	-4.561
11	-5.000	-1.178	-6.259	1.500	-4.891
12	-5.000	-0.498	-6.613	1.500	-5.250

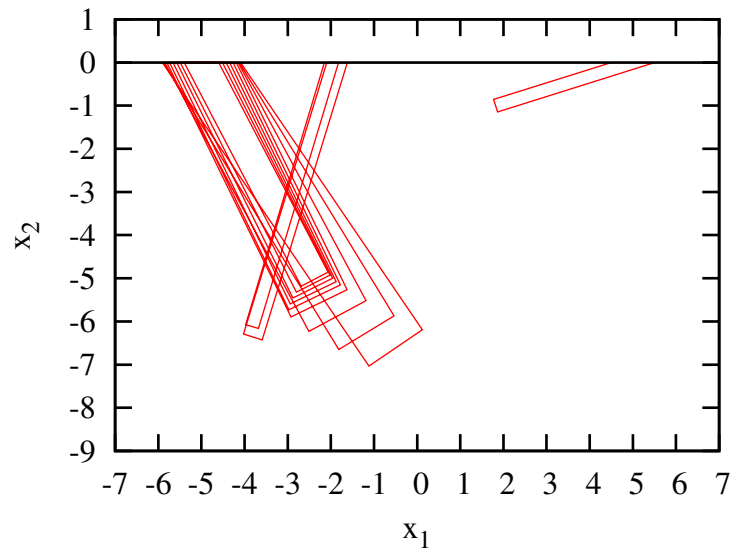Table 5.5: Optimization results when $\mathbf{a}_{start} = (-4, 4, -8, 0.5)$

Figure 5.6: Layout of the optimized wave barrier varying A_{max}, $\mathbf{a}_{start} = (-4, 4, -8, 0.5)$.

trying to be very explicit and pedagogic. If one compares the results of the validation problems, it is clear the superiority of the BEM over the FEM for wave propagation problems. Its error levels for the same element size are much lower.

As it is well known, there are problems where neither the FEM nor the BEM is able to solve them efficiently. For this reason, we have described and explained the classical coupling conditions applied to the sensitivity analysis. It was shown that the direct coupling is similar to any standard zero-order analysis, except that is more involved.

There are several aspects of these formulations that could be improved or expanded:

- The analytical differentiation of the matrices related to the solid isoparametric elements can be applied to structural elements, as shown by Olhoff et al. [49]. This is very interesting in order to optimize designs where structural elements appear.

- Although this report is concerned with the shape optimization, it is not difficult to include material optimization (sensitivities of material properties). This could be used on identification problems.

- Concerning the DDM-BEM formulation, the δHBIE for the already studied problems (Laplace, Helmholtz, elastostatics and elastodynamics) could be obtained thanks to the experience acquired when working on the present research.

- Formulate and implement the variational coupling of Belytschko [41] in the context of sensitivity analysis. To author's best knowledge, this is something that has not been done. It would be interesting to evaluate if the improvement in accuracy that this coupling would bring compensate its involved formulation.

- Obtain these formulations for three-dimensional problems.

- Study the possibilities of hybridization of gradient-based optimization and genetic algorithms in order to get rid of the local minima.

The developed formulation could be applied to more interesting problems:

- The simple wave barrier studied in the present work is useful as an application problem. A more complex wave barrier would be more interesting designs with better performance and less costs. Also, in order to get a more robust design, the objective function would be modified, which could be done in several directions. Instead of considering a single frequency, a range of frequencies could be studied, and hence the objective function must be modified accordingly. In the same way, instead of using just one receiver, a zone of receivers can be defined.

- Given that we have developed BEM–BEM and BEM–FEM couplings for sensitivity analysis in the two-dimensional context, it would be interesting to study of Fluid-Structure, Structure-Soil-Structure, or Fluid-Soil-Structure Interaction problems.

Appendix A

Free-term b^i_{lkjm} of the δSBIE for elastostatics

In this appendix, the values of the free-term b^i_{lkjm} existing in the elastostatic (and elasto-dynamic) δSBIE for boundary collocation points are presented, see Equation (3.150).

$$B = -\frac{1}{4\pi(1-\nu)} \tag{A.1}$$

$$b^i_{1111} = \frac{B}{2}\sin(\theta_1 - \theta_2)\Big[-4(\nu-1)\cos(\theta_1 + \theta_2) + \cos(3\theta_1 + \theta_2) + \cos(\theta_1 + 3\theta_2)\Big] \tag{A.2}$$

$$b^i_{1112} = -\frac{B}{2}\Big[\cos(2\theta_1) - \cos(2\theta_2)\Big]\Big[\cos(2\theta_1) + \cos(2\theta_2) - 2\nu + 1\Big] \tag{A.3}$$

$$b^i_{1121} = -\frac{B}{2}\Big[\cos(2\theta_1) - \cos(2\theta_2)\Big]\Big[\cos(2\theta_1) + \cos(2\theta_2) - 2\nu + 3\Big] \tag{A.4}$$

$$b^i_{1122} = -\frac{B}{2}\sin(\theta_1 - \theta_2)\Big[-4(\nu-1)\cos(\theta_1 + \theta_2) + \cos(3\theta_1 + \theta_2) + \cos(\theta_1 + 3\theta_2)\Big] \tag{A.5}$$

$$b^i_{1211} = -\frac{B}{2}\Big[\cos(2\theta_1) - \cos(2\theta_2)\Big]\Big[\cos(2\theta_1) + \cos(2\theta_2) - 2\nu + 1\Big] \tag{A.6}$$

$$b^i_{1212} = \frac{B}{4}\Big[4\nu\sin(2\theta_1) - \sin(4\theta_1) - 4\nu\sin(2\theta_2) + \sin(4\theta_2)\Big] \tag{A.7}$$

$$b^i_{1221} = -\frac{B}{2}\sin(\theta_1 - \theta_2)\Big[-4(\nu-1)\cos(\theta_1 + \theta_2) + \cos(3\theta_1 + \theta_2) + \cos(\theta_1 + 3\theta_2)\Big] \tag{A.8}$$

$$b^i_{1222} = \frac{B}{2}\Big[\cos(2\theta_1) - \cos(2\theta_2)\Big]\Big[\cos(2\theta_1) + \cos(2\theta_2) - 2\nu + 1\Big] \tag{A.9}$$

$$b^i_{2111} = -\frac{B}{2}\Big[\cos(2\theta_1) - \cos(2\theta_2)\Big]\Big[\cos(2\theta_1) + \cos(2\theta_2) + 2\nu - 1\Big] \tag{A.10}$$

$$b^i_{2112} = -\frac{B}{2}\sin(\theta_1 - \theta_2)\Big[4(\nu-1)\cos(\theta_1 + \theta_2) + \cos(3\theta_1 + \theta_2) + \cos(\theta_1 + 3\theta_2)\Big] \tag{A.11}$$

$$b^i_{2121} = \frac{B}{4}\Big[-4\nu\sin(2\theta_1) - \sin(4\theta_1) + 4\nu\sin(2\theta_2) + \sin(4\theta_2)\Big] \tag{A.12}$$

$$b^i_{2122} = \frac{B}{2}\Big[\cos(2\theta_1) - \cos(2\theta_2)\Big]\Big[\cos(2\theta_1) + \cos(2\theta_2) + 2\nu - 1\Big] \tag{A.13}$$

$$b^{\mathrm{i}}_{2211} = -\frac{B}{2}\sin(\theta_1 - \theta_2)\Big[4(\nu - 1)\cos(\theta_1 + \theta_2) + \cos(3\theta_1 + \theta_2) + \cos(\theta_1 + 3\theta_2)\Big] \tag{A.14}$$

$$b^{\mathrm{i}}_{2212} = \frac{B}{2}\Big[\cos(2\theta_1) - \cos(2\theta_2)\Big]\Big[\cos(2\theta_1) + \cos(2\theta_2) + 2\nu - 3\Big] \tag{A.15}$$

$$b^{\mathrm{i}}_{2221} = \frac{B}{2}\Big[\cos(2\theta_1) - \cos(2\theta_2)\Big]\Big[\cos(2\theta_1) + \cos(2\theta_2) + 2\nu - 1\Big] \tag{A.16}$$

$$b^{\mathrm{i}}_{2222} = \frac{B}{2}\sin(\theta_1 - \theta_2)\Big[4(\nu - 1)\cos(\theta_1 + \theta_2) + \cos(3\theta_1 + \theta_2) + \cos(\theta_1 + 3\theta_2)\Big] \tag{A.17}$$

$$b^{\mathrm{i}}_{2211} = -\frac{B}{2}\sin(\theta_1 - \theta_2)\Big[4(\nu - 1)\cos(\theta_1 + \theta_2) + \cos(3\theta_1 + \theta_2) + \cos(\theta_1 + 3\theta_2)\Big]$$

$$b^{\mathrm{i}}_{2212} = \frac{B}{2}\Big[\cos(2\theta_1) - \cos(2\theta_2)\Big]\Big[\cos(2\theta_1) + \cos(2\theta_2) + 2\nu - 3\Big]$$

Appendix B

Decomposition of elastodynamic fundamental solution and its derivatives

The elastodynamic fundamental solution and its derivatives were presented in Equations (3.201-3.205). In the present appendix, their main terms U_i, V_i, T_i and R_i are decomposed by using the decomposition of Bessel functions shown in Equation (3.113). Note that terms V_3, R_1, R_4 and R_6 have been omitted for brevity, see Equations (3.202) and (3.205).

$$
\begin{aligned}
U_1 = & -\frac{1}{2}\left(\frac{k_1^2}{k_2^2} + 1\right)\ln r - \frac{1}{2}\left[\gamma + \ln\frac{ik_2}{2} + \frac{1}{2} + \frac{k_1^2}{k_2^2}\left(\gamma + \ln\frac{ik_1}{2} - \frac{1}{2}\right)\right] + K_0^R\left(ik_2 r\right) \\
& -\frac{k_1^2}{k_2^2}\frac{1}{ik_1 r}K_1^R\left(ik_1 r\right) + \frac{1}{ik_2 r}K_1^R\left(ik_2 r\right)
\end{aligned}
\tag{B.1}
$$

$$
\begin{aligned}
U_2 = & \frac{1}{2}\left(\frac{k_1^2}{k_2^2} - 1\right) + \frac{1}{8}\left(k_2^2 - \frac{k_1^4}{k_2^2}\right)r^2\ln r \\
& + \frac{1}{8}\left[k_2^2\left(\gamma + \ln\frac{ik_2}{2} - \frac{3}{4}\right) - \frac{k_1^4}{k_2^2}\left(\gamma + \ln\frac{ik_1}{2} - \frac{3}{4}\right)\right]r^2 - \frac{k_1^2}{k_2^2}K_2^R\left(ik_1 r\right) + K_2^R\left(ik_2 r\right)
\end{aligned}
\tag{B.2}
$$

$$
\begin{aligned}
V_1 = & -\frac{1}{2}\left(\frac{k_1^2}{k_2^2} + 1\right)\frac{1}{r} + \frac{1}{8}\left(\frac{k_1^4}{k_2^2} + 3k_2^2\right)r\ln r \\
& + \frac{1}{2}\left\{\frac{1}{4}\left[\frac{k_1^4}{k_2^2}\left(\gamma + \ln\frac{ik_1}{2} - \frac{3}{4}\right) - k_2^2\left(\gamma + \ln\frac{ik_2}{2} - \frac{3}{4}\right)\right] + k_2^2\left(\gamma + \ln\frac{ik_2}{2} - \frac{1}{2}\right)\right\}r \\
& - ik_2 K_1^R\left(ik_2 r\right) + \frac{k_1^2}{k_2^2}\frac{1}{r}K_2^R\left(ik_1 r\right) - \frac{1}{r}K_2^R\left(ik_2 r\right)
\end{aligned}
\tag{B.3}
$$

$$
\begin{aligned}
V_2 = & \left(\frac{k_1^2}{k_2^2} - 1\right)\frac{1}{r} + \frac{1}{8}\left(\frac{k_1^4}{k_2^2} - k_2^2\right)r - ik_1\frac{k_1^2}{k_2^2}K_1^R\left(ik_1 r\right) + ik_2 K_1^R\left(ik_2 r\right) \\
& - \frac{k_1^2}{k_2^2}\frac{4}{r}K_2^R\left(ik_1 r\right) + 4K_2^R\left(ik_2 r\right)
\end{aligned}
\tag{B.4}
$$

$$
\begin{aligned}
T_1 = & 2\left(\frac{k_1^2}{k_2^2} - 1\right)\frac{1}{r} + \frac{1}{4}\left(\frac{k_1^4}{k_2^2} - k_2^2\right)r - 2ik_1\frac{k_1^2}{k_2^2}K_1^R\left(ik_1 r\right) + 2ik_2 K_1^R\left(ik_2 r\right) \\
& - \frac{k_1^2}{k_2^2}\frac{8}{r}K_2^R\left(ik_1 r\right) + \frac{8}{r}K_2^R\left(ik_2 r\right)
\end{aligned}
\tag{B.5}
$$

$$T_2 = -\frac{k_1^2}{k_2^2}\frac{1}{r} + \frac{1}{4}\left(\frac{k_1^4}{k_2^2} + k_2^2\right)r\ln r + \frac{1}{4}\left[\frac{k_1^4}{k_2^2}\left(\gamma + \ln\frac{ik_1}{2} - \frac{3}{4}\right) + k_2^2\left(\gamma + \ln\frac{ik_2}{2} - \frac{1}{4}\right)\right]r$$
$$- ik_2 K_1^R(ik_2 r) + \frac{k_1^2}{k_2^2}\frac{2}{r}K_2^R(ik_1 r) - \frac{2}{r}K_2^R(ik_2 r) \tag{B.6}$$

$$T_3 = \frac{k_1^2}{k_2^2}\frac{1}{r} + \frac{1}{4}\left(2k_1^2 - k_2^2 - 3\frac{k_1^4}{k_2^2}\right)r\ln r$$
$$+ \frac{1}{4}\left[2k_1^2\left(\gamma + \ln\frac{ik_1}{2} - \frac{1}{2}\right) - k_2^2\left(\gamma + \ln\frac{ik_2}{2} - \frac{3}{4}\right) - 3\frac{k_1^4}{k_2^2}\left(\gamma + \ln\frac{ik_1}{2} - \frac{5}{12}\right)\right]r \tag{B.7}$$
$$+ ik_1\left(2\frac{k_1^2}{k_2^2} - 1\right)K_1^R(ik_1 r) + \frac{k_1^2}{k_2^2}\frac{2}{r}K_2^R(ik_1 r) - \frac{2}{r}K_2^R(ik_2 r)$$

$$R_2 = 2\frac{k_1^2}{k_2^2}\frac{1}{r^2} + \frac{1}{4}\left(\frac{k_1^4}{k_2^2} + k_2^2\right) - k_2^2 K_0^R(ik_2 r) - 2ik_1\frac{k_1^2}{k_2^2}\frac{1}{r}K_1^R(ik_1 r) + 4ik_2\frac{1}{r}K_1^R(ik_2 r)$$
$$- 8\frac{k_1^2}{k_2^2}\frac{1}{r^2}K_2^R(ik_1 r) + 8\frac{1}{r^2}K_2^R(ik_2 r) \tag{B.8}$$

$$R_3 = 8\left(1 - \frac{k_1^2}{k_2^2}\right)\frac{1}{r^2} + \frac{1}{2}\left(k_2^2 - \frac{k_1^4}{k_2^2}\right) - 2\frac{k_1^4}{k_2^2}K_0^R(ik_1 r) + 2k_2^2 K_0^R(ik_2 r)$$
$$+ 16ik_1\frac{k_1^2}{k_2^2}\frac{1}{r}K_1^R(ik_1 r) - 16ik_2\frac{1}{r}K_1^R(ik_2 r) + 48\frac{k_1^2}{k_2^2}\frac{1}{r^2}K_2^R(ik_1 r) - 48\frac{1}{r^2}K_2^R(ik_2 r) \tag{B.9}$$

$$R_5 = -2\frac{k_1^2}{k_2^2}\frac{1}{r^2} + \frac{1}{4}\left(-3\frac{k_1^4}{k_2^2} + 2k_1^2 - k_2^2\right) + \left(2\frac{k_1^4}{k_2^2} - k_1^2\right)K_0^R(ik_1 r)$$
$$+ 2ik_1\left(1 - 3\frac{k_1^2}{k_2^2}\right)\frac{1}{r}K_1^R(ik_1 r) + 2ik_2\frac{1}{r}K_1^R(ik_2 r) - 8\frac{k_1^2}{k_2^2}\frac{1}{r^2}K_2^R(ik_1 r) + 8\frac{1}{r^2}K_2^R(ik_2 r) \tag{B.10}$$

Bibliography

[1] M. Abramowitz and I.A. Stegun, editors. *Handbook of Mathematical Functions: with Formulas, Graphs,and Mathematical Tables*. Number 55 in National Bureau of Standards - Applied Mathematics. New York, Dover Publications, 10th printing with corrections, december 1972 edition, 1964.

[2] S. Ahmad and T. M. Al-Hussaini. Simplified design for vibration screening by open and in-filled trenches. *Journal of Geotechnical Engineering*, 117:67–88, 1991.

[3] R. Aithal and S. Saigal. Adjoint structure approach for shape-sensitivity analysis using bem. *Journal of Engineering Mechanics*, 116:2663–2680, 1990.

[4] R. Aithal and S. Saigal. Shape sensitivity analysis in thermal problems using bem. *Engineering Analysis with Boundary Elements*, 15:115–120, 1995.

[5] S. Arnout. *Optimization of shell and truss structures based on size and shape parameterization*. PhD thesis, Katholieke Universiteit Leuven – Faculty of Engineering Science, 2012.

[6] J. S. Arora. An exposition of the material derivative approach for structural shape sensitivity analysis. *Computer Methods in Applied Mechanics and Engineering*, 1993.

[7] J. Avilés and F. J. Sánchez-Sesma. Foundation isolation from vibrations using piles as barriers. *Journal of Engineering Mechanics*, 114:1854–1870, 1988.

[8] P. K. Banerjee. *The Boundary Element Methods in Engineering*. McGraw-Hill Book Company, Inc., 1994.

[9] P. K. Banerjee, S. Ahmad, and K. Chen. Advanced application of BEM to wave barriers in multi-layered three-dimensional soil media. *Earthquake Engineering and Structural Dynamics*, 16:1041–1060, 1988.

[10] D. D. Barkan. *Dynamics of bases and foundations*. McGraw-Hill Book Company, Inc., 1962.

[11] M. R. Barone and D. A. Caulk. Optimal arrangement of holes in a two-dimensional heat conductor by a special boundary integral method. *International Journal for Numerical Methods in Engineering*, 18:675–685, 1982.

[12] M. R. Barone and R. J. Yang. Boundary integral equations for recovery of design sensitivities in shape optimization. *AIAA Journal*, 26:589–594, 1988.

[13] M. R. Barone and R. J. Yang. A boundary element approach for recovery of shape sensitivities in three-dimensional elastic solids. *Computer Methods in Applied Mechanics and Engineering*, 74:69–82, 1989.

[14] T. Belytschko, H. S. Chang, and Y. Y. Lu. A variationally coupled finite element - boundary element method. *Computers & Structures*, 33:17–20, 1989.

[15] T. Belytschko and Y. Y. Lu. Singular integration in variationally coupled FE-BE method. *Journal of Engineering Mechanics*, 117:820–835, 1991.

[16] D. E. Beskos, B. Dasgupta, and I. G. Vardoulakis. Vibration isolation using open or filled trenches. Part 1: 2-D homogeneous soil. *Computational Mechanics*, 1:43–63, 1986.

[17] K.U. Bletzinger, M. Firl, and F. Daoud. Approximation of derivatives in semi-analytical structural optimization. *Computers and Structures*, 86:1404–1416, 2008.

[18] M. Bonnet. BIE and material differentiation applied to the formulation of obstacle inverse problems. *Engineering Analysis with Boundary Elements*, 15:121–136, 1995.

[19] M. Bonnet. Regularized BIE formulations for first- and second-order shape sensitivity of elastic fields. *Computers & Structures*, 56:799–811, 1995.

[20] M. Bonnet. Differentiability of strongly singular and hypersingular boundary integral formulations with respect to boundary perturbations. *Computational Mechanics*, 19:240–246, 1997.

[21] M. Bonnet. *Boundary Integral Equation Methods for Solids and Fluids*. Wiley, 1999.

[22] M. Bonnet. Boundary element based formulations for crack shape sensitivity analysis. *Engineering Analysis with Boundary Elements*, 25:347–362, 2001.

[23] M. Bonnet, T. Burczynski, and M. Nowakowski. Sensitivity analysis for shape perturbation of cavity or internal crack using BIE and adjoint variable approach. *International Journal of Solids and Structures*, 39:2365–2385, 2002.

[24] C. A. Brebbia and J. Domínguez. *Boundary Elements - An Introductory Course*. WIT Press - Computational Mechanics Publications, 1989.

[25] K. K. Choi and N. H. Kim. *Structural Sensitivity Analysis and Optimization 1: Linear Systems*. Mechanical Engineering Series. Springer, 2005.

[26] K. K. Choi and N. H. Kim. *Structural Sensitivity Analysis and Optimization 2: Nonlinear Systems and Applications*. Mechanical Engineering Series. Springer, 2005.

[27] B. Dasgupta, D. E. Beskos, and I. G. Vardoulakis. Vibration isolation using open or filled trenches. Part 2: 3-D homogeneous soil. *Computational Mechanics*, 6:129–142, 1990.

[28] K. Deb. *Multi-Objective Optimization using Evolutionary Algorithms*. John Wiley & Sons, 2001.

[29] J. Domínguez. *Boundary Elements in Dynamics*. International Series on Computational Engineering. Computational Mechanics Publications, 1993.

[30] K. Emad and G. D. Manolis. Shallow trenches and propagation of surface waves. *Journal of Engineering Mechanics*, 111:279–282, 1985.

[31] R. Gallego and J. Domínguez. Hypersingular BEM for transient elastodynamics. *International Journal for Numerical Methods in Engineering*, 39:1681–1705, 1996.

[32] R. Gallego and J. Suárez. Numerical solution of the variation boundary integral equation for inverse problems. *International Journal for Numerical Methods in Engineering*, 49:501–518, 2000.

[33] R. Gallego and J. Suárez. Solution of inverse problems by boundary integral equations without residual minimization. *International Journal of Solids and Structures*, 37:5629–5652, 2000.

[34] D. E. Goldberg. *Genetic Algorithms in Search, Optimization and Machine Learning*. Addison-Wesley Longman Publishing Co., Inc., Boston, MA, USA, 1st edition, 1989.

[35] C. Van hoorickx, O. Sigmund, M. Schevenels, B. S. Lazarov, and G. Lombaert. Topology optimization of two-dimensional wave barriers for the reduction of ground vibration transmission. In V. Papadopoulos M. Papadrakis and V. Plevris, editors, *COMPDYN 2015 5th ECCOMAS Thematic Conference on Computational Methods in Structural Dynamics and Earthquake Engineering*, May 2015.

[36] P. R. Johnston and D. Elliott. A sinh transformation for evaluating nearly singular boundary element integrals. *International Journal for Numerical Methods in Engineering*, 62:564–578, 2005.

[37] L. Jun, G. Beer, and J.L. Meek. Efficient evaluation of integrals of order $1/r$, $1/r^2$ and $1/r^3$ using Gauss quadrature. *Engineering Analysis*, 2(3):118–123, 1985.

[38] J. H. Kane and S. Saigal. Design-sensitivity analysis of solids using bem. *Journal of Engineering Mechanics*, 114:1703–1722, 1988.

[39] S. E. Kattis, D. Polyzos, and D. E. Beskos. Vibration isolation by a row of piles using a 3-D frequency domain BEM. *International Journal for Numerical Methods in Engineering*, 46:713–728, 1999.

[40] K. L. Leung, D. E. Beskos, and I. G. Vardoulakis. Vibration isolation using open of filled trenches: Part 3: 2-D non-homogenous soil. *Computational Mechanics*, 7:137–148, 1990.

[41] Y. Y. Lu, T. Belytschko, and W. K. Liu. A variationally coupled fe-be method for elasticity and fracture mechanics. *Computer Methods in Applied Mechanics and Engineering*, 85:21–37, 1991.

[42] S. C. Mellings and M. H. Aliabadi. Dual boundary element formulation for inverse potential problems in crack identification. *Engineering Analysis with Boundary Elements*, 12:275–281, 1993.

[43] S. C. Mellings and M. H. Aliabadi. Flaw identification using the boundary element method. *International Journal for Numerical Methods in Engineering*, 38:399–419, 1995.

[44] R. A. Meric. Boundary integral equation and conjugate gradient methods for optimal boundary heating of solids. *International Journal of Heat and Mass Transfer*, 26:261–268, 1983.

[45] R. A. Meric. Boundary element methods for optimization of distributed parameter systems. *International Journal for Numerical Methods in Engineering*, 20:1291–1306, 1984.

[46] R. A. Meric. Optimal loading of solids by the boundary element method. *International Journal of Engineering Science*, 23:1101–1111, 1985.

[47] N. Nishimura and S. Kobayashi. Determination of cracks having arbitrary shapes with the boundary integral equation method. *Engineering Analysis with Boundary Elements*, 15:189–195, 1994.

[48] J. Nocedal and S. J. Wright. *Numerical optimization*. Springer Series in Operations Research. Springer, 1999.

[49] N. Olhoff, J. Rasmussen, and E. Lund. A method of "exact" numerical differentiation for error elimination in finite-element-based semi-analytical shape sensitivity analyses. *Mechanics of Structures and Machines*, 21:1–66, 1993.

[50] E. Oñate. *Structural Analysis with the Finite Element Method: Linear Statics*, volume 1 Basis and Solids. CIMNE/Springer, 2009.

[51] G. Rus. *Numerical methods for nondestructive identification of defects*. PhD thesis, University of Granada, 2001.

[52] G. Rus and R. Gallego. Boundary integral equation for inclusion and cavity shape sensitivity in harmonic elastodynamics. *Engineering Analysis with Boundary Elements*, 29:77–91, 2005.

[53] G. Rus and R. Gallego. Hypersingular shape sensitivity boundary integral equation for crack identification under harmonic elastodynamic excitation. *Computational Methods in Applied Mechanics and Engineering*, 196:2596–2618, 2007.

[54] J. A. Samareh. A survey of shape parameterization techniques. CP-1999-209136, NASA, 1999.

[55] C.A. Mota Soares, H. C. Rodrigues, and K. K. Choi. Shape optimal structural design using boundary elements and minimum compliance techniques. *Journal of Mechanisms, Transmissions, and Automation in Design*, 106:518–523, 1984.

[56] J.C.F. Telles. A self-adaptive co-ordinate transformation for efficient numerical evaluation of general boundary element integrals. *International Journal for Numerical Methods in Engineering*, 24:959–973, 1987.

[57] J.C.F. Telles and R.F. Oliveira. Third degree polynomial transformation for boundary element integrals: further improvements. *Engineering Analysis with Boundary Elements*, 13:135–141, 1994.

[58] J. C. Townsend, J. A. Samareh, R. P. Weston, and W. E. Zorumski. Integration of a CAD system into an MDO framework. TM-1998-207672, NASA, 1998.

[59] F. van Keulen, R. T. Haftka, and N. H. Kim. Review of options for structural design sensitivity analysis. Part 1: Linear systems. *Computational Methods in Applied Mechanics and Engineering*, 2005.

[60] R. D. Woods. *Screening of elastic surface waves by trenches*. PhD thesis, University of Michigan, 1967.